ON THE UNSTEADY AERODYNAMICS OF STATIONARY ELLIPTIC CYLINDERS DURING ORGANISED WAKE CONDITION

by

AJAI KUMAR DIKSHIT
B.Sc., Gorakhpur University, U.P., India
B.Tech., Indian Institute of Technology, Madras, India

A THESIS SUBMITTED IN PARTIAL FULFILLMENT OF
THE REQUIREMENTS FOR THE DEGREE OF
M.A.Sc.

in the Department
of
Mechanical Engineering

We accept this thesis as conforming to the
required standard

THE UNIVERSITY OF BRITISH COLUMBIA
July, 1970

In presenting this thesis in partial fulfillment of the requirements for an advanced degree at the University of British Columbia, I agree that the Library shall make it freely available for reference and study. I further agree that permission for extensive copying of this thesis for scholarly purposes may be granted by the Head of my Department or by his representatives. It is understood that copying or publication of this thesis for financial gain shall not be allowed without my written permission.

A.K. Dikshit

Department of Mechanical Engineering

The University of British Columbia
Vancouver 8, B.C., Canada

Date 16th Aug' 70.

ABSTRACT

The aerodynamics of a set of two-dimensional, stationary elliptic cylinders with eccentricity of 0.44, 0.92 and 0.98 is studied experimentally during the organised wake condition ($R=2x10^4-10^5$). The results indicate the effect of eccentricity and angle of attack on mean and unsteady pressure coefficients, Strouhal number and wake geometry, the three important parameters in the aeroelastic instability study. In conjunction with the available literature, the information presented here attempts at providing better understanding of the bluff body aerodynamics in the region between the two extreme cases of circular cylinder (e=0) and flat plate ($e=\infty$).

The cylinder eccentricity and attitude has considerable effect on vortex shedding frequency, with variation of the Strouhal number in the range 0.037-0.274. Although basing Strouhal number on projected dimension or wake width reduces its dependence on angle of attack, the use of transverse distance between the separation points provides, in addition, a smoother transition even at higher eccentricities and smaller angles of attack.

The measurement of fluctuating pressure in the

narrow band around the Strouhal frequency showed substantial dependence on the Reynolds number at zero angle of attack, particularly for the ellipses of high eccentricity. Considerable phase difference may exist between the pressure signals, however, it has negligible effect on the unsteady lift.

The thesis also presents analytical results on the location of shear layer separation as obtained using Görtler's series in conjunction with mean pressure profile. The analytical data compared favourably with the results of flow visualisation through Schlieren technique. The high speed movie of the near wake region gave preliminary information about the location of the first vortex and the oscillations of the separating shear layers. The rise and decay of the unsteady pressure in the vortex formation region appeared to substantiate the visual observations. In general, the wake geometry ratio varied around the Kármán stability value of 0.281.

The correlation of spanwise results clearly emphasized the three dimensional character of the unsteady aerodynamics. In general, the spanwise variation of fluctuating pressure is enhanced with increase in angle of attack. The phase data suggest inclination of the vortex line at the model to be $\lesssim 11°$. Increase in angle of attack results in improved alignment of the vortex line with the cylinder axis.

TABLE OF CONTENTS

LIST OF TABLES

LIST OF FIGURES

Figure | Page

Figure | Page

LIST OF SYMBOLS

C_D	mean drag coefficient, pressure drag/ $\{(1/2)\ \rho V_\infty^2\ 2ac\}$
C_L	mean lift coefficient, lift/$\{(1/2)\rho V_\infty^2\ 2ac\}$
C_M	mean pitching moment coefficient, moment about mid-chord/ $\{(1/2)\rho V_\infty^2\ 4a^2c\}$
C_p	mean static pressure coefficient, $(p-p_\infty)$/ $\{(1/2)\rho V_\infty^2\}$
$C_{L'}$	amplitude of fluctuating sectional lift coefficient, based on rms value
$C_{\bar{p}'}$	fluctuating pressure coefficient, $\bar{p}'$/ $\{(1/2)\rho V_\infty^2\}$
D	diameter of circular cylinder or length of square cylinder side
F	stream function, $\psi(X,Y) = \nu \sqrt{2\xi}\ F(\xi,n)$
$\bar{F}$	ratio of the maximum fluctuating pressure (average amplitude) at a transverse station in the wake to the corresponding value on the surface of the model for a given angle of attack, $\bar{p}'_w/(\bar{p}'_m)_{max}$
L	longitudinal spacing between vortices
N	the number of pedestals at which correlation output reaches the maximum value
R	Reynolds number, $V_\infty 2a/\nu$
S	percentage circumference, measured anti-clockwise from tap 0
S_R, S_S, S_{2b}, S_h	Strouhal numbers based on Roshko's criterion $(fW/[V_\infty^2\{1-(C_p)_b\}]^{1/2})$, spacing between separation points $(fh'/[V_\infty^2\{1-(C_p)_b\}]^{1/2})$, minor axis $(f2b/V_\infty)$ and projected height of the model (fh/V_∞), respectively

$U(X)$	outer potential flow velocity parallel to circumference of ellipse at the edge of boundary layer
V_v	streamwise vortex velocity
V_∞	free stream velocity
W	lateral spacing between vortices
X	distance measured along circumference of ellipse from front stagnation point
Y	distance from circumference of ellipse along the normal
a	semi-major axis of model
b	semi-minor axis of model
c	length of model
e	eccentricity of elliptic cylinder, $[1-(b/a)^2]^{1/2}$
f	frequency of vortex shedding, Strouhal frequency
h	projected height of model, $2(a^2\sin^2\alpha+b^2\cos^2\alpha)^{1/2}$
h'	transverse distance between the separation points
p	mean pressure
p'	amplitude of the fluctuating pressure signal
$\bar{p}'$	unsteady pressure (average amplitude based on the rms value) about mean
p_∞	mean static pressure in the free stream
s	circumferential location of minimum pressure from front stagnation expressed as a fraction of sectional perimeter
t	time delay setting in computing cross correlation function
x, y, z	reference coordinate system with origin on the axis of a model at the central section, Figure 3-2

α	angle of attack
θ	inclination of the vortex line to z-axis of the model
ν	kinematic viscosity of air
ρ	air density
$\tau(X)$	shear stress at the surface of ellipse
ϕ	phase angle between fluctuating pressure signals

Subscripts

b	base value of parameter
l, u	value of parameter on lower and upper surfaces, respectively
m	parameter value on model surface
max	maximum value of parameter
w	parameter value in wake

ACKNOWLEDGEMENT

The author wishes to express his sincere appreciation for the guidance and and assistance given by Dr. V.J. Modi throughout the program. His help during Schlieren photography and in the preparation of the thesis deserves special mention.

Thanks are also due to the Department of Mechanical Engineering for the use of their facilities, and to the technicians Ed Abell, Fred Knowles, John Hoar and Phil Hurren for their invaluable and skilled contribution in the preparation of the experimental facilities. Sincere appreciations are conveyed to Dr. Z. Rotem for the use of his semi-focusing Schlieren system and Mr. F.W. Anderson for his assistance during this part of the experiment.

Financial support was received from the National research Council of Canada, Grant A-2181.

1. INTRODUCTION

The problem of self-induced oscillations of elastically mounted bluff bodies, when exposed to a fluid stream, is not new. Several instances of vibration and subsequent breakdown of smoke stacks, transmission lines, aircraft wings, bridges etc., have been reported. The nature of the forcing function, Strouhal number and wake geometry represent three important parameters in an aeroelastic instability study. The determination of the corresponding information for a set of two dimensional, stationary, elliptic cylinders in the Reynolds number range of 2×10^4-10^5 forms the subject of this investigation.

In general, the elastically supported bluff bodies exhibit two distinct forms of aerodynamically induced vibration transverse to the flow direction. In the first type, commonly known as vortex resonance, the periodicity of the organised wake due to vortex shedding coincides with the natural frequency of the structure. This represents forced vibration since the sustaining alternating force exists independent of the motion and persists even when the motion is stopped. Although any bluff body of arbitrary cross-section, when suitably mounted, would exhibit vortex excited oscillation, the available literature is largely confined to such studies on circular

cylinders because of the geometric simplicity of the section.

The second form of instability, referred to as galloping, represents an important type of self-excited vibration. The fluid forces which create a condition of instability arise due to the fact that the cross-section of the body is aerodynamically unstable to small disturbances. These forces result in oscillations which grow in amplitude until the energy extracted from the fluid stream balances that dissipated through various forms of damping. Galloping oscillations are referred to as "self-excited" because the fluid forces that sustain the motion are created and controlled by the motion itself, and if the motion stops, the unsteady forces disappear. The main features of galloping are that the vibration can occur in a single degree of freedom and the steady-state amplitude tends to increase with increasing wind velocity.

Strouhal[1] was the first to correlate the periodic vortex shedding with the diameter of a circular cylinder and fluid velocity. This was followed by the classical study of Von Kármán[2], wake analysis by Heisenberg[3] and experiments on wake geometry by Bénard[4]. Ever since, academic and practical interest in the vortex shedding phenomenon has resulted in many theoretical and experimental investigations by Roshko[5-10], Kovásznay[11], Rosenhead[12,13], Schaefer and Eskinazi[14], Gerrard[15-21] and others.

Rosenhead[22], Wille[23,24], Marris[25], Morkovin[26] and Slater[27] have reviewed this literature at some length. It would be, therefore, sufficient to emphasize only the important features of the available information relevent to the present investigation.

Among the numerous papers written on the aspects of fluid mechanics and dynamics of bluff bodies, only a few are concerned with the actual measurements of unsteady pressures. McGregor[28] and Gerrard[15] measured fluctuating forces on stationary circular cylinders using a condenser microphone system built into the model. The pressure distribution was obtained by turning the cylinder. Keefe[29] carried out fluctuating force measurements with the help of a carefully designed strain-gauge transducer which also acted as a test model. Molyneux[30] has also described a low frequency strain-gauge type transducer mounted inside the model to measure pressures on oscillating wings. More recently, Humphreys[31], Fung[32], Grove[33] et al., Bishop and Hassan[34], and Ferguson and Parkinson[35] measured unsteady loading on fixed circular cylinder over different ranges of the Reynolds number.

The study of three-dimensional structure of the wake, through flow-visualisation and/or correlation of aerodynamic coefficients, associated with circular cylinder has been reported by several investigators[18,31,36-42]. In general, two-dimensional character of the flow was

maintained only over two to three diameters in the neighbourhood of the central section. Both sharp edged separation and oscillation of the model led to improved correlation.

So far as the effect of turbulence on the unsteady aerodynamics of a stationary circular cylinder is concerned, the investigation carried out by Surry[43] appears to be the most significant one. He observed that mean drag coefficient and vortex shedding frequency are consistent with an effective increase in the Reynolds number which now depends both on intensity and scale of the turbulence. The fluctuating lift is dominated by broadened Strouhal peak while the unsteady drag is primarily due to streamwise turbulence. In general, the presence of turbulence resulted in the reduction of spanwise correlation length.

The available information concerning bluff body interaction with the separated flow of stable vortex type is not limited to the cylinders of circular cross-section. Investigations with square, rectangular, triangular and hexagonal cylinders, Structural H and angle sections, as well as several irregular geometries are also reported[44-56]. But it must be emphasized that the bulk of the literature is indeed devoted to the circular geometry. This point is well emphasized by the fact that the previous work on elliptical cylinders seems to be limited to rather preliminary unsteady pressure measurements by Modi and Heine[49],

Strouhal number study by Schramm[50], together with fluctuating loading and vortex shedding frequency study (e=0.60,0.80) by Modi and Wiland[57].

A comment concerning the related but somewhat modified problem involving calculation of the boundary layer separation would be appropriate here. Although Hiemenz[58], Chiu[59] and Achenbach[60] have provided experimental data for two-dimensional stationary circular cylinders, the major research efforts in this area have been analytic in character. Schlichting[61] has presented an excellent review of this literature.

The aeroelastic instability of bluff bodies has been under investigation in this department since 1958. The review of the progress made has been reported in two survey papers[62,63]. The investigation described here forms the part of this continuing programme and intends to study, experimentally, the effect of eccentricity of the cylindrical bluff body on the fundamental parameters listed before.

2. PURPOSE AND SCOPE OF THE INVESTIGATION

A systematic study of the aeroelastic instability of bluff bodies, which has been progressing in this department for over a decade, has contributed to our understanding of wind effects on buildings and structures. The investigation reported here forms a part of this broad-based programme.

The significance of elliptic geometry in such a study becomes apparent when one recognises the fact that a circular cylinder, in yawed condition, presents elliptic cross-section along the relative wind. Furthermore, an elliptic section represents a more general configration permitting realization of a wide range of geometrical shapes, from circular cylinder ($e=0$) to flat plate ($e=\infty$), by a systematic variation of eccentricity.

The project aims at studying the aerodynamics of stationary, two-dimensional, elliptic cylindrical models of eccentricities 0.44, 0.92 and 0.98. In particular, it presents experimental results on:

(i) mean lift, drag and pitching moment;

(ii) variation of Strouhal number with Reynolds number;

(iii) mean and fluctuating static pressure distributions;

(iv) fluctuating lift;

(v) wake geometry;

as functions of angle of attack and eccentricity. The growth and decay of the fluctuating pressure in the wake are studied in some detail to obtain information concerning the position of the first vortex. In most cases the Reynolds number range was confined to $2x10^4$-10^5. Whenever available, results for flat plate, circular cylinder and Wiland's[64] data on elliptic cylinders (e=0.60, 0.80) are included to permit comparison and establish trend.

The flow field was also examined visually through Schlieren technique in conjunction with high speed photography to provide, at least, qualitative understanding of the complex phenomenon. The position of the separating shear layer as given by flow visualization is compared with the analytical results obtained using Görtler series solution[65] approach.

Since the influence of wind tunnel walls on the aerodynamic coefficients is not well established, the results presented are uncorrected for that effect.

3. MODELS AND SUPPORTING SYSTEM

Three elliptic cylindrical models, each 27 inches long, were designed to span the wind tunnel cross-section thus approximating the two-dimensional flow condition. The constructional details of a typical model are shown in Figure 3-1 and physical parameters are listed in the table below. As Wiland's data have been quoted extensively throughout the thesis for comparison, the geometrical features of his models are also included.

Table 3-1 Model data

e	a/b In./In.	Material	Weight lb.	Number of Bulkheads	Skin Thickness in.
0.44	5.0/4.5	Plexiglas	1.81	7	0.020
*0.60	5.0/4.0	Aluminum	4.20	7	0.020
*0.80	5.0/3.0	Plexiglas	1.45	7	0.020
0.92	5.0/2.0	Plexiglas	1.38	7	0.015
0.98	5.0/1.0	Plexiglas	2.00	Modular Construction	-

*Wiland's models[64]

Although the present set of experiments employ models under stationary condition, the dynamic tests planned for future required careful consideration of weight and strength. The model design permitted them to be mounted on the wind tunnel balance or supported by the existing air bearing system for measurement under vibrating condition. The pronounced slenderness of ellipse with e=0.98 required slightly different constructional technique. Here plexiglas modules were accurately finished and bonded together.

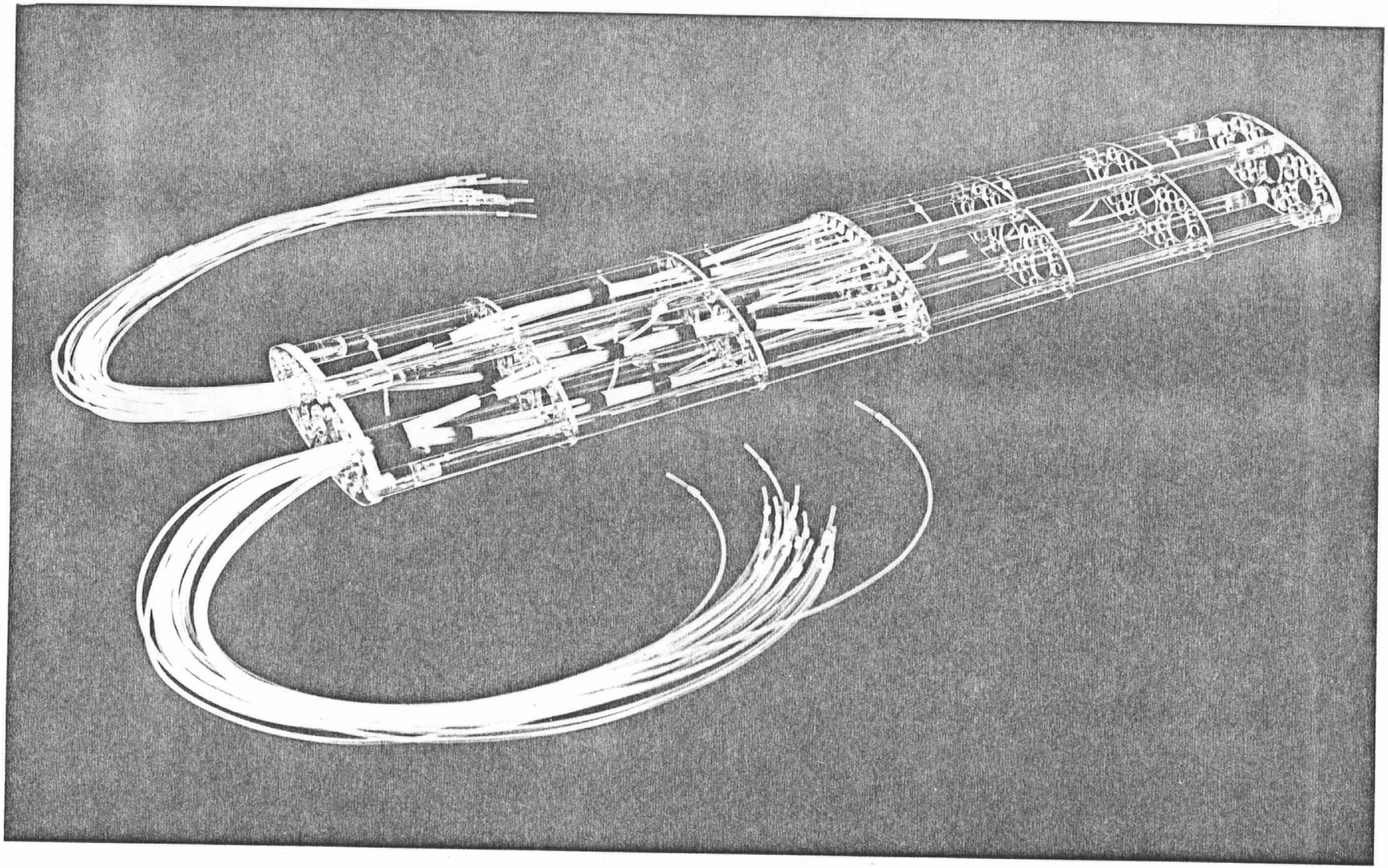

Figure 3-1 Constructional details of a typical model

The central bulkhead of each model carried 32 pressure taps (dia.=0.025 in.) equally spaced around the circumference. In addition the model was provided with 8 pressure taps in spanwise direction as indicated in Figure 3-2. The pressure taps are connected to 5 ft. long "Intramediac" polyethelene tubings of inside diameter 0.066 in. which are brought out from the bottom end of the models (Figure 3-1).

The models were tested in a low speed, low turbulence, return type wind tunnel where the air speed can be varied from 4-150 ft./sec.with a turbulence level less than 0.1%. A Betz micromanometer, with an accuracy of 0.2 mm. of water, is used to measure the pressure differential across the contraction section of 7:1 ratio. The test section velocity is calibrated against the above pressure differential. The rectangular cross-section, 36 in. x 27 in., is provided with 45° corner fillets which vary from 6 in. x 6 in. to 4.75 in. x 4.75 in.to partly compensate for the boundary layer growth. The spatial variation of mean velocity in the test section is less than 0.25%. The tunnel is powered by a 15 horsepower direct current motor driving a commercial axialflow fan with a Ward-Leonard system of speed control. Figure 3-3 shows the outline of the tunnel.

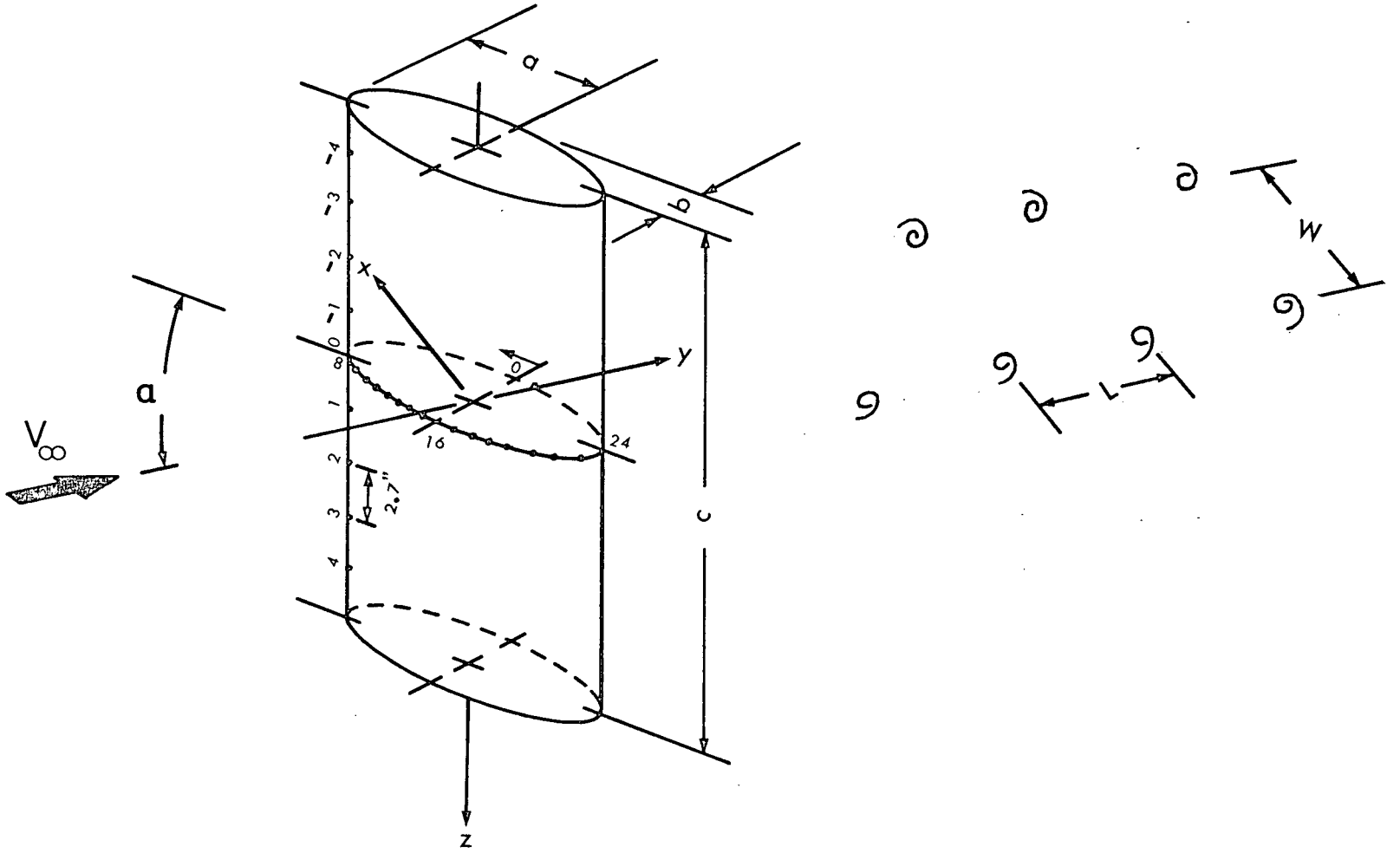

Figure 3-2 Notation for model and wake geometry

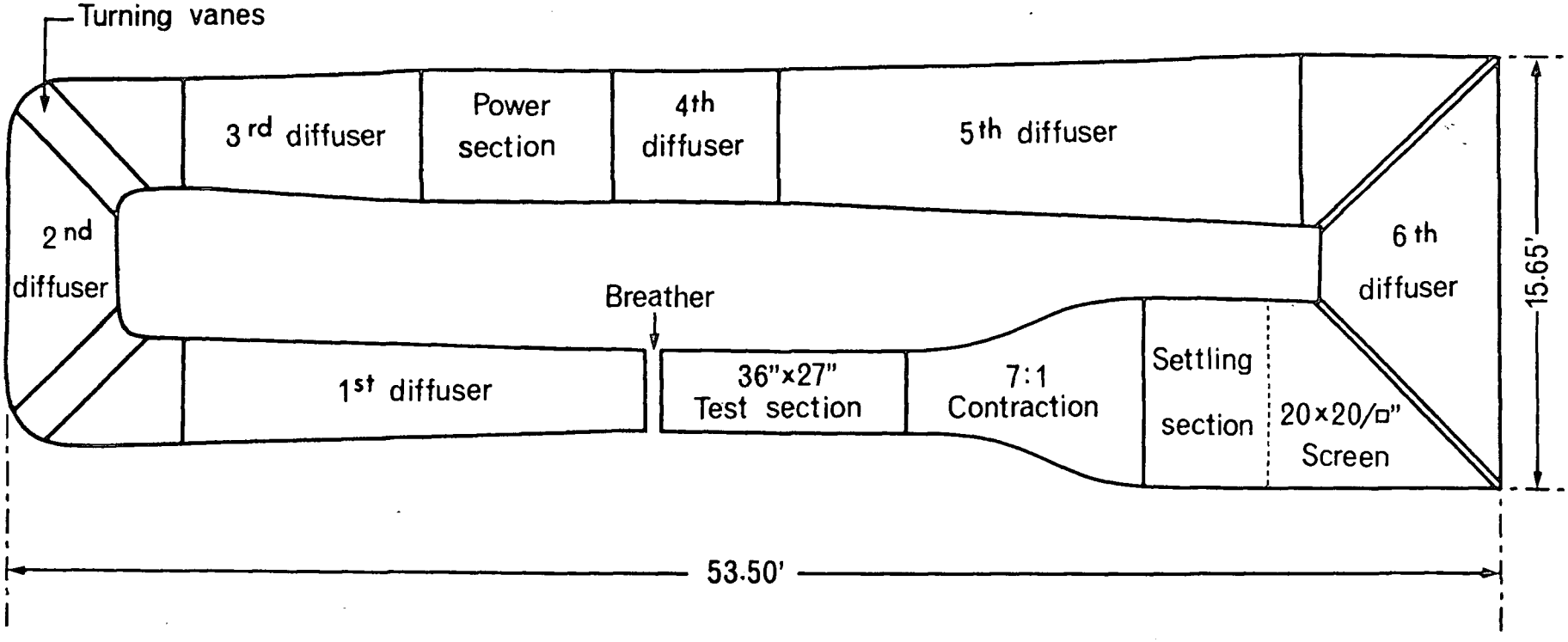

Figure 3-3 Schematic diagram of the low speed wind tunnel used in test programme

4. TEST PROCEDURES

4.1 Instrumentation and Calibration

Most of the instrumentation used for the experimental programme, e.g., wind tunnel balance, manometers, filters, rms meter, etc., constitute standard equipment in any aerodynamics laboratory and hence needs no elaboration. However, a brief account of the unsteady pressure and wake geometry measurement procedure would be appropriate.

In 1963 Datametrics Inc. of Waltham, Massachusetts developed a pressure transducer called Barocel Modular Pressure Transducing system. It is a high precision sensitive instrument consisting of a stable capacitive voltage divider with a stainless steel diaphragm separating the two pressure chambers. When exposed to a pressure signal, the diaphragm deflects attaining a voltage level determined by its relative position between the plates. With Barocel appropriately arranged in a bridge circuit, the output voltage is determined by the ratio of capacitance of the diaphragm to each of the stationary electrodes. It can now be read on any of the 8 sensitivity ranges (5V d.c. full scale) which have a linearity of ±0.1% and stability of ±0.1% over ±15°F ambient temperature changes. The prestressed diaphragm has a natural frequency of 2500 cps

and the transient response of the pressure sensor head is less than 2 ms. to a step pressure input. From experiment the Helmholtz resonator frequency of the cavity and connection on one side of diaphragm was found to be approximately 210 cps.

The Barocel is accurately calibrated for steady pressures. However, for fluctuating signals transmitted through relatively long, small diameter tubes considerable attenuation would occur. Therefore, the output electrical signal required calibration against known input fluctuating pressure at the model surface. This was achieved using the calibration system developed by Wiland[64]. Figure 4-1 shows the calibration plot for the transducer in terms of attenuation as a function of signal frequency.

The wake survey was carried out using a disc probe constructed by Ferguson[66] in accordance with the design discussed in detail by Bryer et al.[67] It was mounted on a 1 in. hypodermic needle which in turn was connected to a 14 in. long, 1/4 in. diameter sting. The mean pressure calibration results for the probe are shown in Figure 4-2. The measurements indicate the probe to be relatively insensitive to a pitch of ±5° and Yaw of ±20°. The wake traversing gear designed by Ferguson[66] was used to position the probe at a desired location in the wind tunnel test section. The accuracy in positioning the probe was approximately 0.02 in.

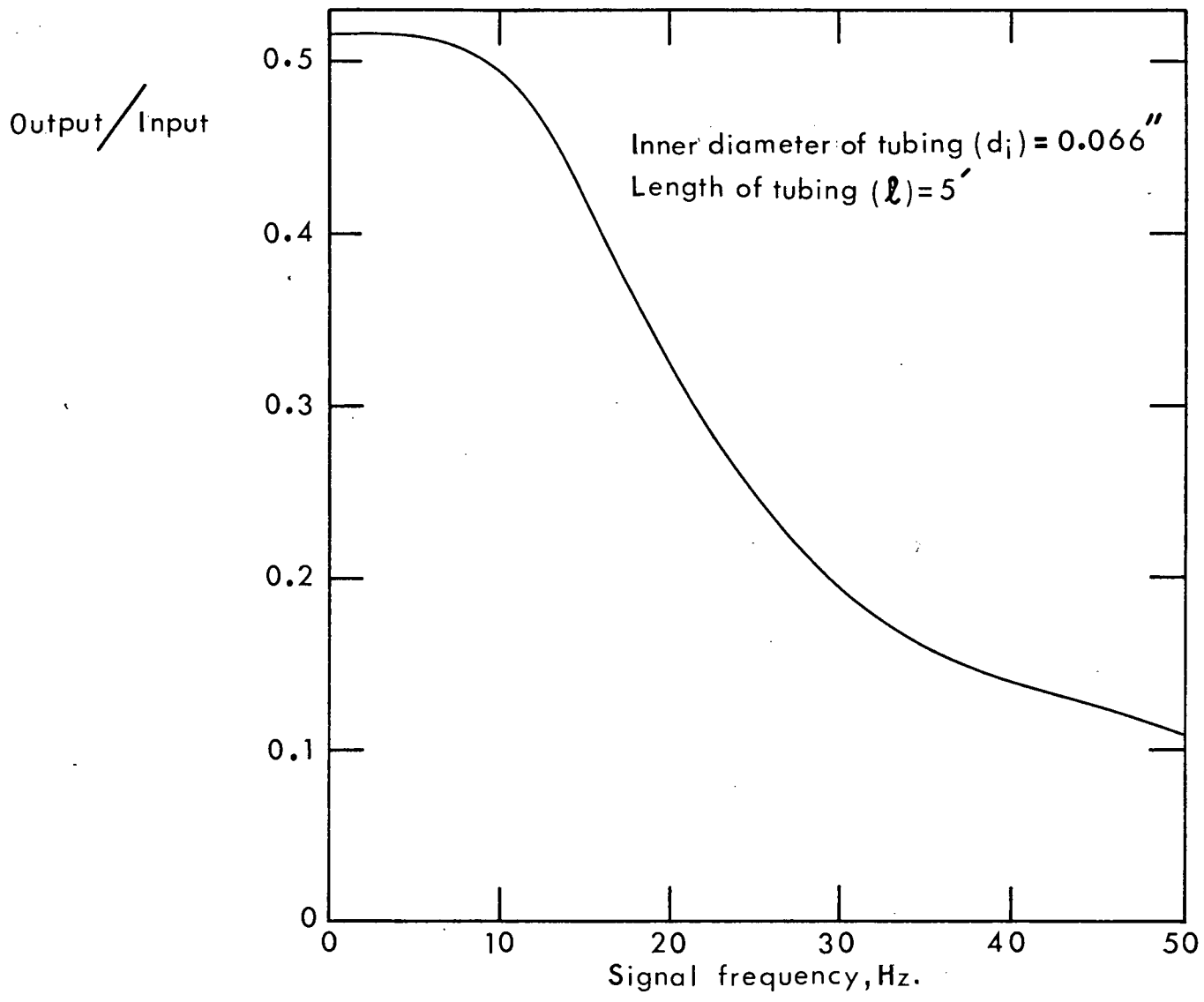

Figure 4-1 Calibration plot for Barocel pressure transducer with damping bottle

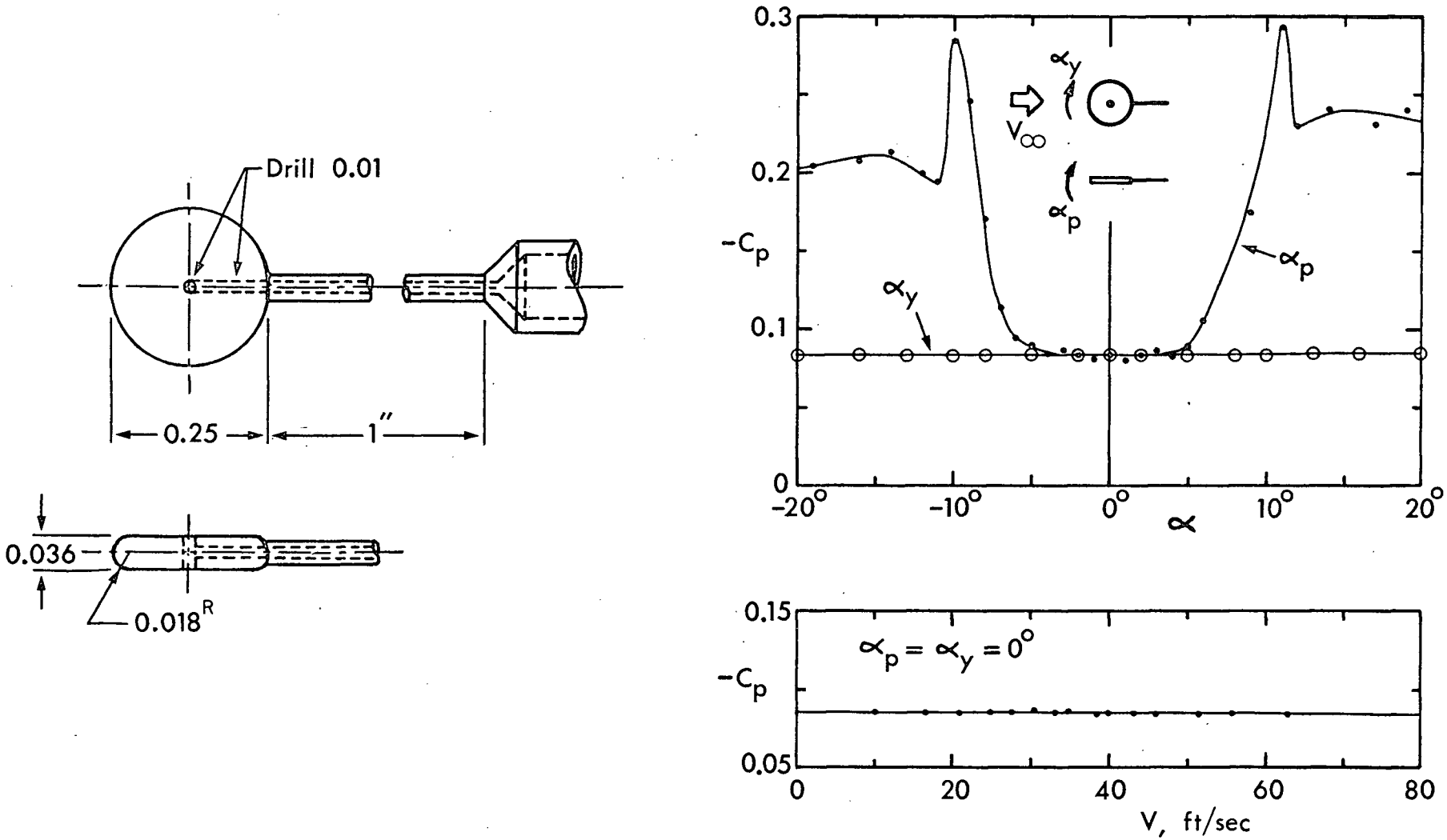

Figure 4-2 Disc probe and calibration plots

4.2 Balance Measurements

For force and moment measurements, the models were mounted on the wind tunnel balance through a bracket. To ensure nearly two-dimensional flow condition, the clearance between the tunnel ceiling and the model end was kept to a minimum ($\simeq$1/32 in.). Having set the model at a preselected value of angle of attack, the wind tunnel speed was brought to the desired value and the lift, drag and pitching moment results recorded. The procedure was repeated at several wind speeds to study Reynolds number dependency. The angle of attack was varied systematically over the range 0-90° in the step of 5° except near the ends of the interval where finer changes were required to establish trend.

As indicated by Pankhurst and Holder[68] the interference from wind tunnel walls during steady flow conditions may be subdivided into:

(i) Solid blockage;
(ii) Wake blockage;
(iii) Lift effect;
(iv) Interference due to static pressure gradient;
(v) Wall-boundary layer interference.

In case of an elliptic cross-section model, symmetrically placed in a flow field, (iii) does not exist. For the

wind tunnel at the University of British Columbia, the wall boundary layer thickness in the test section is relatively small partly due to the filleted corners which compensate for boundary layer growth. Furthermore, the pressure integrated and balance measured aerodynamic coefficients showed good correlation (Figure 5-1). Thus, (v) appears to be negligible. Similarly, for the tunnel (iv) was found to be of minor significance (<1%). Therefore solid and wake blockage represent major wall interference on model aerodynamics.

Approximate correction to the drag coefficient was obtained using the method described by Whitbread[69]. It amounts to 13%, 14%, and 17% for ellipses of e=0.44, 0.92 and 0.98, respectively, at α=90°. At α=0 it is 12%, 6% and 1% for e=0.44, 0.92, 0.98 respectively. For the ellipses tested by Wiland[64] (e=0.60, 0.80) these corrections were in the range of 8-12%. As suggested by Whitbread the same correction can be applied to the lift and moment coefficients.

4.3 Mean Static Pressure on Model Surface

The mean pressure distribution was obtained using a Lambrecht manometer. Hypodermic needles were introduced in the tubing connecting the pressure tap to the manometer to minimize oscillation of the alcohol column caused by the fluctuating component of the static pressure. The

pressure on the model was measured relative to the total head in the settling section of the wind tunnel to facilitate reduction of the data. This eliminated the effect of atmospheric pressure changes during the tests and produced a pressure differential which was always positive. The tests were conducted over a range of wind speed and angle of attack.

4.4 Vortex Shedding Frequency

The Strouhal frequency was determined by displaying a fluctuating pressure signal on a storage oscilloscope. A band pass filter was introduced in the circuit to eliminate extraneous noise. The models were tested for vortex shedding frequency variation with angle of attack and Reynolds number. In general, the signals were stronger for ellipses at higher angles of attack. With the slender ellipse of e=0.98, the system failed to record any signal for $\alpha<12°$, probably, due to poor response characteristics of the pressure transducer at high frequency. The flow visualisation study indicated the presence of well defined Kármán vortex street, even at $\alpha=0°$, for the same ellipse.

4.5 Fluctuating Pressure on Model Surface

Fluctuating pressure, relative to the mean static pressure at the tap in question, was measured using the

instrumentation set-up shown in Figure 4-3. Due to large seemingly random amplitude modulations of fluctuating pressure, it was necessary to present the results as time-average values. Under certain conditions it was necessary to average results over several minutes to obtain reproducible results. This was accomplished through the use of true rms voltmeter which converts the fluctuating pressure signal into an equivalent D.C. output level. An external r-c damping circuit was used to reduce the variation of the signal caused by amplitude modulations. The final steady d.c. level was measured on a vaccum tube voltmeter. Because of the extremely high input resistance of the latter no measurable voltage drop occurred over the damping resistors. The extent of the amplitude modulation was obtained by determining the average peak signal over more than 2,000 cycles as recorded on a storage oscilloscope.

The band pass filter attenuation was determined for each wind speed and filter cut-off frequency settings by using a sinusoidal signal from a low frequency function generator.

The phase difference between the fluctuating pressure at the model taps was obtained using function correlator manufactured by Princeton Applied Research Corporation. For cross correlation mode the phase is given by a simple formula,

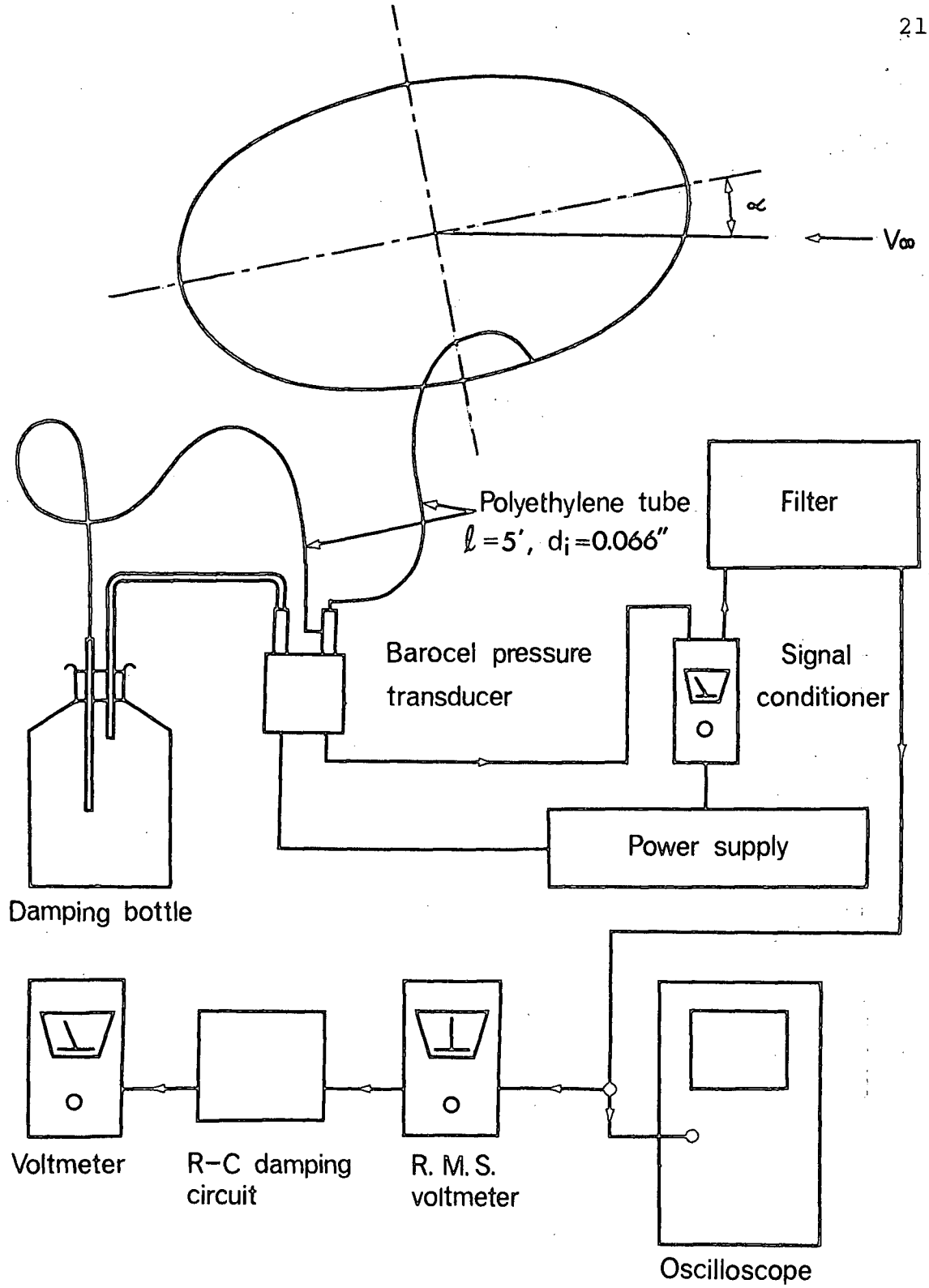

Figure 4-3 Fluctuating pressure measuring set up

$$\phi = 3.6\ Ntf \qquad (4.1)$$

The effect of any phase change inherent to the instrumentation was nullified by measuring all phase data with respect to reference taps at 90° to the wind direction. The schematic diagram of the phase measuring system is shown in Figure 4-4.

4.6 Wake Survey

The determination of wake geometry was accomplished by examining the fluctuating pressure field, associated with the vortices shed from the model, using the instrumentation layout shown in Figure 4-5. Traversing the disc probe lateral to the wake at various downstream stations and recording the rms value of the pressure signal gave a set of curves each having two peaks near the vortex centre lines. The distance between these maxima, at each y-station, was taken to be a measure of the lateral spacing between the two rows of vortices. It was convenient to present the results of lateral traverse as a ratio of probe to model tap rms signals. The selection of the model tap for the ratio was somewhat arbitrary, but represented the position on the model having a near maximum value of the unsteady pressure. Variation of the peak pressure values along the y-coordinate gave an indication as to the position

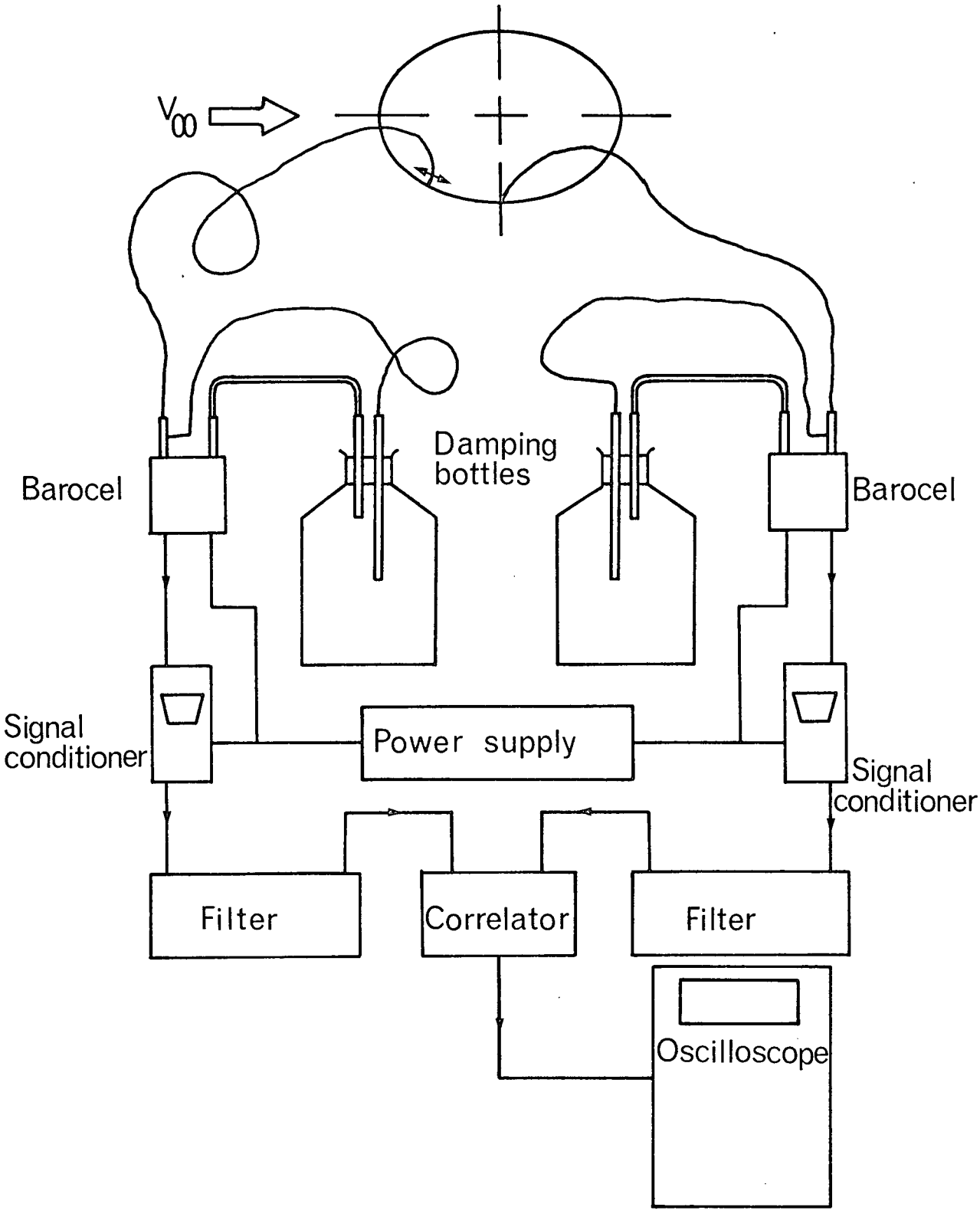

Figure 4-4 Instrumentation for measurement of phase

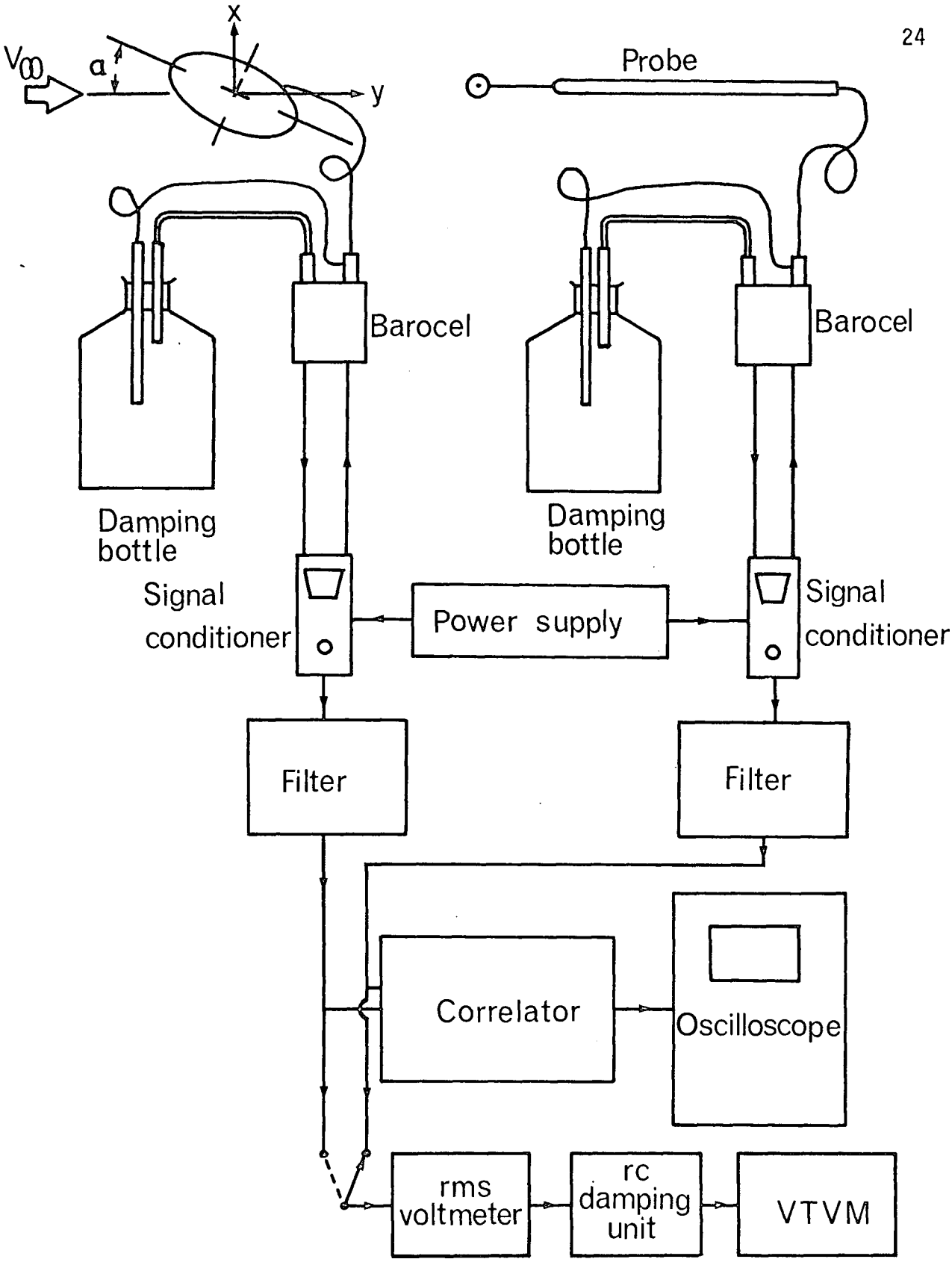

Figure 4-5 Schematic diagram of instrumentation used in wake survey

of the first vortex formation and its decay in downstream direction.

The longitudinal spacing between the consecutive vortices was obtained through recognition of the fact that the distance corresponds to a 360° phase difference between the fluctuating pressure signals associated with them. Using a pressure tap on the model as reference, the disc probe was moved downstream near the centre line of a vortex row. The phase data, obtained using the correlator, was recorded as a function of downstream coordinate (y). The process was continued until limited by the travel of the traversing gear (40 in.). The plot of phase vs. y-coordinate gave continuous variation of the longitudinal spacing through the relation

$$L = \frac{dy}{d\phi^\circ} (360^\circ) \qquad (4.2)$$

The Strouhal frequency being known, the vortex velocity in the wake was also determined. The wake traverse measurements were confined to the midspan of the cylinder.

5. TEST RESULTS AND DISCUSSION

5.1 Steady Aerodynamic Coefficients

The mean lift, drag and pitching moment experienced by elliptic cylinders were measured over a range of Reynolds number and angle of attack using the Aerolab six component strain-gauge balance. The results are presented in Figure 5-1. It is apparent that over the wind-speed range investigated, the force and moment coefficients are essentially independent of the Reynolds number, except for the few isolated discrepancies. Pertinent results for flat plate[70], circular[5] and elliptic[64] cylinders as quoted in literature are also included. The pressure integrated results, available for α=0, 30°, 60° and 90°, are indicated for comparison. Their close agreement with the balance data suggests essentially two-dimensional flow condition. A degree of similarity between the lift and moment plots together with the presence of hump near $\alpha \simeq 10°$ for slender ellipses is of interest. The sudden drop in these aerodynamic coefficients along the leeward side of the hump may be attributed to the shift in top surface separation point from the vicinity of the trailing end to the leading edge. This behavior was confirmed during the flow visualisation.

In general, lift and pitching moment increase with eccentricity and angle of attack reaching their peak values

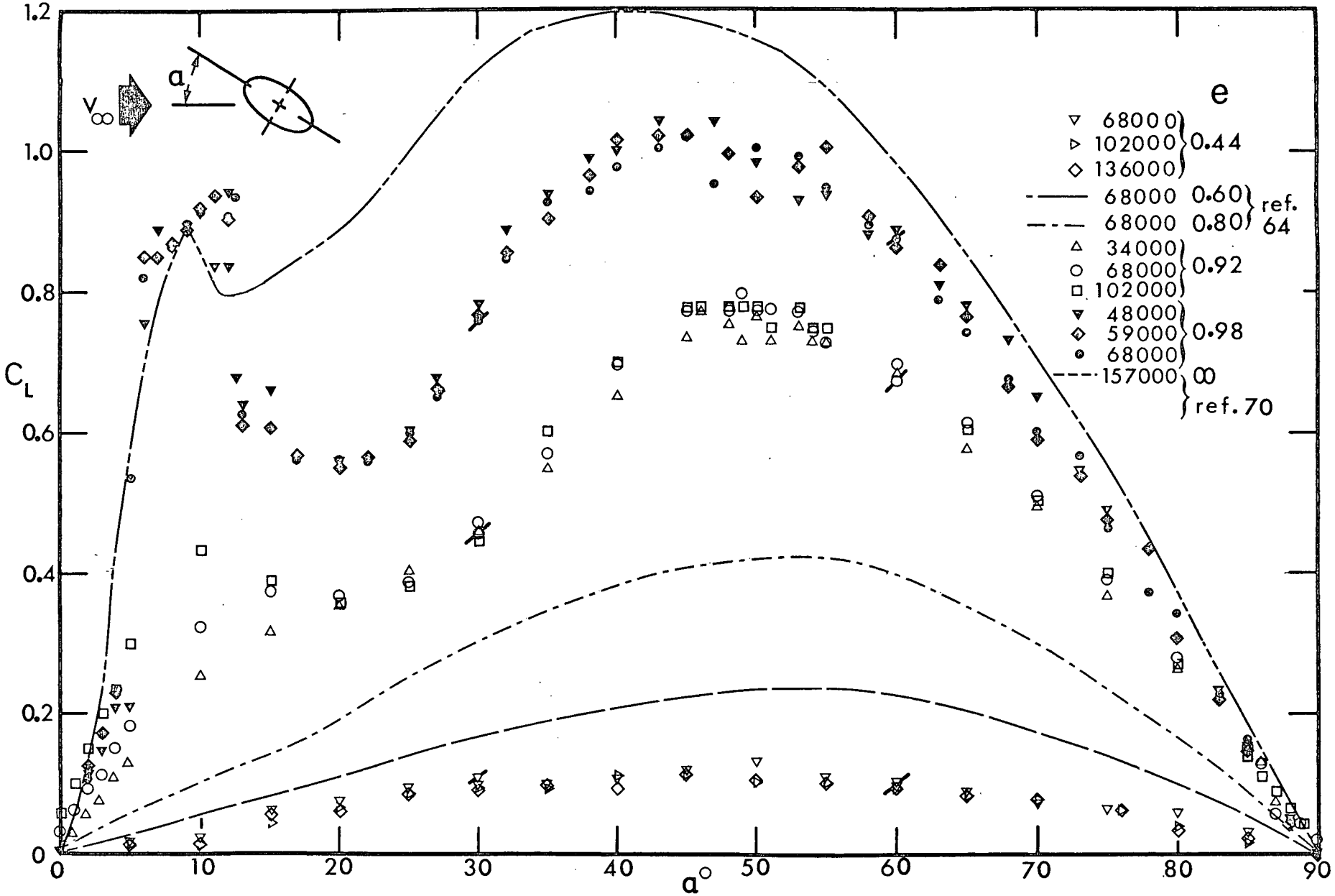

Figure 5-1 Variation of mean aerodynamic coefficients with angle of attack (symbols with slash indicate pressure integrated values): (a) Lift

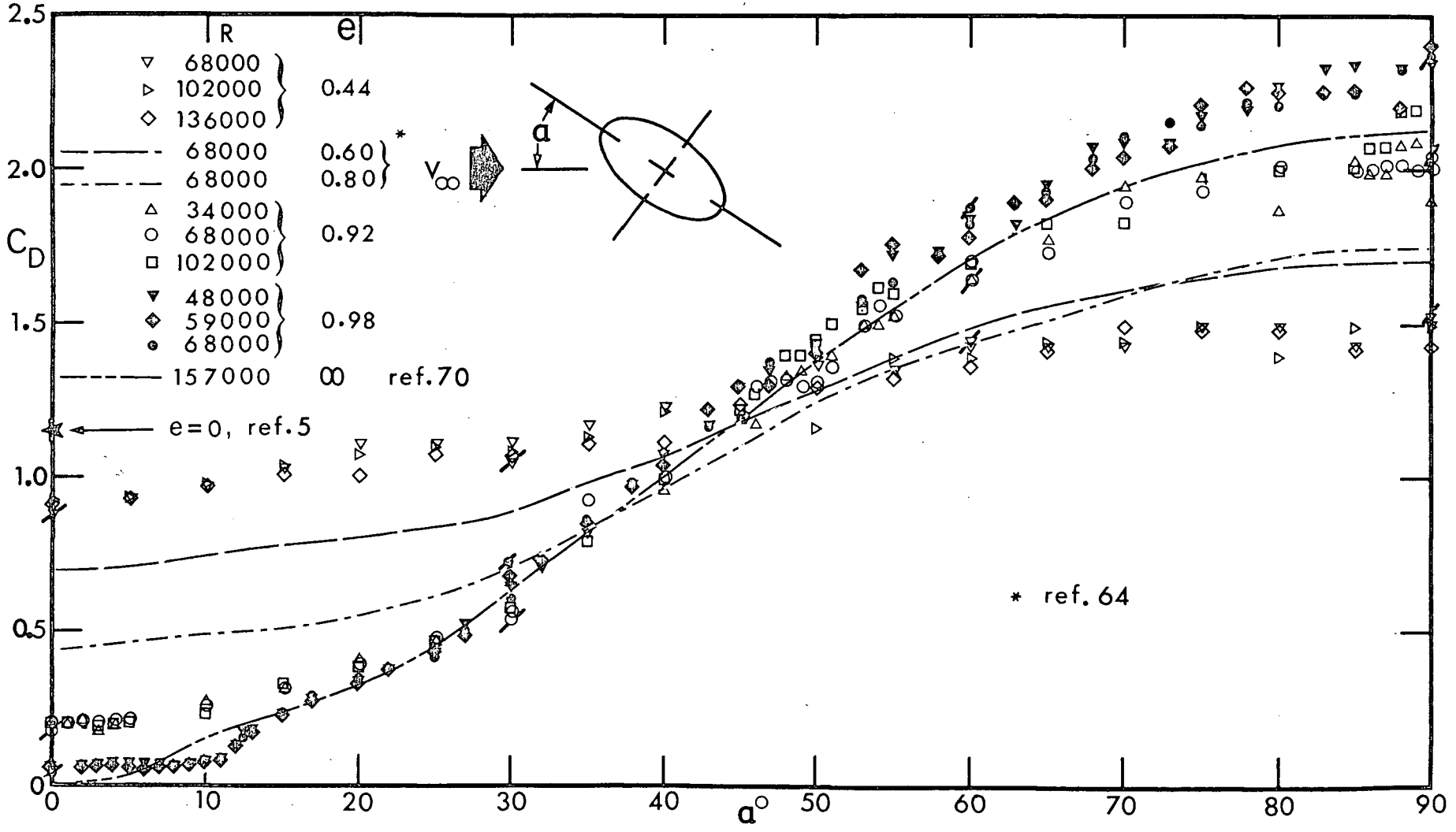

Figure 5-1 Variation of mean aerodynamic coefficients with angle of attack (symbols with slash indicate pressure integrated values): (b) Drag

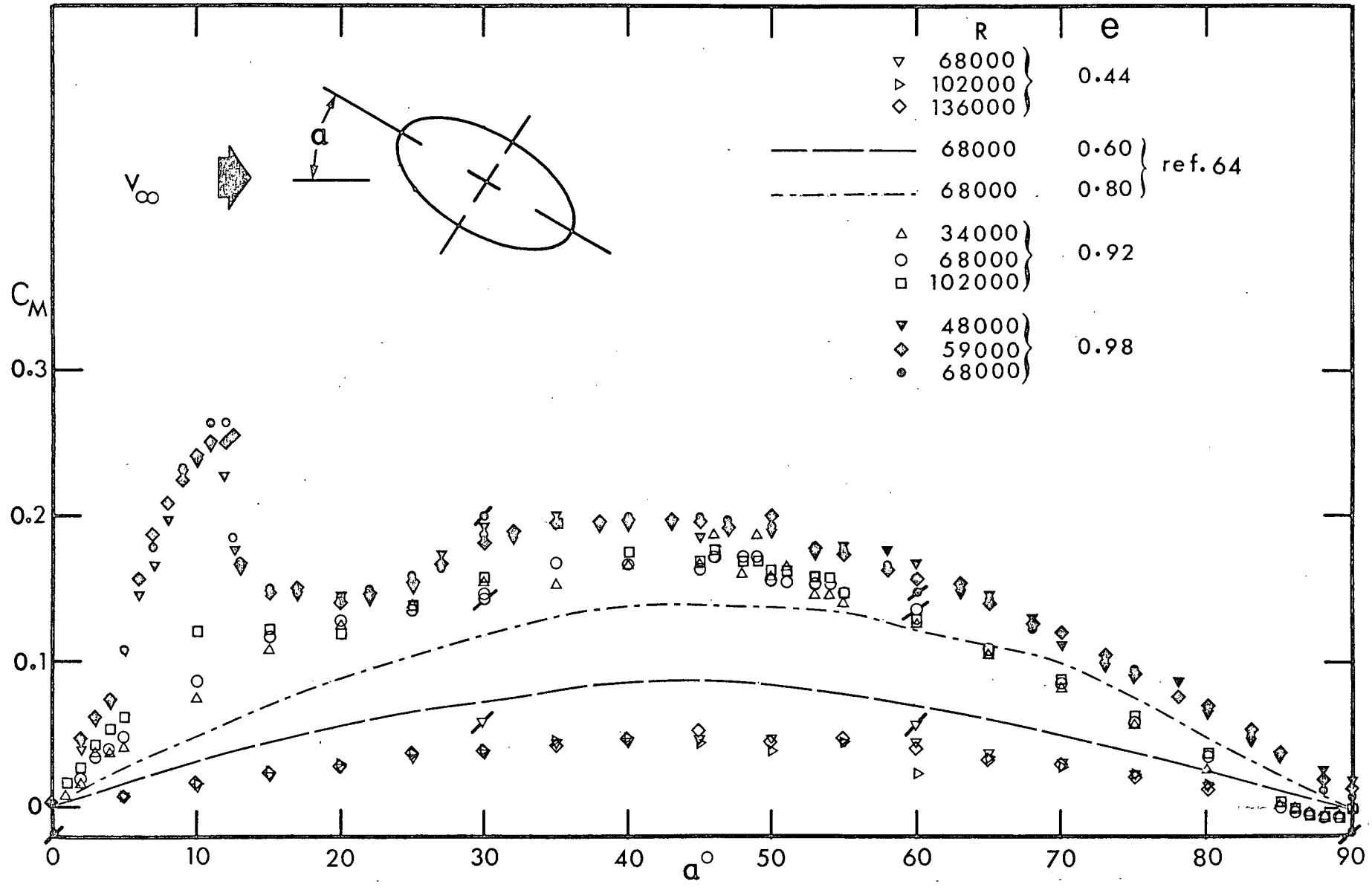

Figure 5-1 Variation of mean aerodynamic coefficients with angle of attack (symbols with slash indicate pressure integrated values): (c) Pitching moment about mid-chord

around 40°-55°. The maximum value of the mean lift for the slender ellipse of e=0.98 was found to be 1.0 which compares with the flat plate value of 1.2. It is of interest to note that α corresponding to the maximum lift increases with decreasing eccentricity ($^{\alpha}|C_{L_{max}}$ = 40°, 55° for e=∞, 0.44 respectively). On the other hand, $^{\alpha}|C_{M_{max}} \simeq 45°$ and is relatively unaffected by the cylinder eccentricity. Beyond this, lift and moment gradually decrease and vanish completely at α=90° due to symmetry.

As expected, drag coefficient increases with bluffness in the angle of attack range of 0-45°. However, in general, the trend is reversed beyond this point. The maximum drag coefficient of 2.3 for e=0.98 is slightly higher than the flat plate value of 2.12 reported by Fage and Johansen[70], probably due to wall confinement. Using the measured base pressure value for the cylinder with e=0.98 at α=90°, Roshko's[7] notched hodrograph solution predicts a value of C_D=2.62, which is somewhat higher than the balance data. The attitude of around 45° appears to play an important role in the steady state aerodynamics of the elliptic cylinders. Besides attaining the stall accompanied by the maximum rate of increase in drag, the elliptic models, irrespective of their eccentricities, offer approximately the same resistance as the circumscribing circular cylinder.

For a given ellipse, variation of the drag coefficient with angle of attack can be reduced by basing it on the projected height. However, the drag coefficient does not become completely independent of the model orientation.

It may be emphasized that such a systematic study of lift, drag and pitching moment coefficients as a function of angle of attack and eccentricity of the ellipse, though routine, has not been recorded in literature. Only available data are for ellipses at zero angle of attack as reported by Hoerner[71]. They compare quite well with the corresponding results in Figure 5-1(b).

Various other aerodynamic parameters such as flucuating pressure, Strouhal number, wake geometry, etc., were found to be substantially independent of the Reynolds number. Therefore, the results presented henceforth are for R=68,000 unless otherwise specified.

5.2 Mean Static Pressure Distribution

The mean pressure on the surface of the elliptic cylinder was found to be essentially independent of the Reynolds number over the range 2×10^4-10^5. Midspan pressure distributions for the ellipses are shown in Figure 5-2. The plots not only proved useful in the analytical determination of the separation points, but also provided data on location of front stagnation and base pressure coefficient necessary in evaluating wind tunnel wall corrections and

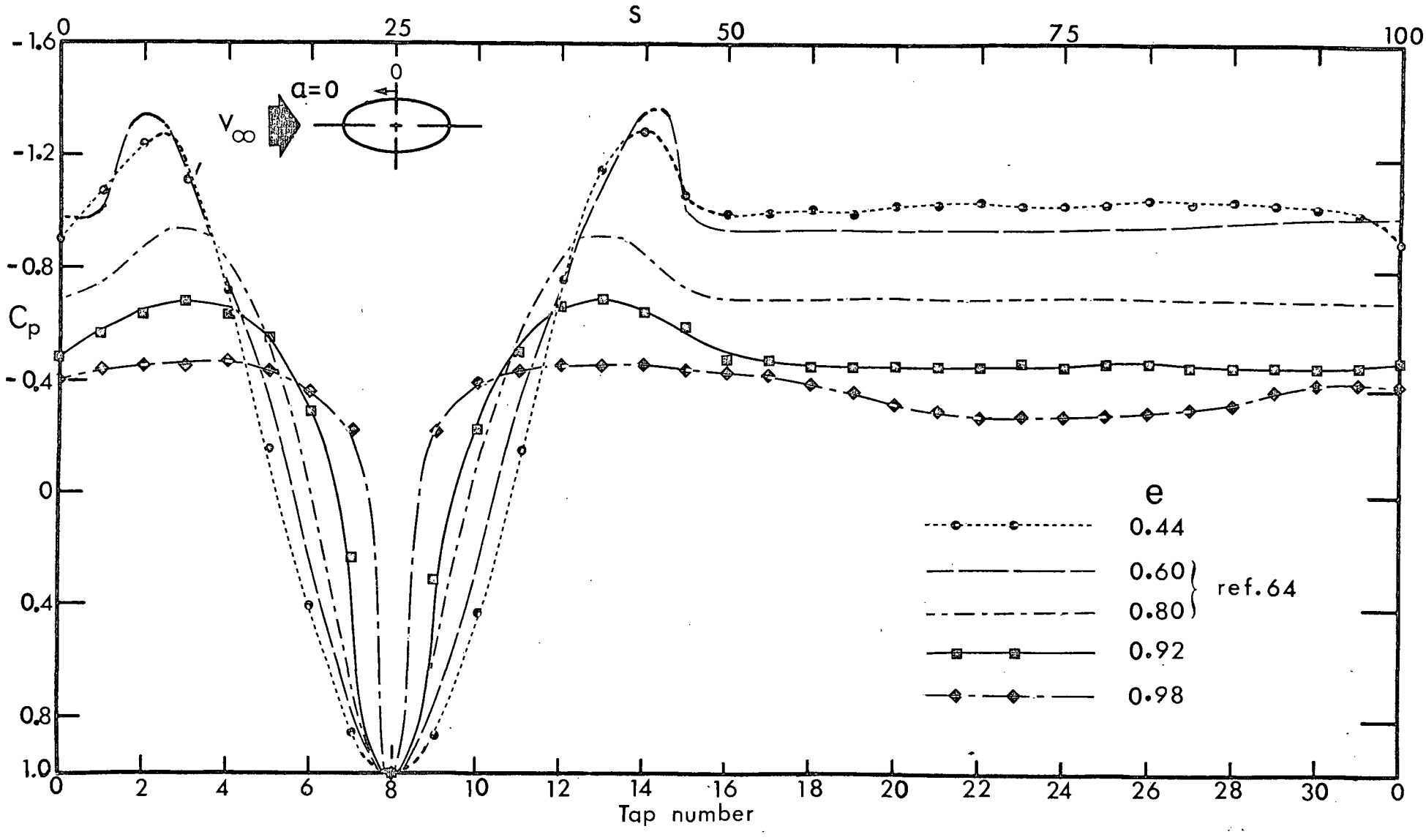

Figure 5-2 Midspan distribution of mean pressure coefficient: (a) $\alpha = 0$

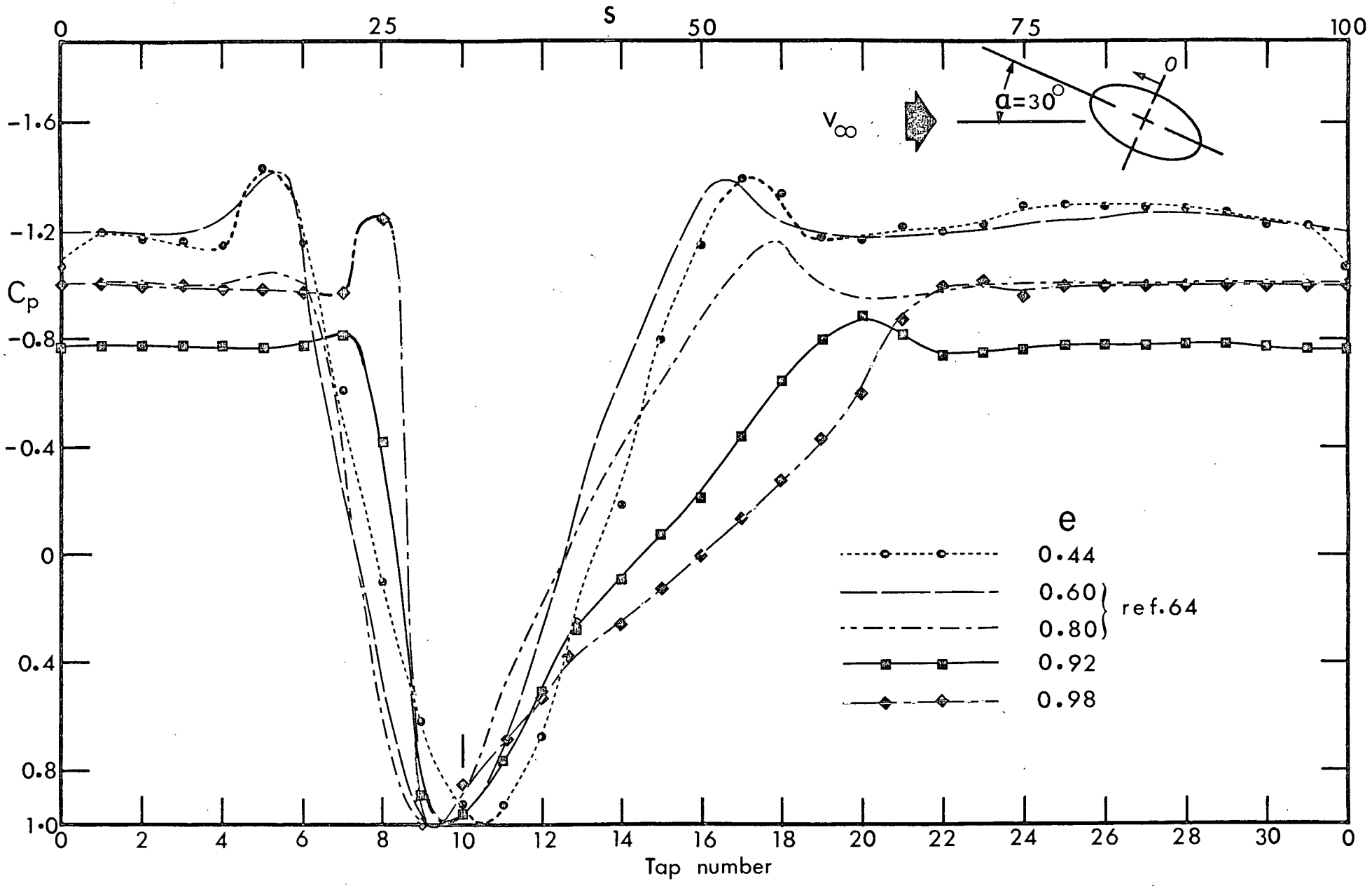

Figure 5-2 Midspan distribution of mean pressure coefficient: (b) α = 30°

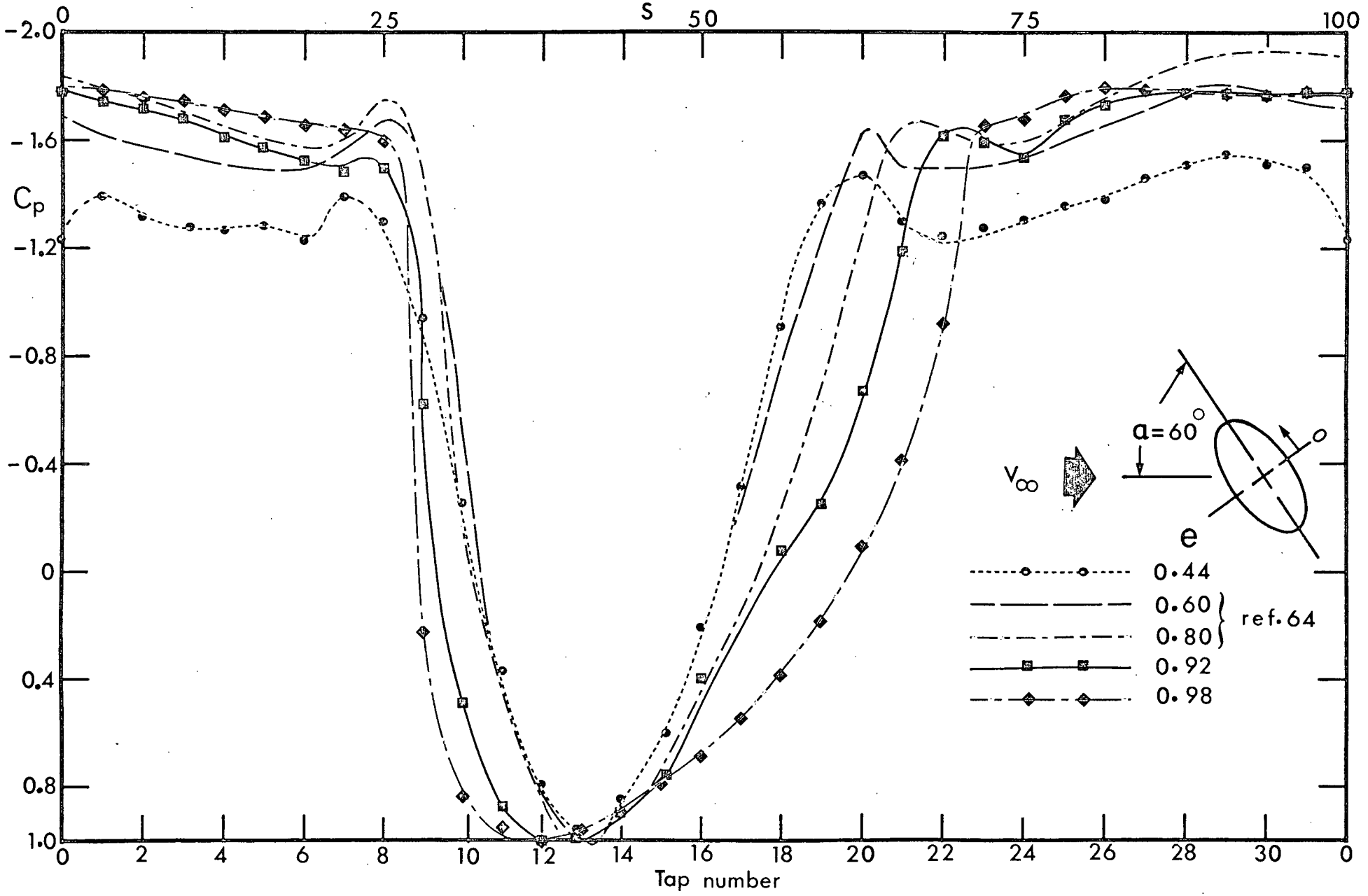

Figure 5-2 Midspan distribution of mean pressure coefficient: (c) α = 60°

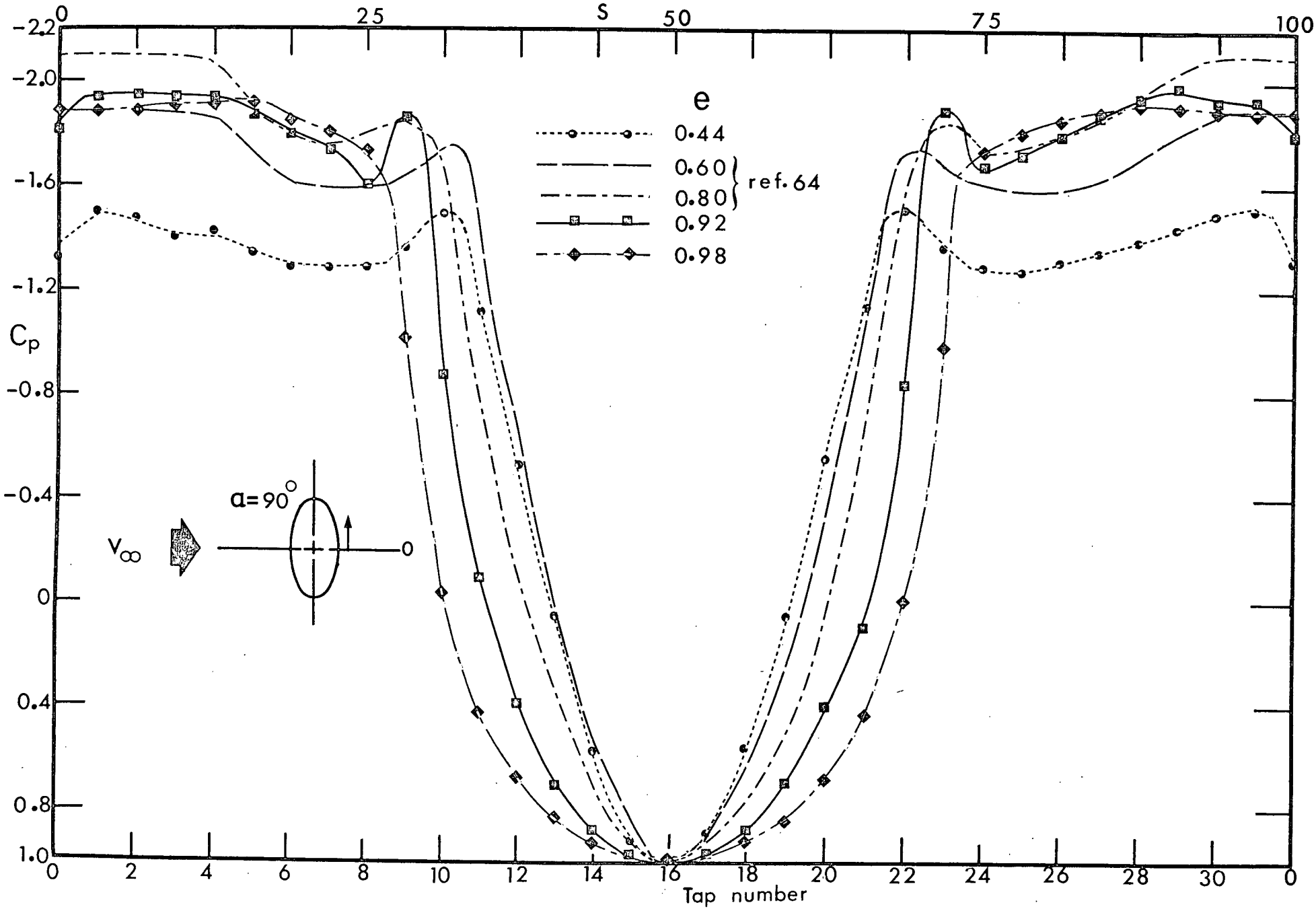

Figure 5-2 Midspan distribution of mean pressure coefficient: (d) α = 90°

separated shear layer velocity. They also served as a check on balance data.

As the flow moves downstream from the stagnation point along the contour of an ellipse, the pressure increases negatively, attaining a peak value near separation points. Beyond this, in the wake, the mean pressure remains approximately uniform. As can be expected, the pressure distribution is substantially affected by the eccentricity and angle of attack of the ellipse. However, it is of interest to note that some definite trend can be discerned.

In general, the mean pressure increases negatively with increase in angle of attack. For $\alpha=0$, the steeper change in pressure, in the immediate vicinity of the stagnation point, with increase in eccentricity may be attributed to the higher curvature of the nose. This leads to decreasing pressure with eccentricity, however, the trend is reversed following the separation as shown in Figure 5-2(a). The behaviour, though not quite well defined, appears to undergo complete reversal at higher angles of attack (Figures 5-2c,d). The transition in the trend seems to occur around 30°, where no well defined pattern can be established.

The variation of base pressure with angle of attack and eccentricity is shown in Figure 5-3. The base pressure increases with rise in eccentricity at $\alpha=0$, with the minimum value of -1.07 for $e=0^{72}$. However, this trend begins to change at higher angles of attack, and at $\alpha=90°$, the base

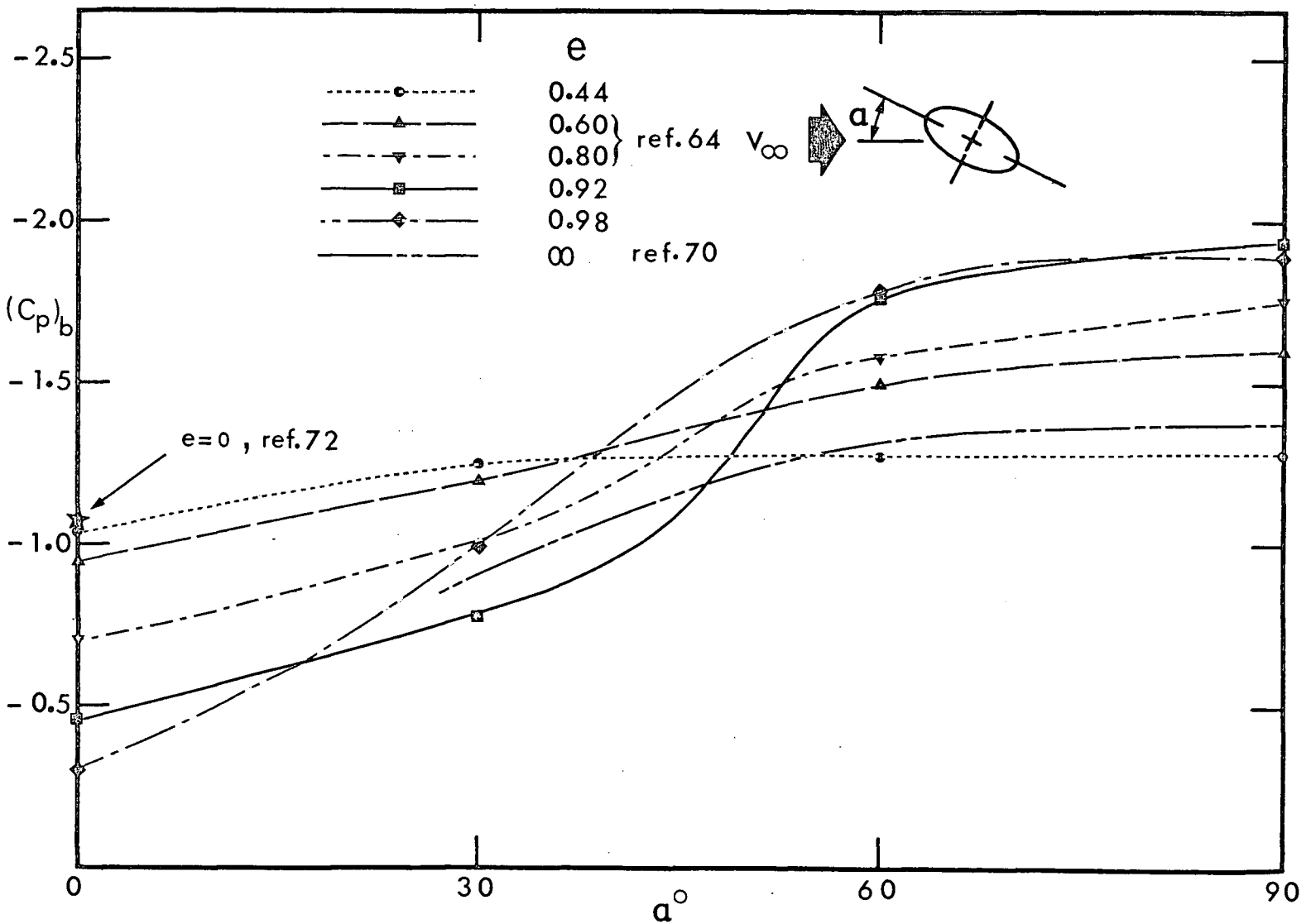

Figure 5-3 Variation of base pressure with angle of attack

pressure is more negative for the ellipses of higher eccentricities. The flat plate data shown in the diagram do not conform to this trend, probably, due to the difference in the blockage ratios for the two sets of experiments. The similarity between the base pressure and the drag coefficient curve should also be recognised.

In Figure 5-4 is shown the dependence of the minimum pressure points (approximate locations of the separation points) on cylinder eccentricity and angle of attack. For $\alpha=0$, the separation appears to occur early for slender ellipses, probably, due to small radius of curvature of the leading edge. It is evident that the minimum pressure point on the top surface moves forward, while that on the lower surface moves rearwards with increase in angle of attack, however, this trend reverses at higher attitude ($\tilde{>}40°$). The effect of increase in eccentricity at $\alpha=90°$ is to shift these points downstream.

5.3 Location of Separation Using Görtler's Method

The location of shear layer separation as indicated by minimum pressure point should be considered only qualitative. Numerous analytical methods have been reported[73], which approximately predict the mean position of separation, e.g., Blasius series method[74], Pohlhausen's approach[75], Schlichting and Ulrich's[76] extension of Pohlhausen's technique to the two dimensional case, etc.

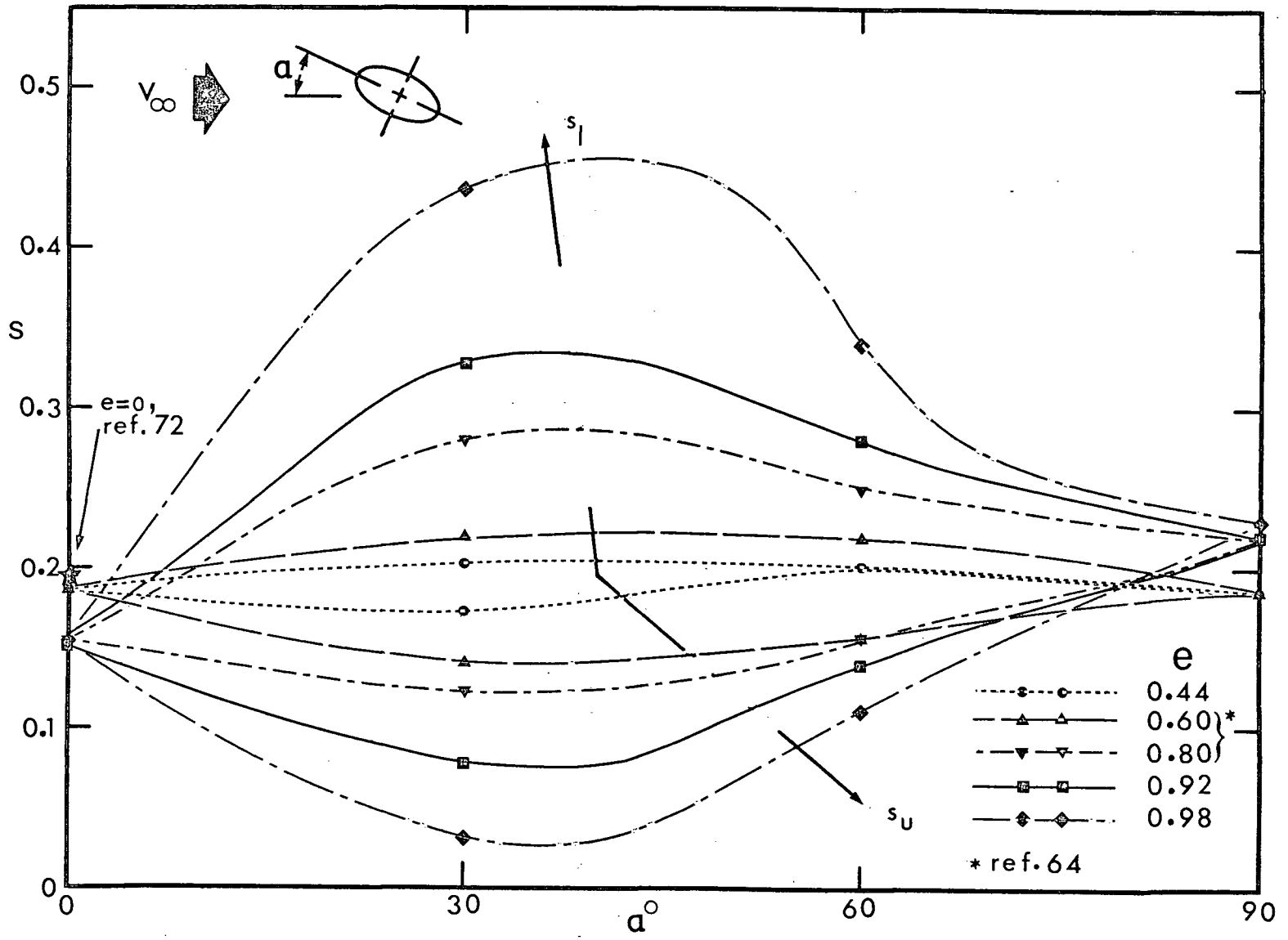

Figure 5-4 Dependence of minimum pressure location on cylinder attitude and eccentricity

However, a relatively recent method by Görtler[65] appears to be quite promising. As against the apparent limitations (use of only fourth degree polynomial by Pohlhausen, restricted application of the Blasius series to cylinders where flow starts with a stagnation point, mostly flat plate relevance of Howarth's[77] and Tani's[78] approaches, and of course, poor convergence characteristics) of the methods mentioned above, Görtler's approach represents generalisation of the available series solution technique, promises better convergence and is applicable to the bodies irrespective of the leading edge condition. This series approach, which does not involve any preferential choice of coordinates, solves the dimensionless form of the boundary layer equation

$$F_{\eta\eta\eta} + \beta(\xi)[1-(F_\eta)^2] + FF_{\eta\eta} = 2\xi(F_\eta F_{\xi\eta} - F_\xi F_{\eta\eta}) \qquad (5.1)$$

where, $\xi = \frac{1}{\nu}\int_0^X U(X)dX$

$$\eta = \frac{YU(X)}{\sqrt{2\nu\int_0^X U(X)dX}}$$

$$\psi(X,Y) = \nu\sqrt{2\xi}\ F(\xi,\eta)$$

$$\beta(X) = 2\frac{U'(X)}{\{U(X)\}^2}\int_0^X U(X)dX$$

As influence of the body geometry appears in the equation through β, Görtler referred to it as the "Principal Function." Using measured pressure distribution, the potential flow field was represented by a series leading to the determination of the coefficient in the principal function expansion. Furthermore, representing dimensionless stream function $F(\xi,\eta)$ in terms of universal functional coefficients lead to the shear stress expression

$$\tau(X) = \frac{\rho U^2(X)}{\sqrt{2\xi}} F_{\eta\eta}(\xi,0) \qquad (5.2)$$

The separation results obtained using Görtler series approach are shown in Table 5-1. The method appears to work quite well for the ellipse of e=0.44 over the entire range of angles of attack. However, for higher eccentricity ellipses, it could be applied only at α=0. The failure of the method at higher attitudes may be attributed to the poor convergence of the polynomial representing potential velocity distribution.

5.4 Separation Study Using Flow-Visualisation

To better appreciate the character of separation, its visual study using semi-focussing Schlieren system[79,80] was undertaken. An open circuit wind tunnel with 6 in. x 12 in. test section with a maximum speed of 20 fps was used for the purpose. The models used were so proportioned

as to provide the blockage condition identical to that observed during the test in the main tunnel. The Reynolds number during this study was typically 20,000. The required density gradient was obtained through streaklines of low density air introduced by placing a heated probe (Nichrome V wires of 0.010 in. diameter) upstream of the model. The position of the probe was adjusted with respect to the model such that the streaklines were close to the region of separating shear layers. The flow patterns were photographed using 35 mm. still (Ashahi Pentax SP) and 16 mm. high speed movie (HYCAM K30S1) cameras.

To provide some indication as to the proper working of the instrumentation, the well known case of flow around circular cylinder was photographed (Figure 5-5). The separation point was found to be at approximately 80°, which is in fair agreement with the accepted value of 82° as obtained by Hiemenz[58]. The Schlieren photographs showing the character of separation as a function of cylinder eccentricity and angle of attack are shown in Figure 5-6. The mean locations of the separating shear layers as obtained through flow visualisation are compared with the corresponding analytical data and experimentally obtained minimum pressure points in Table 5-1. Pertinent results from literature are also included for comparison.

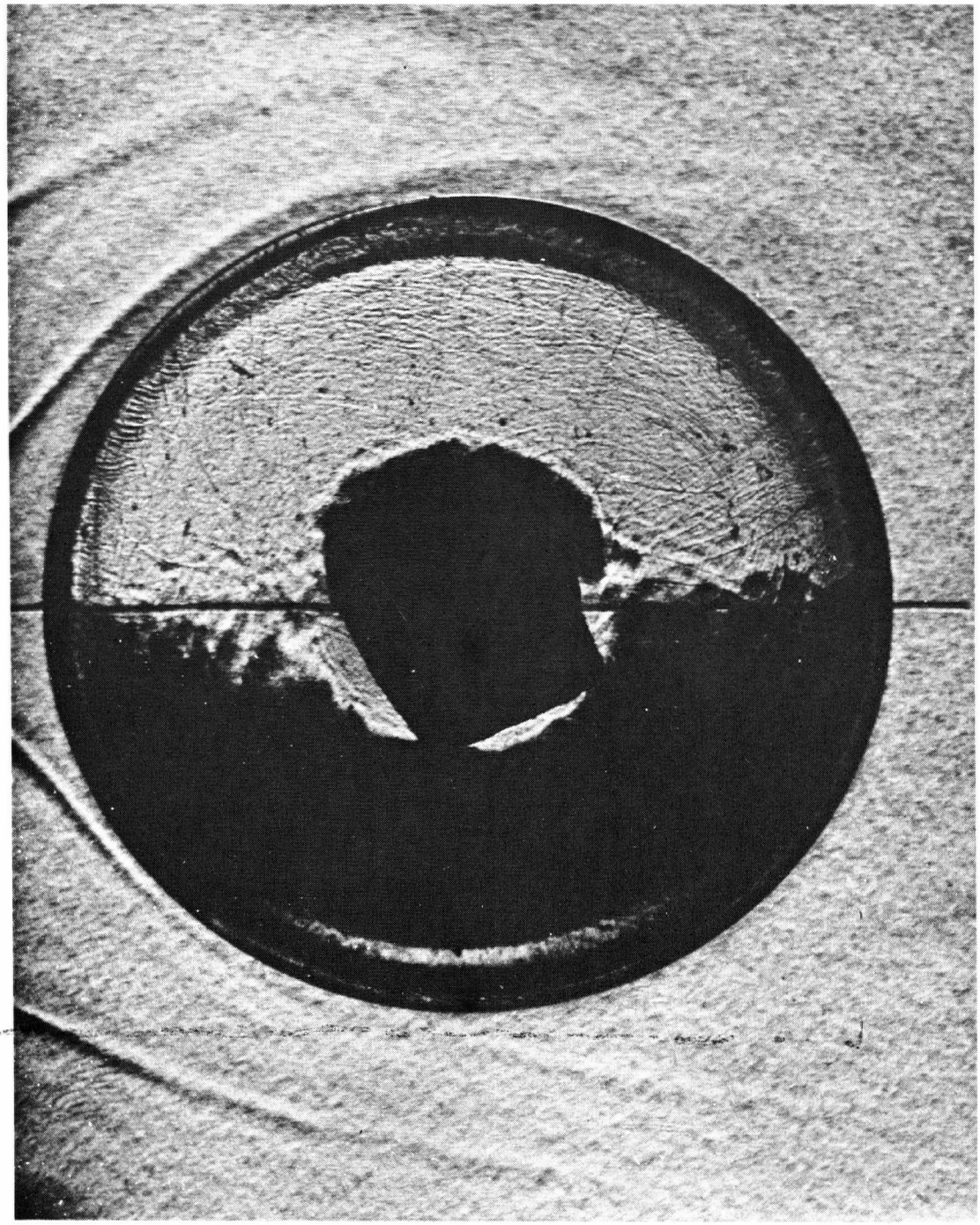

Figure 5-5 Schlieren photograph of flow around a circular cylinder, R = 17,000

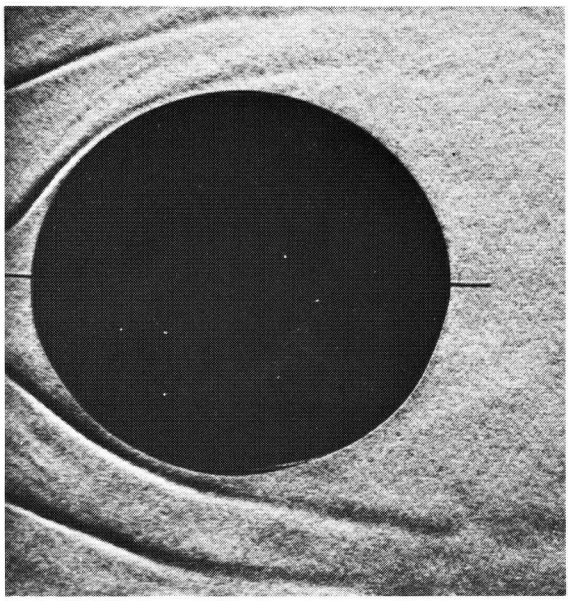

$\alpha = 0^{\circ}$
$S = 0.21$

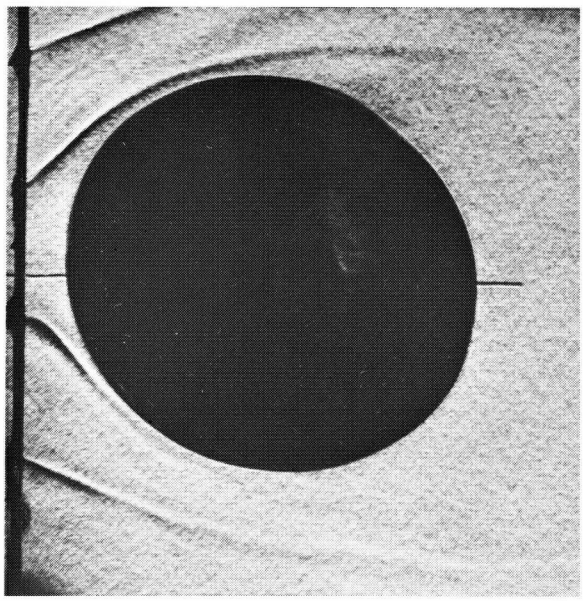

$\alpha = 30^{\circ}$
$S_u = 0.21$; $S_l = 0.21$

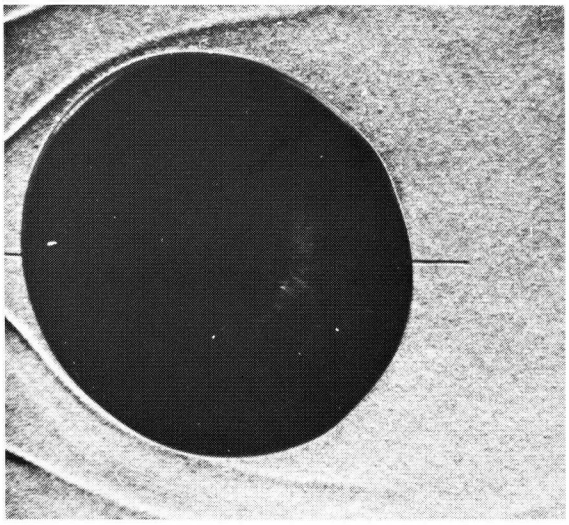

$\alpha = 60^{\circ}$
$S_u = 0.19$; $S_l = 0.24$

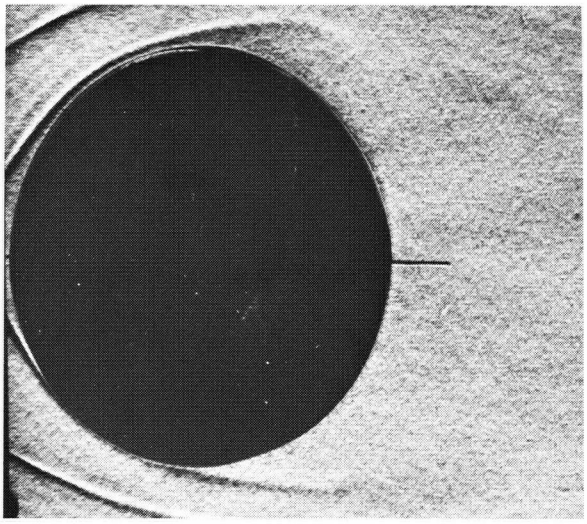

$\alpha = 90^{\circ}$
$S = 0.23$

Figure 5-6 Schlieren study of laminar separation on elliptic cylinders:
(a) e = 0.44

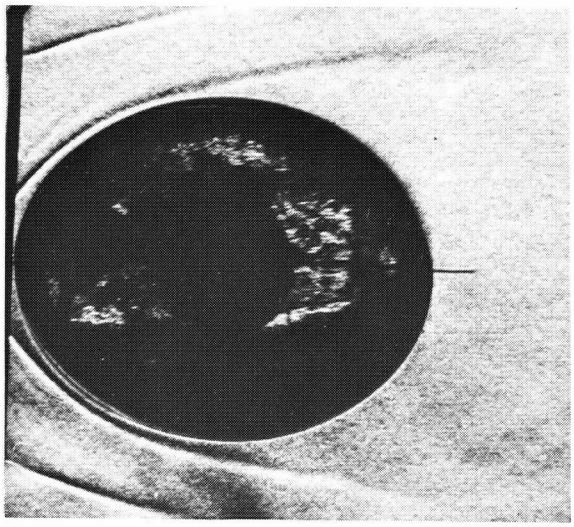

$\alpha = 0^{\circ}$
$s = 0.22$

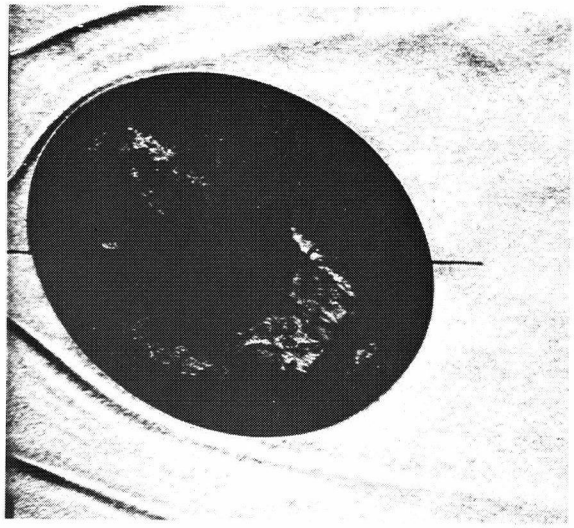

$\alpha = 30^{\circ}$
$s_u = 0.16$; $s_l = 0.29$

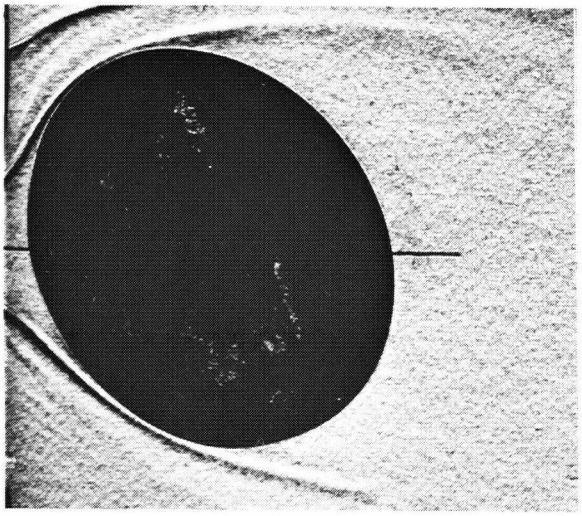

$\alpha = 60^{\circ}$
$s_u = 0.19$; $s_l = 0.25$

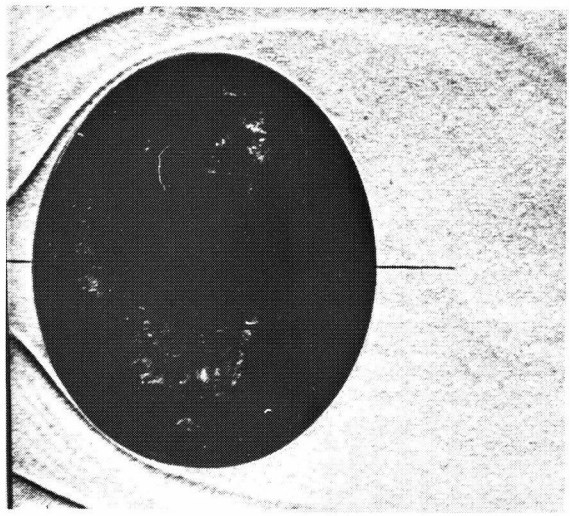

$\alpha = 90^{\circ}$
$s = 0.22$

Figure 5-6 Schlieren study of laminar separation on elliptic cylinders:
(b) e = 0.60

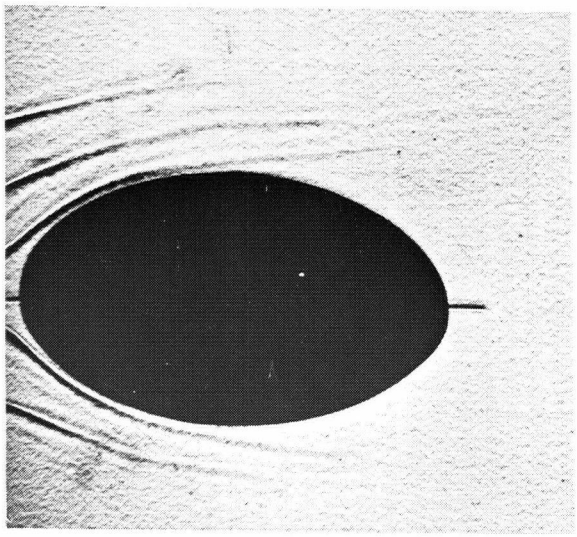

$\alpha = 0^{\circ}$
$S = 0.22$

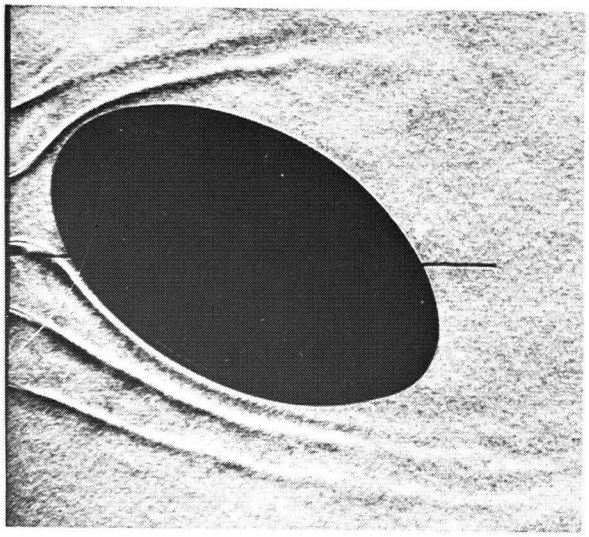

$\alpha = 30^{\circ}$
$S_u = 0.12; S_l = 0.31$

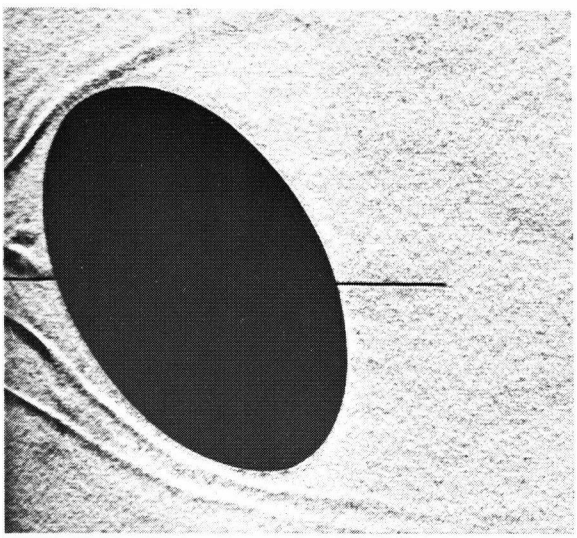

$\alpha = 60^{\circ}$
$S_u = 0.16; S_l = 0.27$

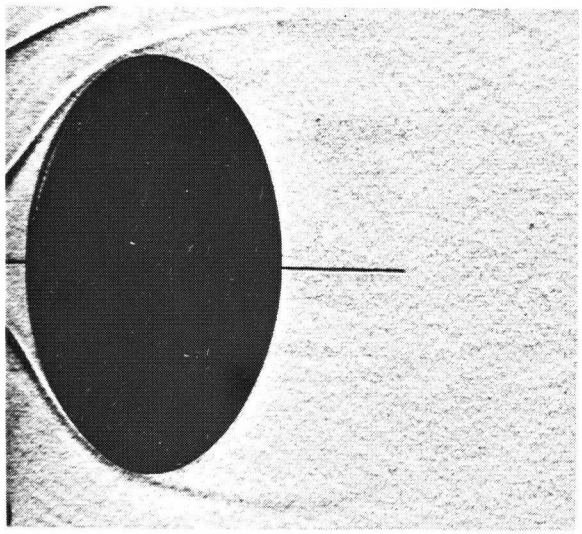

$\alpha = 90^{\circ}$
$S = 0.23$

Figure 5-6 Schlieren study of laminar separation on elliptic cylinders:
(c) e = 0.80

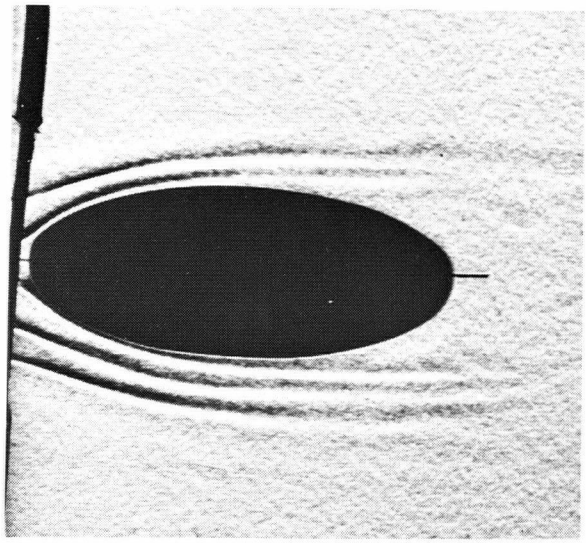

$\alpha = 0^{\circ}$
$S = 0.18$

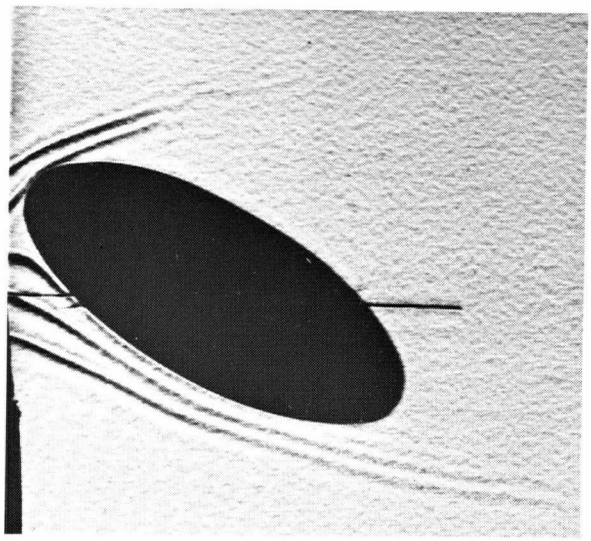

$\alpha = 30^{\circ}$
$S_u = 0.08\ ;\ S_l = 0.33$

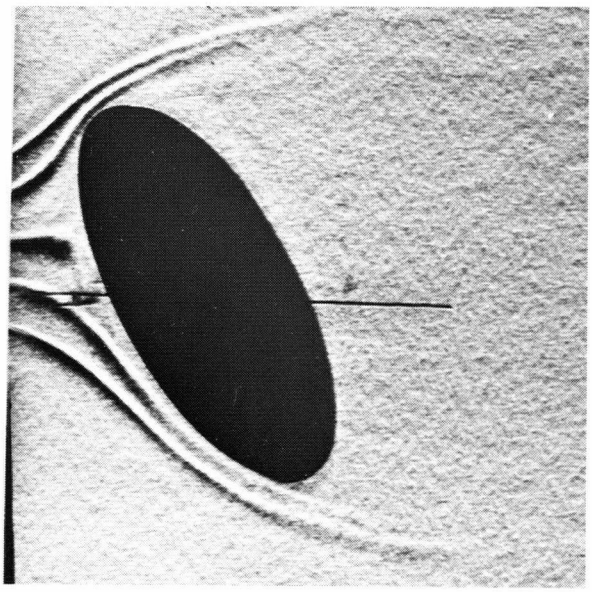

$\alpha = 60^{\circ}$
$S_u = 0.15;\ S_l = 0.31$

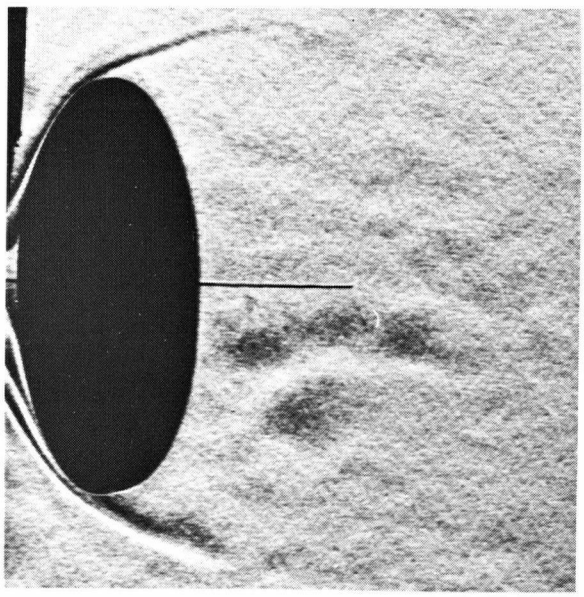

$\alpha = 90^{\circ}$
$S = 0.23$

Figure 5-6 Schlieren study of laminar separation on elliptic cylinders:
(d) e = 0.92

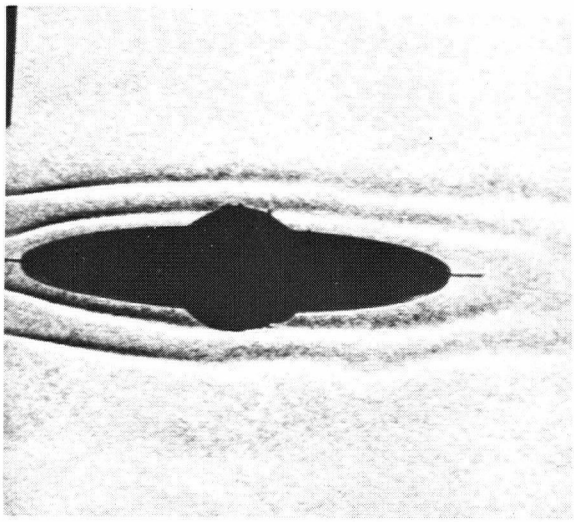

$\alpha = 0^{\circ}$

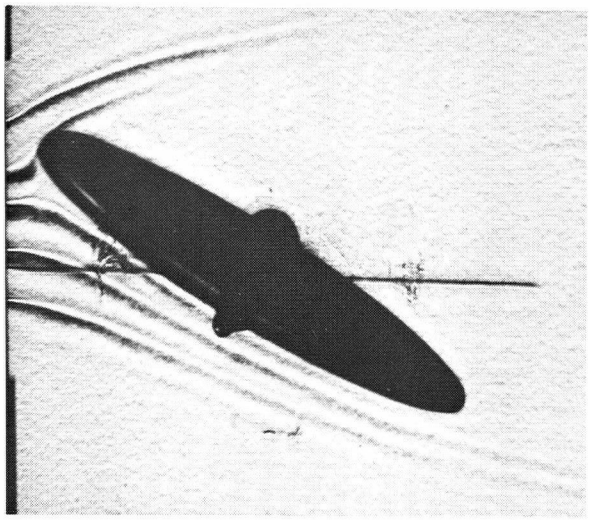

$\alpha = 30^{\circ}$
$S_u = 0.05 ; S_l = 0.44$

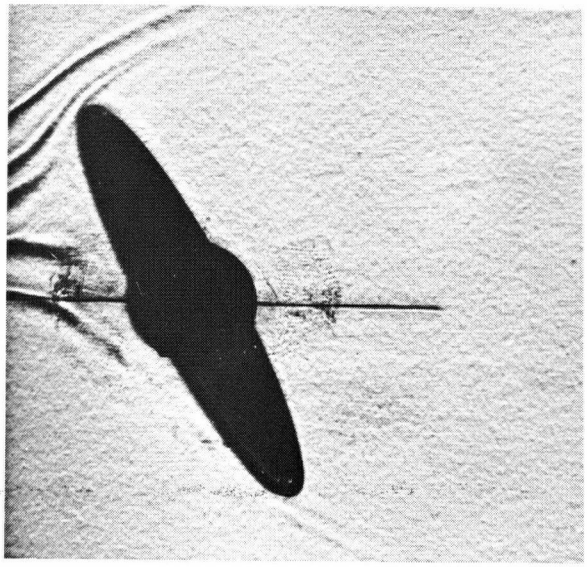

$\alpha = 60^{\circ}$
$S_u = 0.12 ; S_l = 0.35$

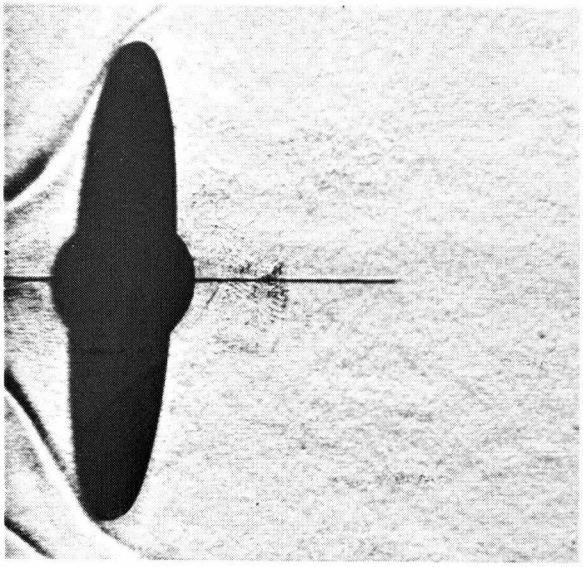

$\alpha = 90^{\circ}$
$S = 0.22$

Figure 5-6 Schlieren study of laminar separation on elliptic cylinders:
(e) e = 0.98

Table 5-1 Comparison of analytically determined separation points and those obtained experimentally

e	α°	Position of minimum pressure point		Analytically determined separation values		Experimental Values	
		S_u	S_l	S_u	S_l	S_u	S_l
0	0	*0.19 **0.20		*0.23 ***0.23 §0.23 †0.30		*0.23	
0.44	0	0.19		0.23		0.21	
	30	0.17	0.20	0.19	0.24	0.21	0.21
	60	0.20	0.20	0.23	0.24	0.19	0.24
	90	0.19		0.25		0.23	
0.60	0	0.20		0.24		0.22	
	30	0.14	0.22			0.16	0.29
	60	0.16	0.22			0.19	0.25
	90	0.19				0.22	
0.80	0	0.16		0.20		0.22	
	30	0.11	0.28			0.12	0.31
	60	0.16	0.25			0.16	0.27
	90	0.22				0.23	
†0.87	0			0.36			
0.92	0	0.16		0.20		0.18	
	30	0.08	0.32			0.08	0.33
	60	0.14	0.28			0.15	0.31
	90	0.22				0.23	
Δ0.94	0	0.19		∇0.29		0.28	
0.97	0			0.42			
0.98	0	0.16		0.21		(?)	
	30	0.03	0.44			0.05	0.44
	60	0.11	0.34			0.12	0.35
	90	0.23				0.22	
†0.998	0			0.46			

*Hiemenz[58], **Flachsbart[72], ***Pohlhausen[75], §Gortler[65], †Schlichting and Ulrich[76], ΔSchubauer[82], ∇Meksyn[81]

In general, the agreement between the analytical and experimental data appears to be quite acceptable. As can be expected, the separation occurs downstream of the minimum pressure positions, however, the difference in their locations appears to diminish with increase in eccentricity. Based on the trend, suggested by the results, concerning the dependence of shear layer separation on the cylinder eccentricity and angle of attack, the following observations can be made:

(i) At α=0 and e in the range of 0-0.80, the location of the separation (s) is substantially independent of cylinder eccentricity, variations being less than 5% around the circular cylinder value. However, for slender ellipses with e greater than 0.80, the separation points move considerably forward. This is in agreement with the observation concerning movement of the minimum pressure points made earlier. It may be pointed out that the analytical results of Schlichting and Ulrich[76] and Schubauer[82] do not confirm to this trend.

(ii) As suggested by the experimental results, the effect of increase in angle of attack, up to a critical value, is to move the lower separation point rearwards and upper separation point forward. However, any further increase in α beyond

the critical value reverses this trend. The critical attitude for all ellipses was observed to be in the range α=30°- 60°.

(iii) At α=30°, 60°, the separation of shear layer from the lower surface tends to move downstream, while that from the upper surface shifts forward with increase in eccentricity.

(iv) In general, at α=90° the location of separation points is relatively independent of eccentricity.

5.5 Strouhal Number

The vortex shedding frequency was measured in the Reynolds number range of 2×10^4-10^5 with the systematic variation in angle of attack. It was observed to vary linearly with increasing wind speed thus indicating independence of the Strouhal number over the Reynolds number range investigated.

Figure 5-7(a) shows the variation of Strouhal number, based on minor axis of the model, as a function of angle of attack. In general, S_{2b} decreases with increase in angle of attack, the drop being more pronounced in the range α=0-50° for the ellipses of high eccentricities. It may be attributed to the fact that high eccentricity ellipses at low angles of attack essentially behave as slender bodies shedding vortices at high frequency. However, at

higher angles of attack, bluff body character predominates leading to the almost uniform Strouhal number. This, together with increase in the Strouhal number with reduction in eccentricity at higher angles of attack ($\alpha \geq 20°$), suggests that basing the dimensionless frequency parameter on projected height h may minimize its dependence on bluffness. It is apparent from Figure 5-7(b) that, in most cases, the Strouhal number is confined to the range 0.18-0.22 irrespective of the eccentricity and angle of attack. It may be pointed out that the test results, being uncorrected for blockage, are somewhat higher than the nearly unconfined flat plate values as given by Fage and Johansen[70]. For the slender ellipse of e=0.98 at small angles of attack ($\alpha < 12°$) no reliable Strouhal data could be obtained due to minute pressure fluctuations and poor response characteristics of the instrumentation in the higher frequency range.

It was decided to explore applicability of Roshko's universal Strouhal number[8], S_R, based on wake width and shear layer separation velocity. The variation of S_R, based on measured minimum base pressure, wake geometry and shedding frequency, with angle of attack and eccentricity is shown in Figure 5-7(c). In general, the results collapsed around the universal value of 0.164 except for the slender ellipses of e=0.92, 0.98 at small angles of attack. Here, as pointed out by Roshko, the theory does not apply directly

probably due to the difference in the history of the boundary layer development.

The dependence of Strouhal number on cylinder bluffness can be minimized further by relating it to the boundary layer separation conditions. Figure 5-7(d) shows the variation of S_S based on transverse distance between separation points and velocity at the outer edge of the boundary layer around the separation point. Although the possibility of collapsing the data on a single curve appears to be remote, this manner of representation reduces the excursion of data with bluffness, even at high eccentricities, as compared to Roshko's approach.

The Strouhal number results can be summarised conveniently, as indicated in Figure 5-8. For clarity only results corresponding to the extreme attitudes of the model (α=0,90°) are included. It is apparent that up to e=0.80 the criterion based on projected height fares quite well. However, for larger eccentricity cylinders, Strouhal number based on separation points shows smoother trend at α=0 and is relatively uniform at α=90°.

5.6 Fluctuating Pressure Distribution

Midspan fluctuating pressure measurements were made for α=0, 30°, 60° and 90.° To determine the dependence of fluctuating pressure on the Reynolds number, the latter was varied from 2.5×10^4-10^5. To better reflect the character

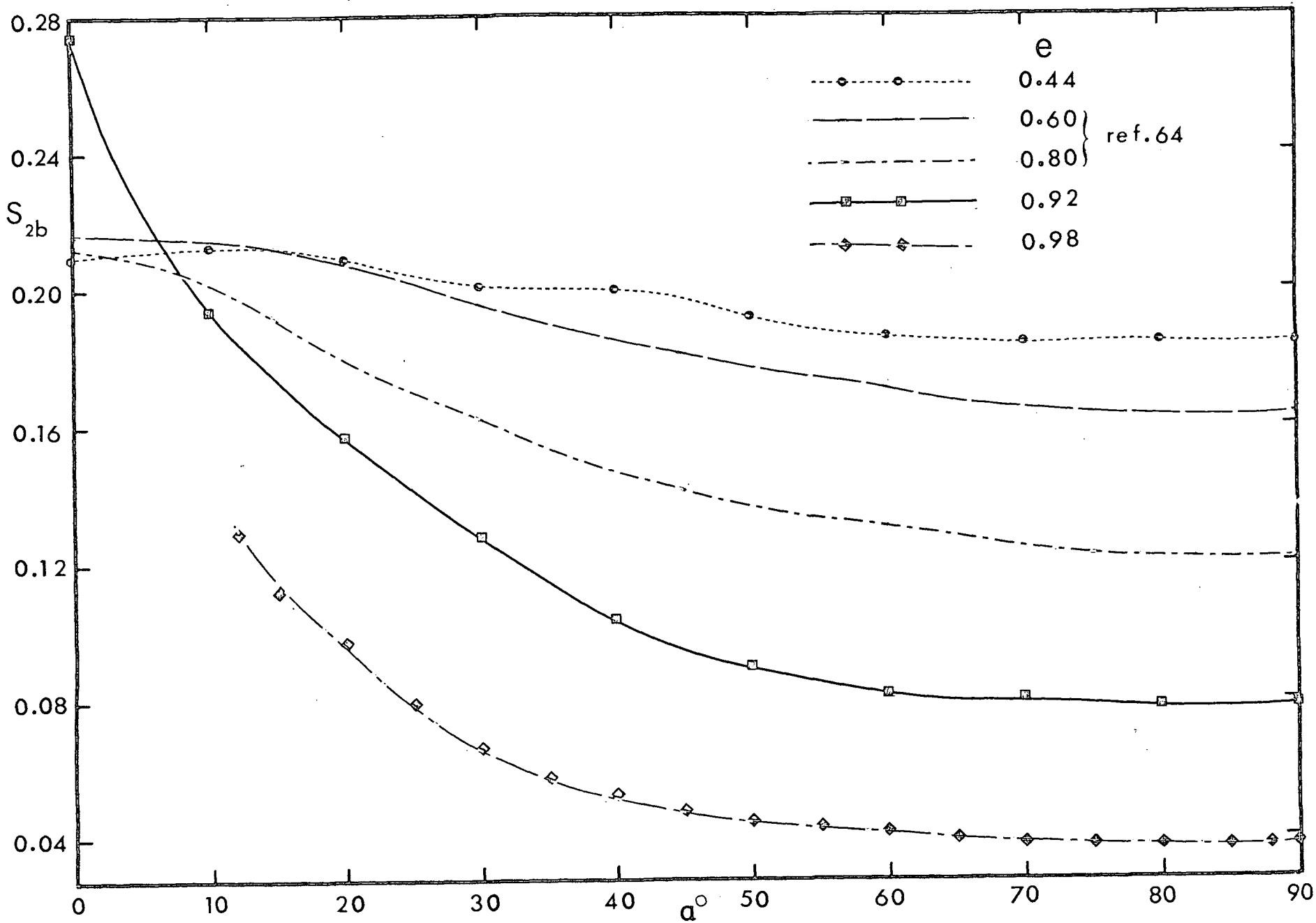

Figure 5-7 Variation of Strouhal number with angle of attack and eccentricity as based on: (a) minor axis of ellipse

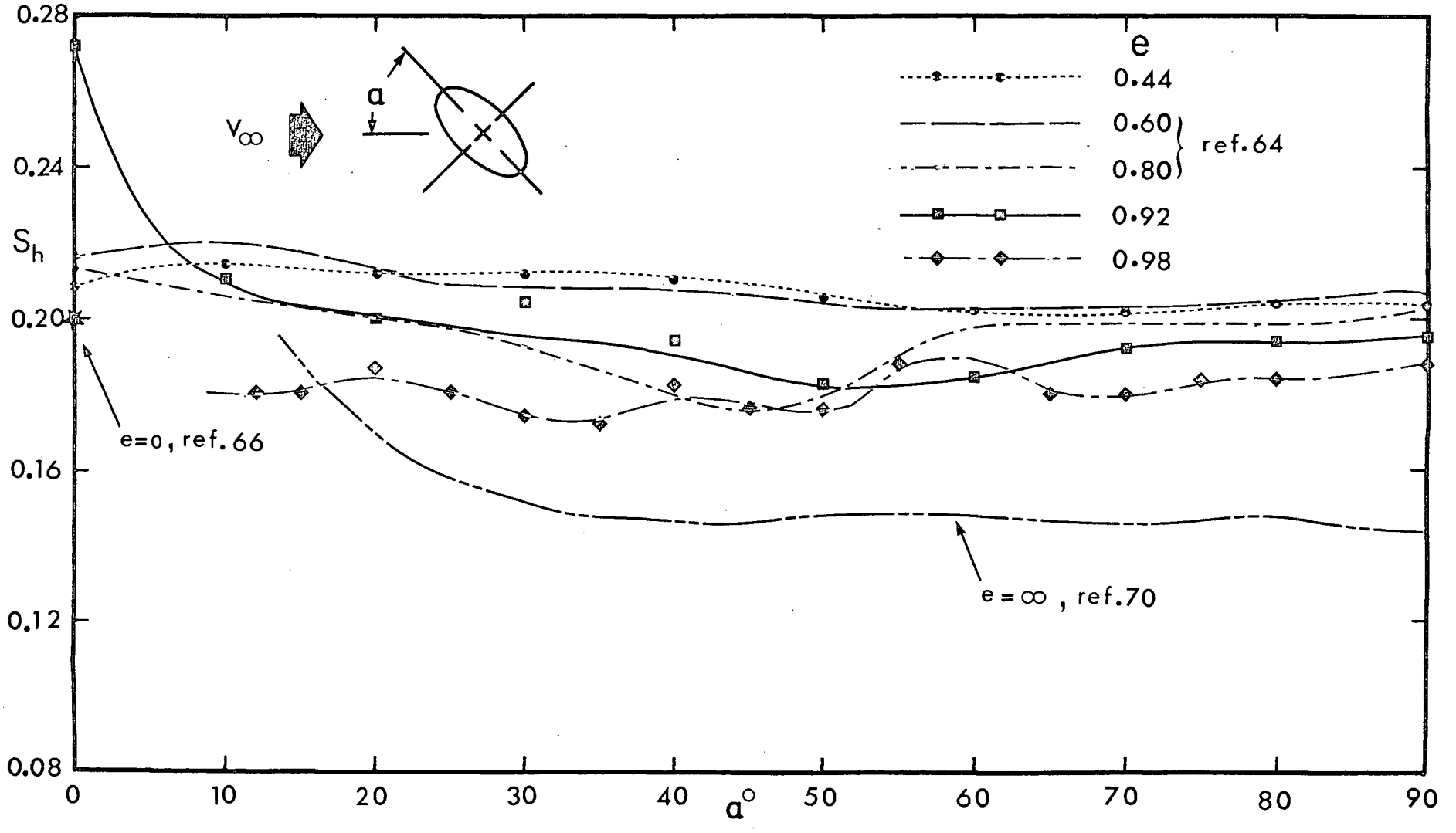

Figure 5-7 Variation of Strouhal number with angle of attack and eccentricity as based on: (b) projected dimension

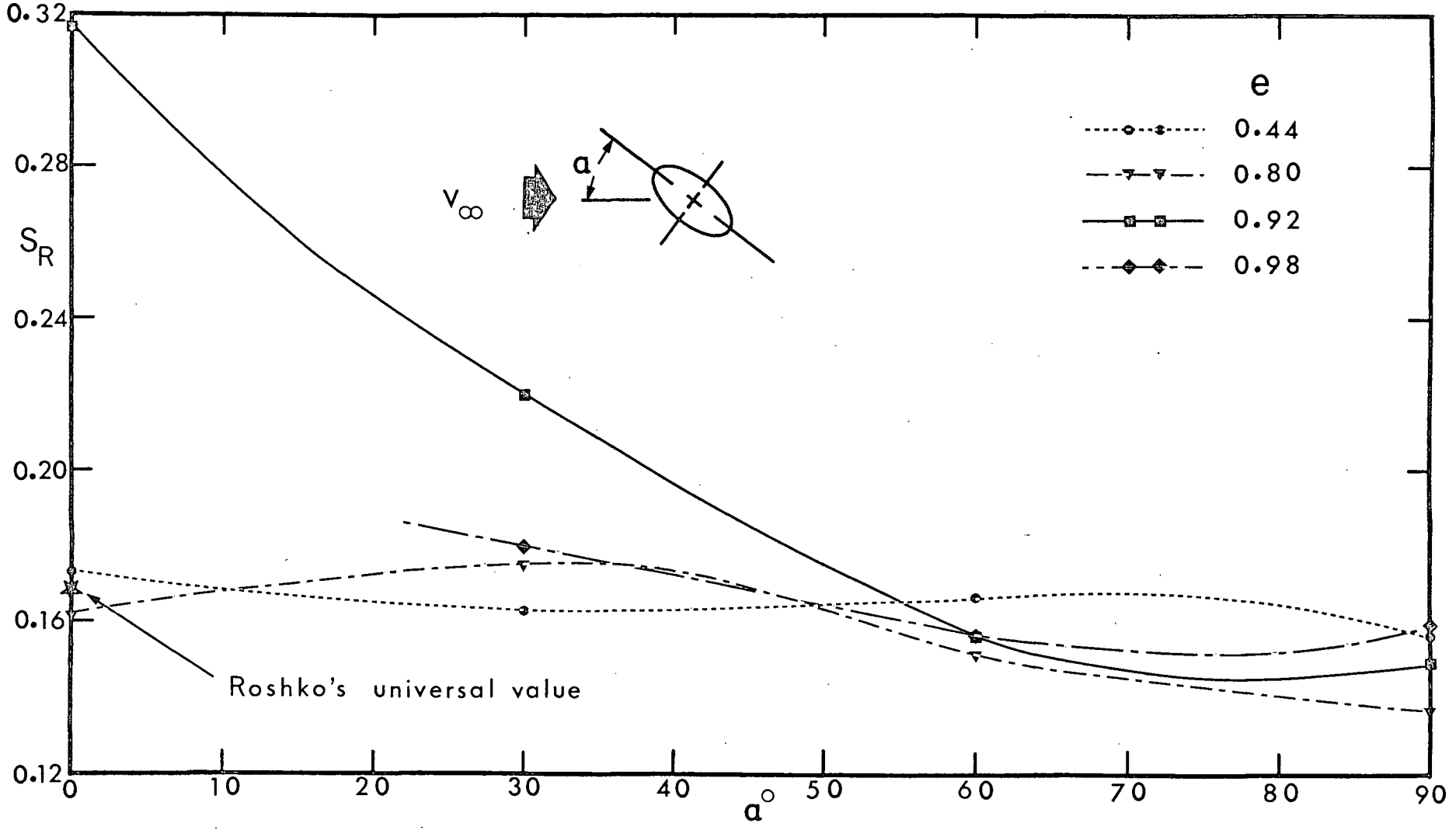

Figure 5-7 Variation of Strouhal number with angle of attack and eccentricity as based on: (c) Roshko's criterion

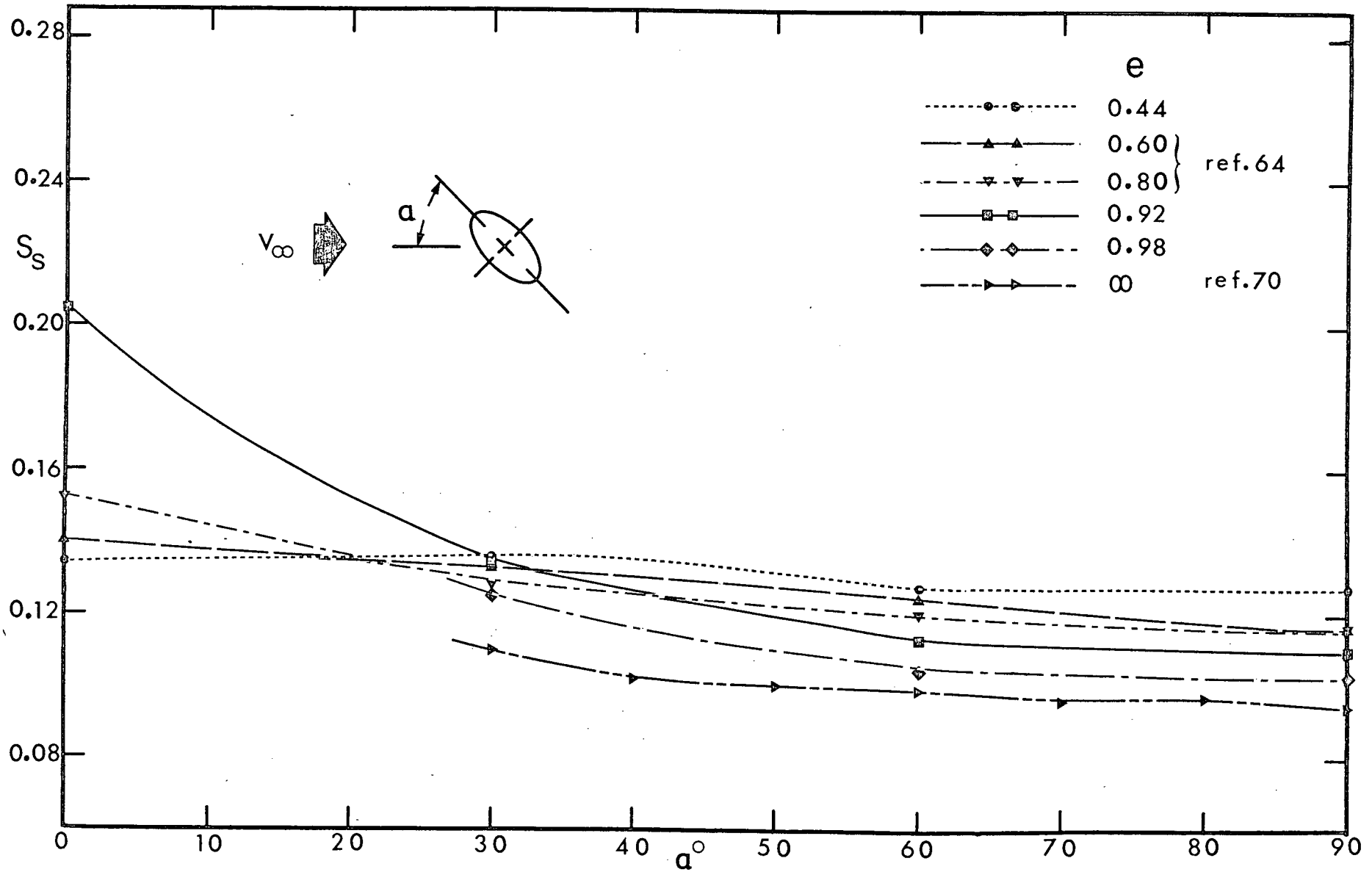

Figure 5-7 Variation of Strouhal number with angle of attack and eccentricity as based on: (d) transverse distance between separation points

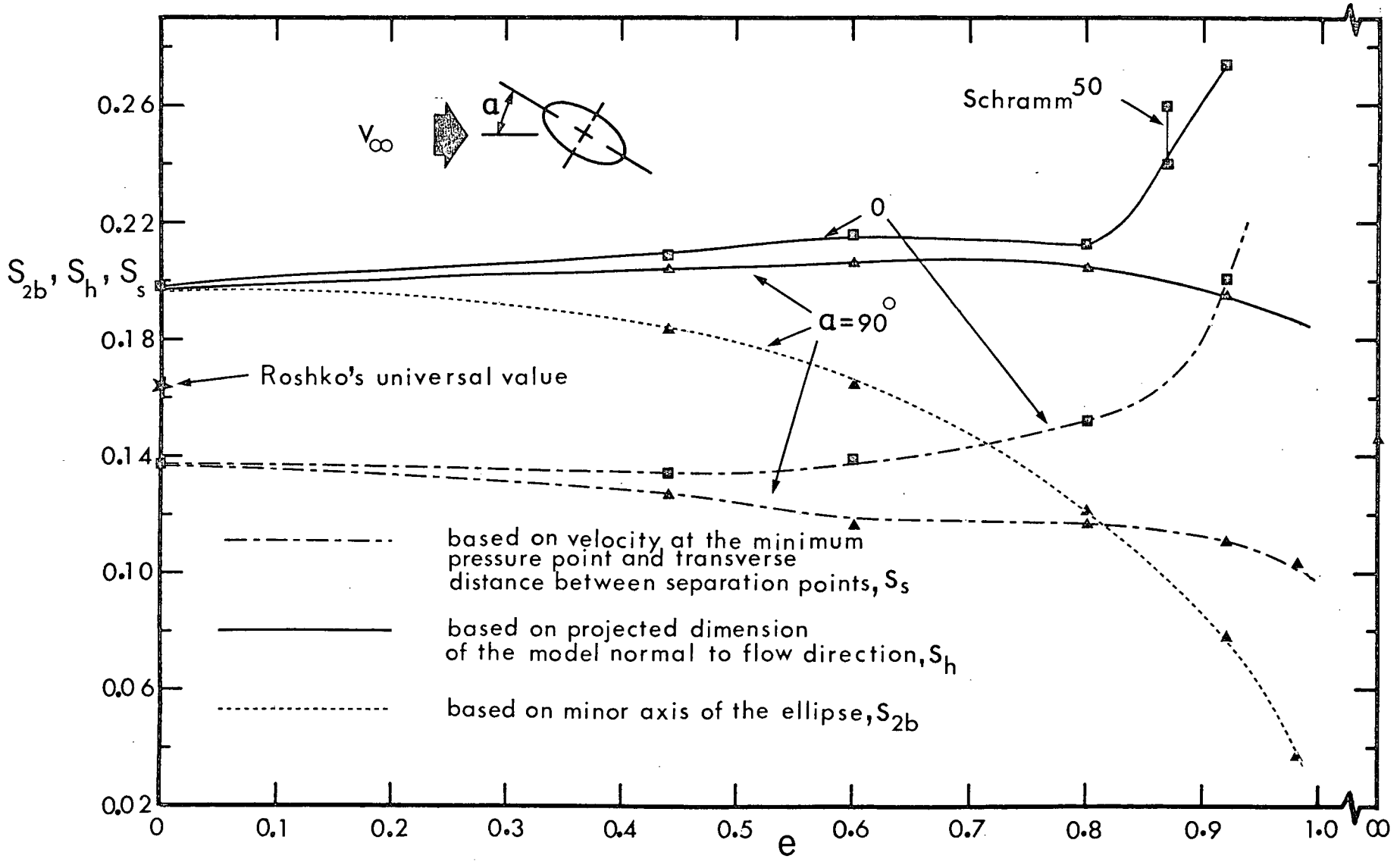

Figure 5-8 Strouhal number as a function of eccentricity of the ellipse at extreme attitudes

of the flow four taps were used, two in the laminar and two in the separated flow regions. The Reynolds number dependency was conveniently expressed as a percentage variation of the fluctuating pressure about a mean value at a tap in question. The selection of the points depended on the location of the separation and hence varied with cylinder eccentricity and attitude. The pressure taps used are tabulated below and the Reynolds number dependency of unsteady pressure is indicated in Figure 5-9.

Table 5-2 Positions of the pressure taps used in the study of fluctuating pressure dependency on the Reynolds number

e \ α	0°	30°	60°	90°
0.44	*L-5,11 *S-21,28	L-8,12 S-20,31	L-11,16 S-20,28	L-13,14 S-3,4
0.92	L-5,11 S-22,26	L-7,13 S-0,4	L-10,18 S-2,24	L-11,21 S-6,26
0.98	no well de- fined signal	L-19,20 S-4,5	L-18,19 S-4,5	L-12,20 S-5,27

* L and S refer to the taps located in laminar and separated regions, respectively.

No significant Reynolds number dependency was noticed except for the ellipses at zero angle of attack. Modi and Wiland[57] also observed similar behavior during the test with elliptic cylinders of e=0.60, 0.80. For comparison

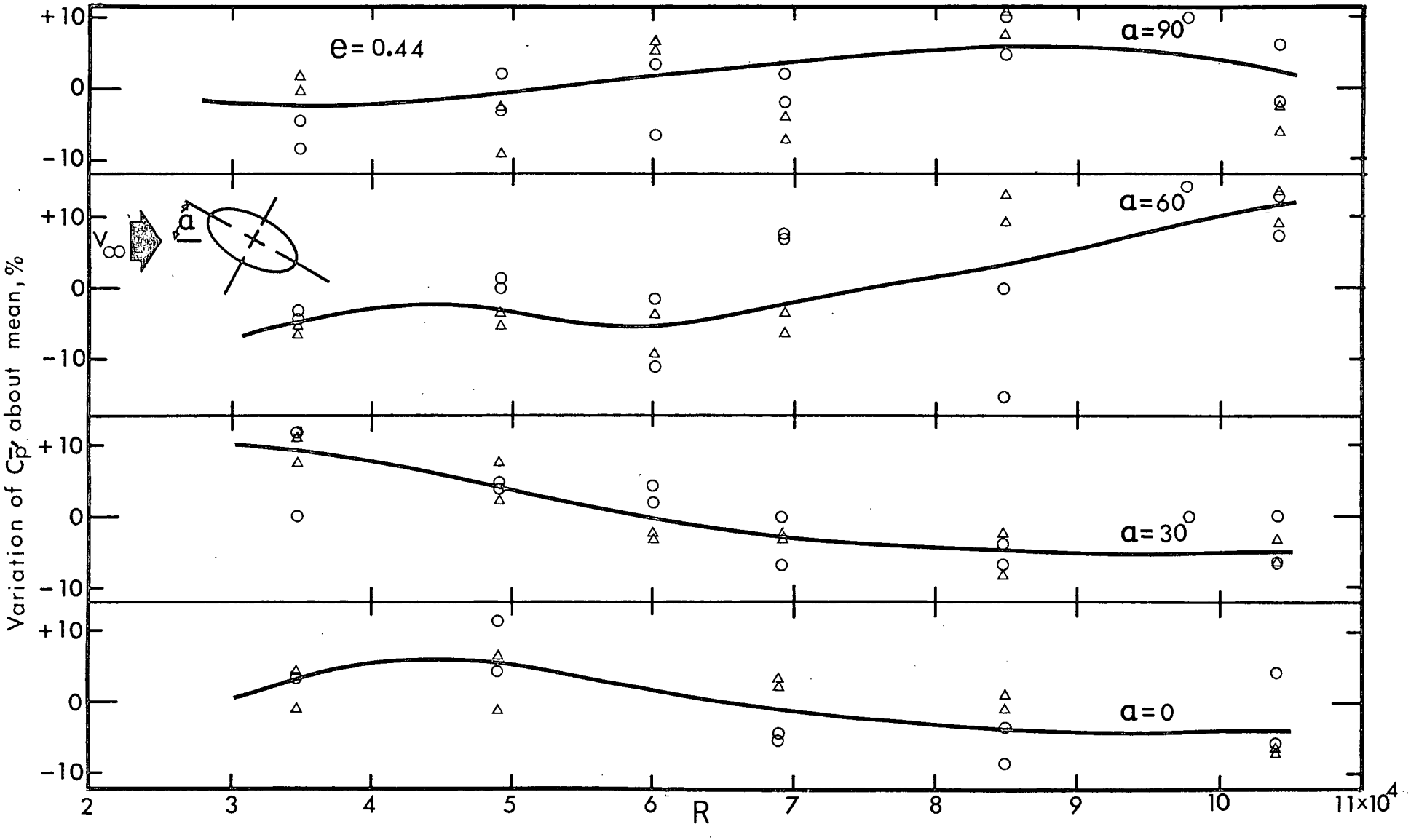

Figure 5-9 Variation of fluctuating pressure coefficient with Reynolds number: (a) e = 0.44

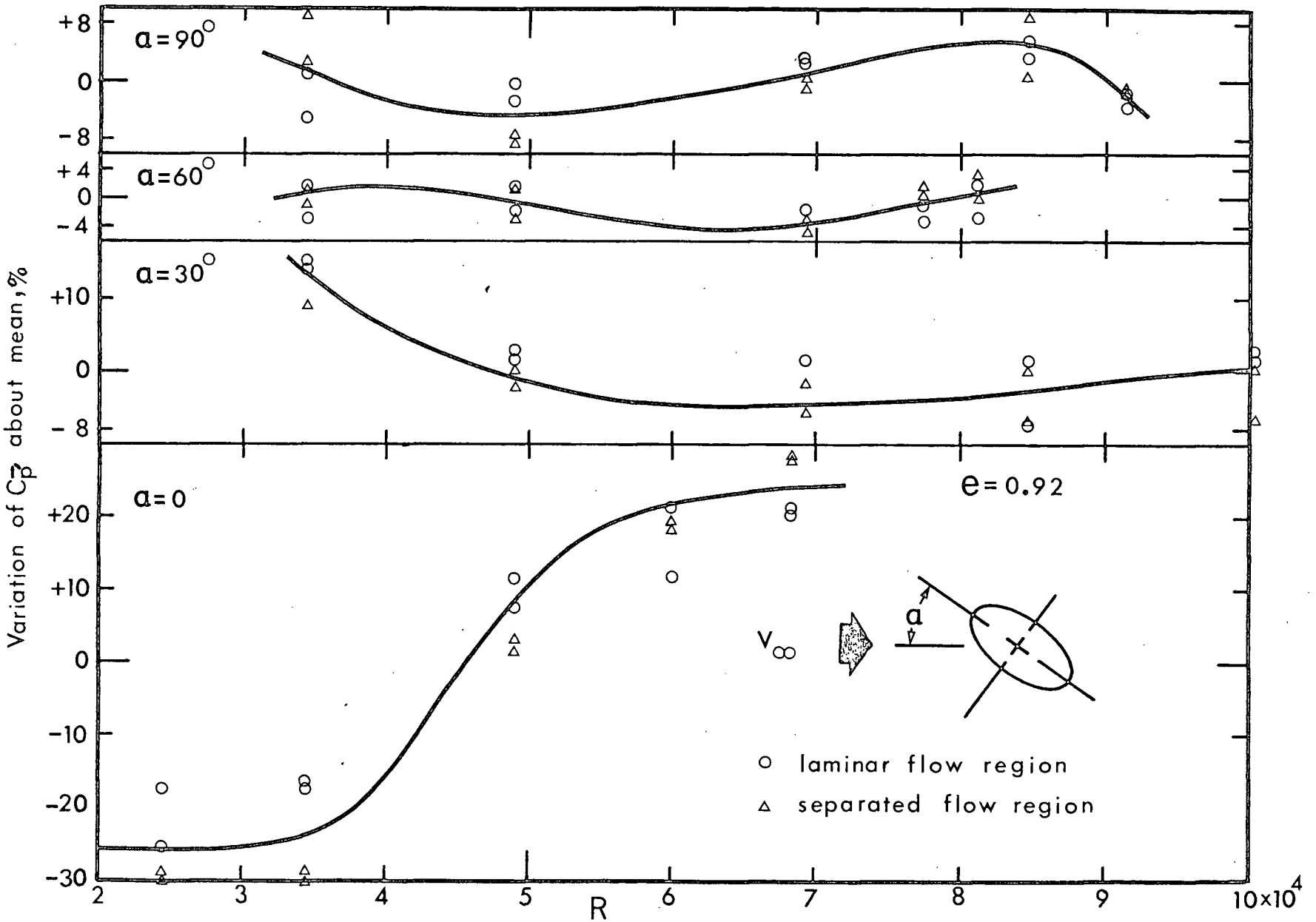

Figure 5-9 Variation of fluctuating pressure coefficient with Reynolds number: (b) e = 0.92

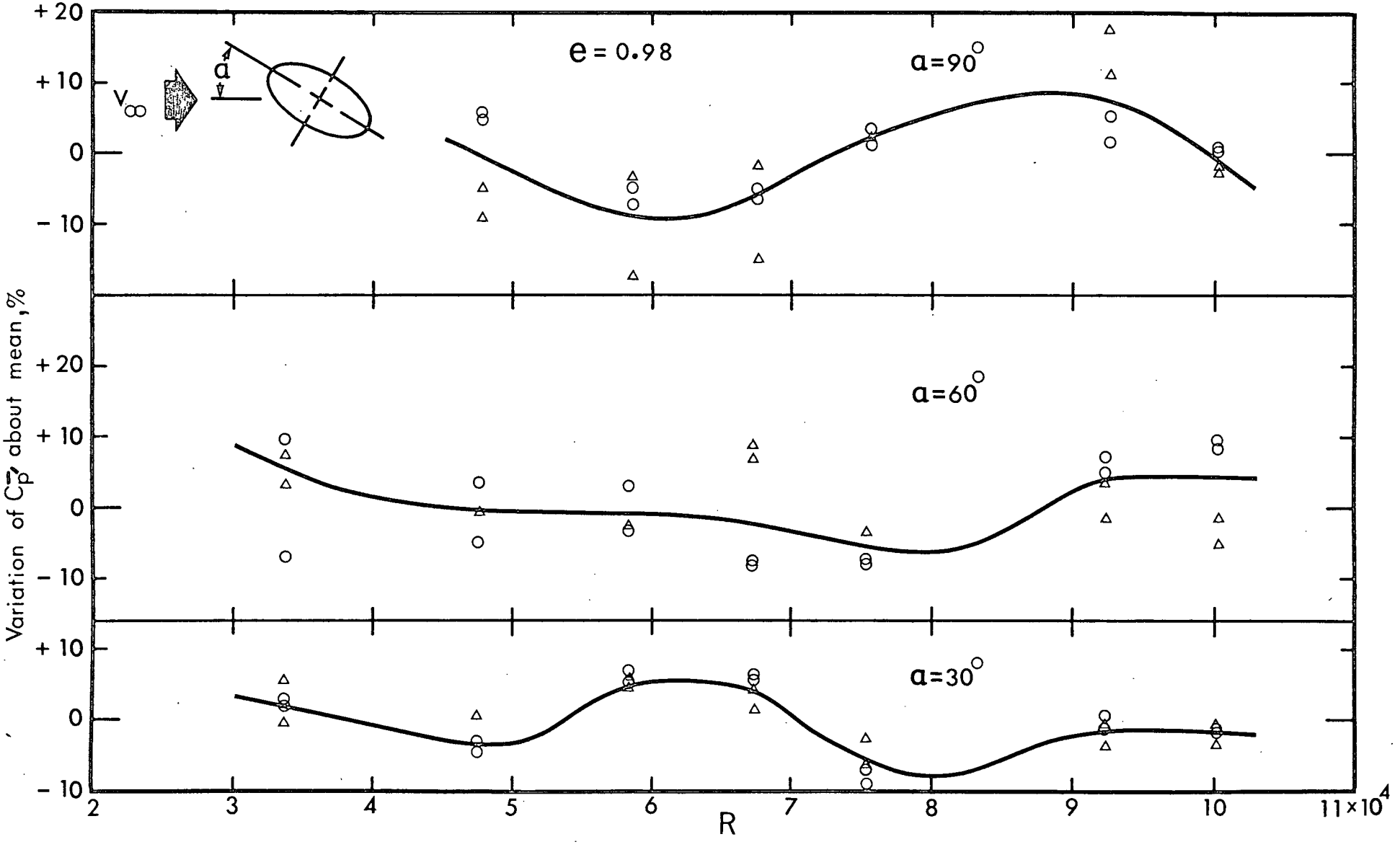

Figure 5-9 Variation of fluctuating pressure coefficient with Reynolds number: (c) e = 0.98

these results are summarized in Figure 5-10(a). Test data on circular cylinders as obtained by Gerrard[15] are also included. The influence of the Reynolds number appears to be confined to the range $3\text{-}7\times10^4$ and increases with eccentricity. However, for circular cylinders, Gerrard observed the Reynolds number effect to extend at least over the range 2,000-180,000 investigated by him. No conclusive explanation concerning this phenomenon is available, but it is likely to be associated with the measured base pressure variations (Figure 5-10b), which in turn may reflect changes in separation condition.

In general, for the cylinder attitude and the Reynolds number conditions under investigation, a decrease in base pressure appears to be accompanied by an increase in fluctuating pressure over the entire range of cylinder eccentricity. For clarity this is shown separately in Figure 5-10(c) for a few representative cases. How this would affect mean location and unsteady movement of the separation points needs to be explored. The measurement of instantaneous pressure profiles, shear stress and/or flow visualisation studies could throw some light on the excursion of separation points. As can be expected, with increase in angle of attack the movement of separation points is minimised leading to a reduced dependency of fluctuating pressure on the Reynolds number.

Fluctuating pressure distribution at the midspan station was measured for R=68,000 and cylinder attitude

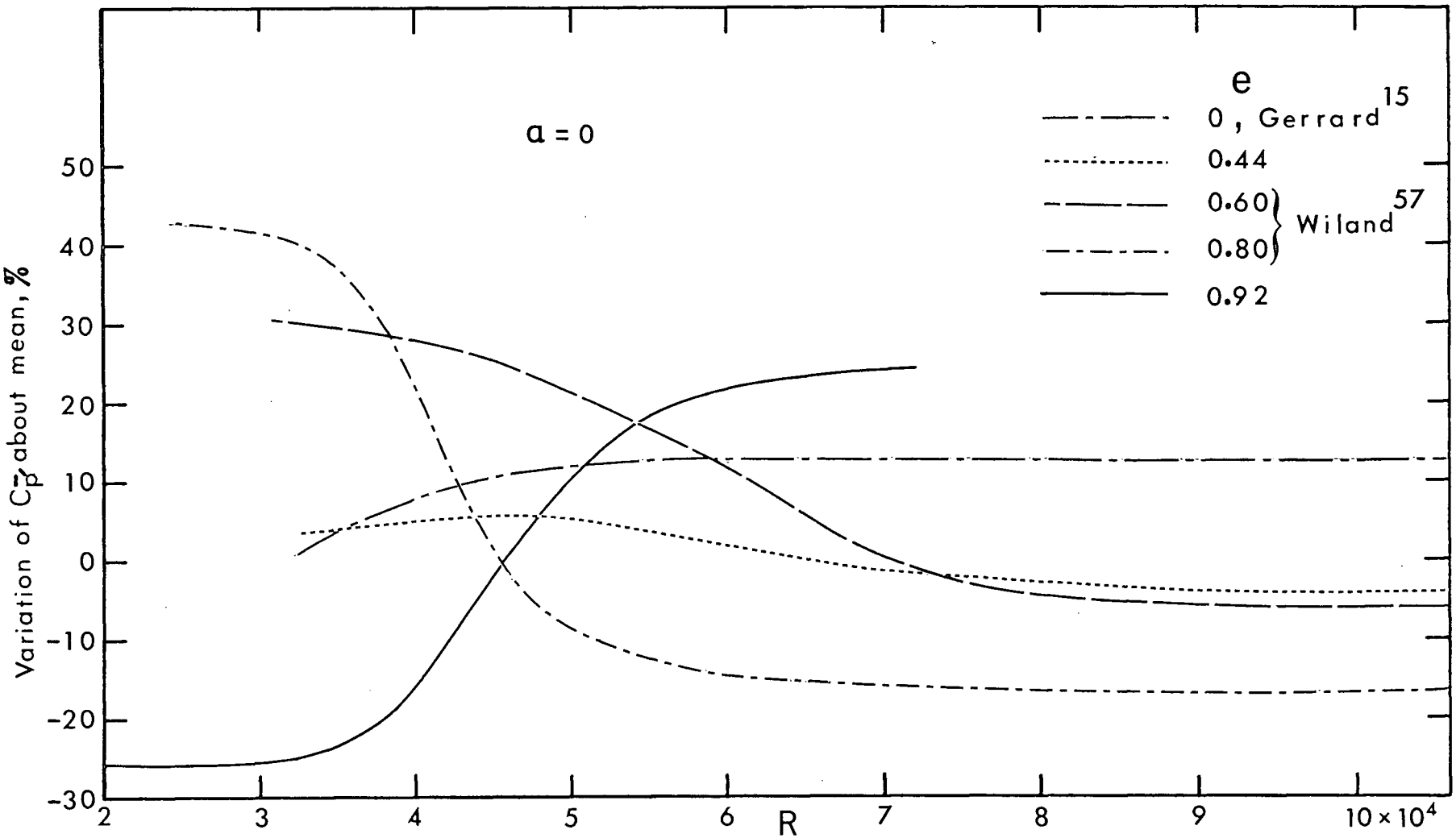

Figure 5-10 Effect of the Reynolds number on aerodynamics of elliptic cylinder at α = 0: (a) unsteady pressure

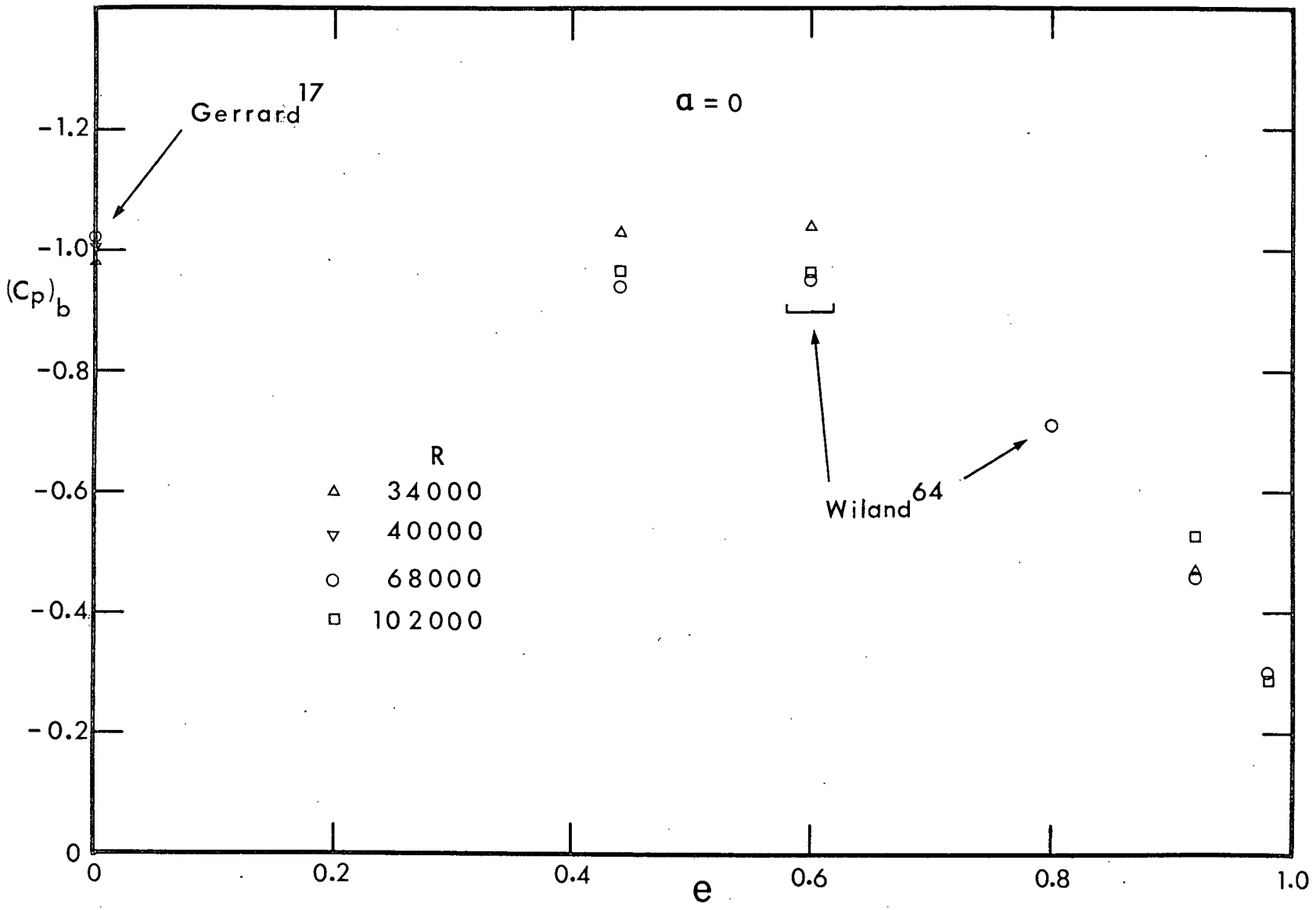

Figure 5-10 Effect of the Reynolds number on aerodynamics of elliptic cylinder at $\alpha = 0$: (b) mean base pressure

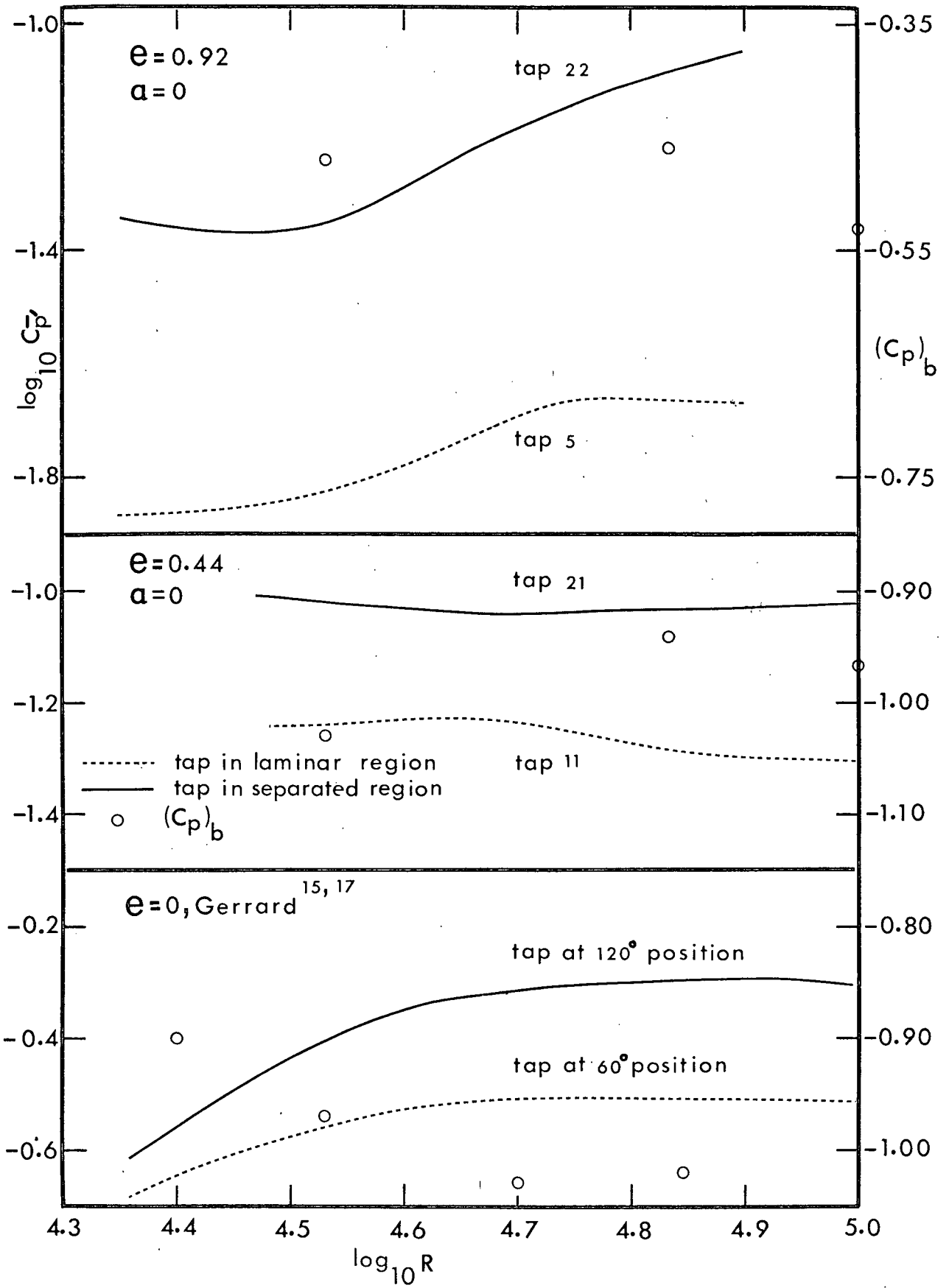

Figure 5-10 Effect of the Reynolds number on aerodynamics of elliptic cylinder at $\alpha = 0$: (c) correspondence between unsteady pressure and base pressure

of 0, 30°, 60° and 90°. The results are presented in Figure 5-11. Based on this data following remarks can be made:

(i) The maximum fluctuating pressure occurs near the region where the mean pressure approaches the minimum value, i.e., close to the separation points. On the other hand, there are two positions, approximately 180° apart, where the fluctuating pressure tends to vanish. One would expect this due to cancellation of pressures which are 180° out of phase. As can be expected this effect is less complete at the rear of the cylinder, probably due to irregularities in the wake.

(ii) For α=0 and 30°, the level of fluctuating pressure appears to increase with bluffness. However, at higher angles of attack, the trend is not well established because of the relatively smaller variations in $C_{\tilde{p}}$, with eccentricity.

(iii) In general, for a given ellipse, the maximum fluctuating pressure increases with increase in angle of attack (Figure 5-12). The fluctuating pressure coefficient can attain a value as high as 0.8 (e=0.60, α=90°).

(iv) It is interesting to note that the fluctuating pressure increases as the mean pressure decreases. Thus a curve presenting variation of the mean

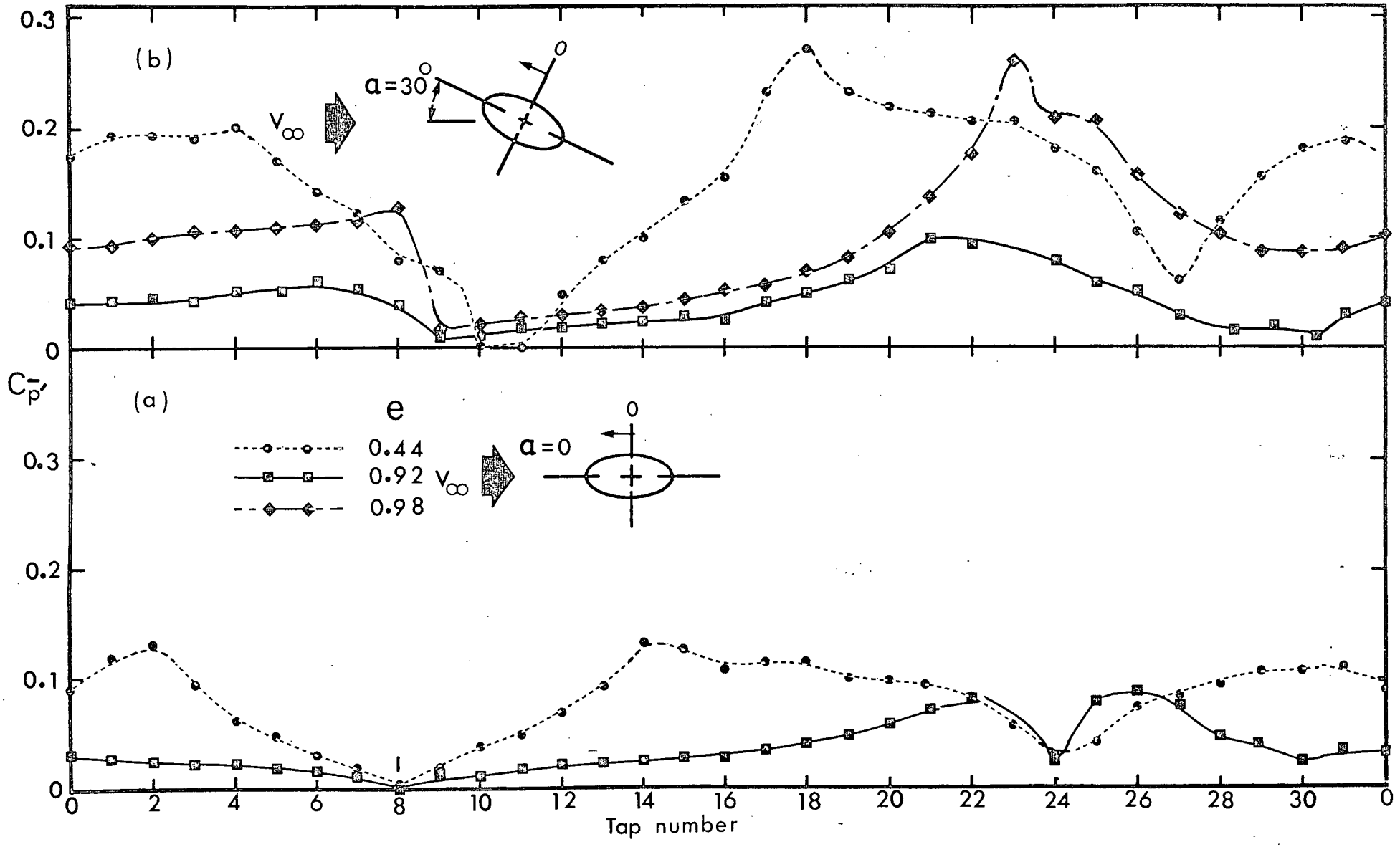

Figure 5-11 Distribution of midspan fluctuating pressure coefficient:
(a) $\alpha = 0$
(b) $\alpha = 30°$

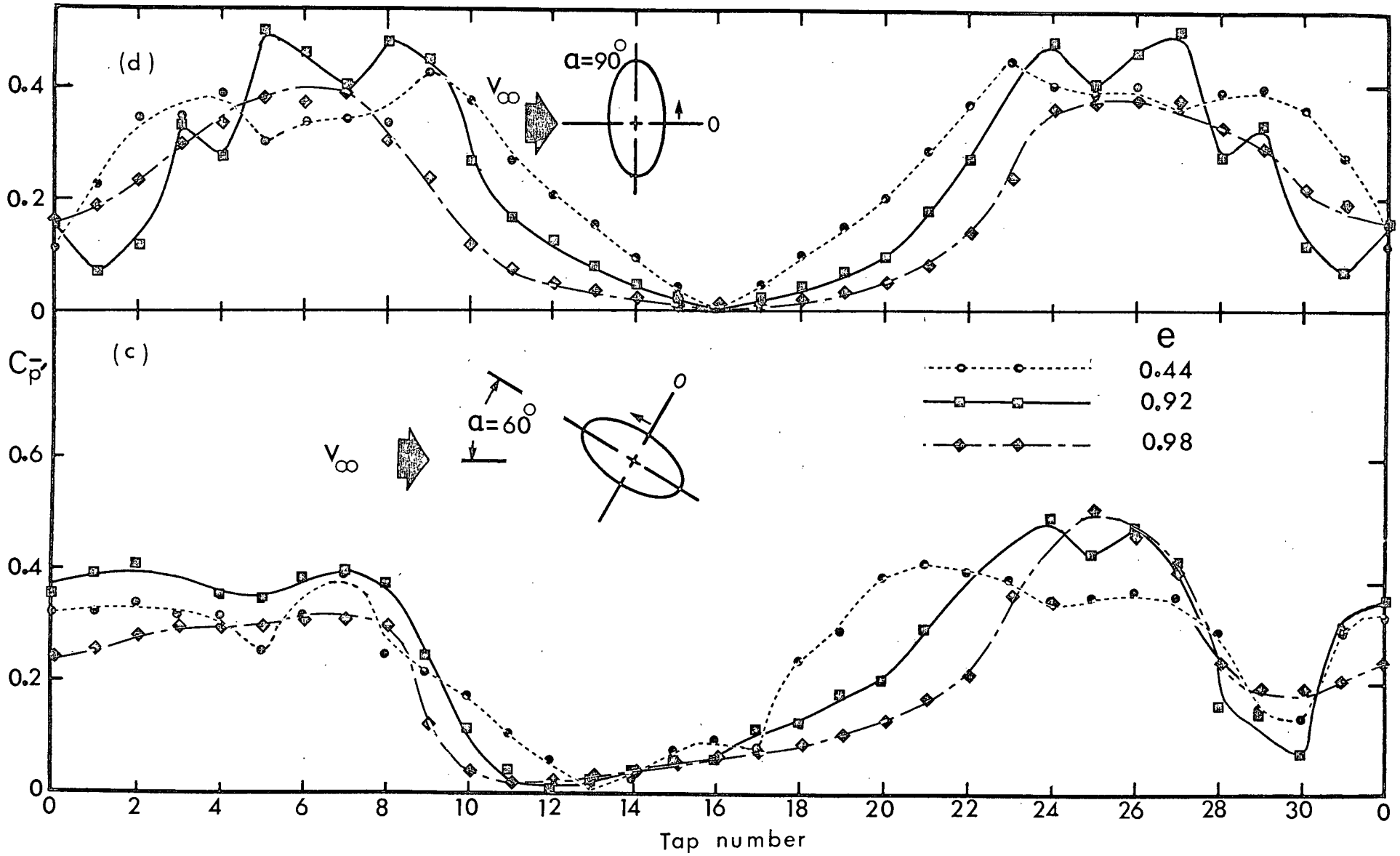

Figure 5-11 Distribution of midspan fluctuating pressure coefficient:
(c) α = 60°
(d) α = 90°

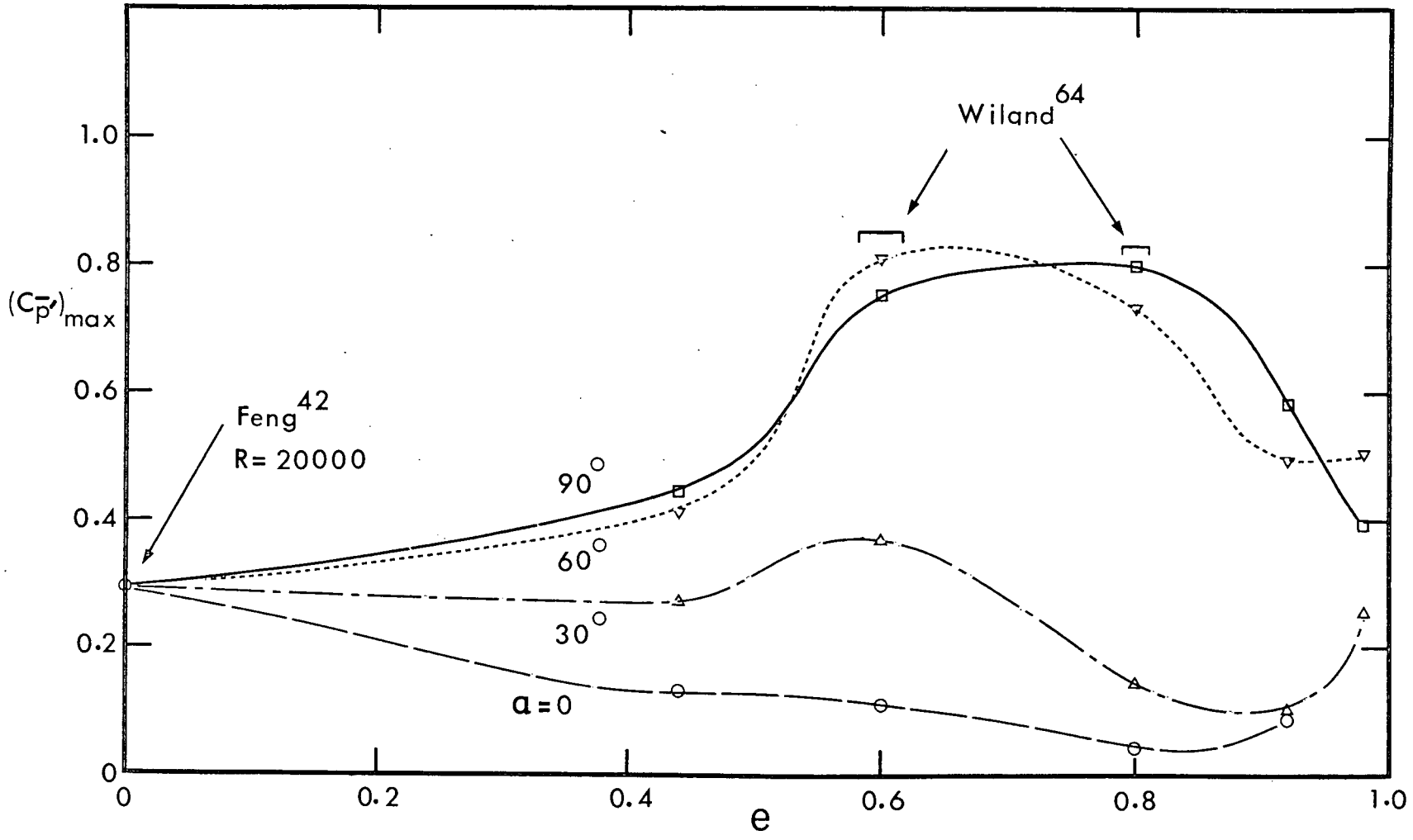

Figure 5-12 The variation of maximum fluctuating pressure with eccentricity and angle of attack

pressure on the surface of a cylinder follows the trend similar to that of $C_{\bar{p}'}$.

The fluctuating pressure signals on the model surface showed random amplitude modulation, which may be attributed to the general instability of the separated shear layer and associated vortices. Figure 5-13 shows extent of the modulation, expressed as a ratio of the maximum to average amplitude, on the model surface. The maximum value was obtained by monitoring the signal over a period of three minutes. In spite of the apparent scatter, a peak value attained by the ratio near the minimum fluctuating pressure point (diametrically opposite to the front stagnation point) is quite distinct. The results also suggest a trend towards reduction of modulation in laminar region.

As suggested by several investigators[15,28,66,83] the amplitude modulation were found to be in phase around the model.

Gerrard[15] was probably the first one to measure the 180° phase character of the pressure signals on the two sides of a circular cylinder. However, contrary to his observation, Modi and Wiland[57] found considerable phase difference between adjacent pressure signals, probably, due to the adjustment of the flow field around the model following the shedding of vortex and formation of the next

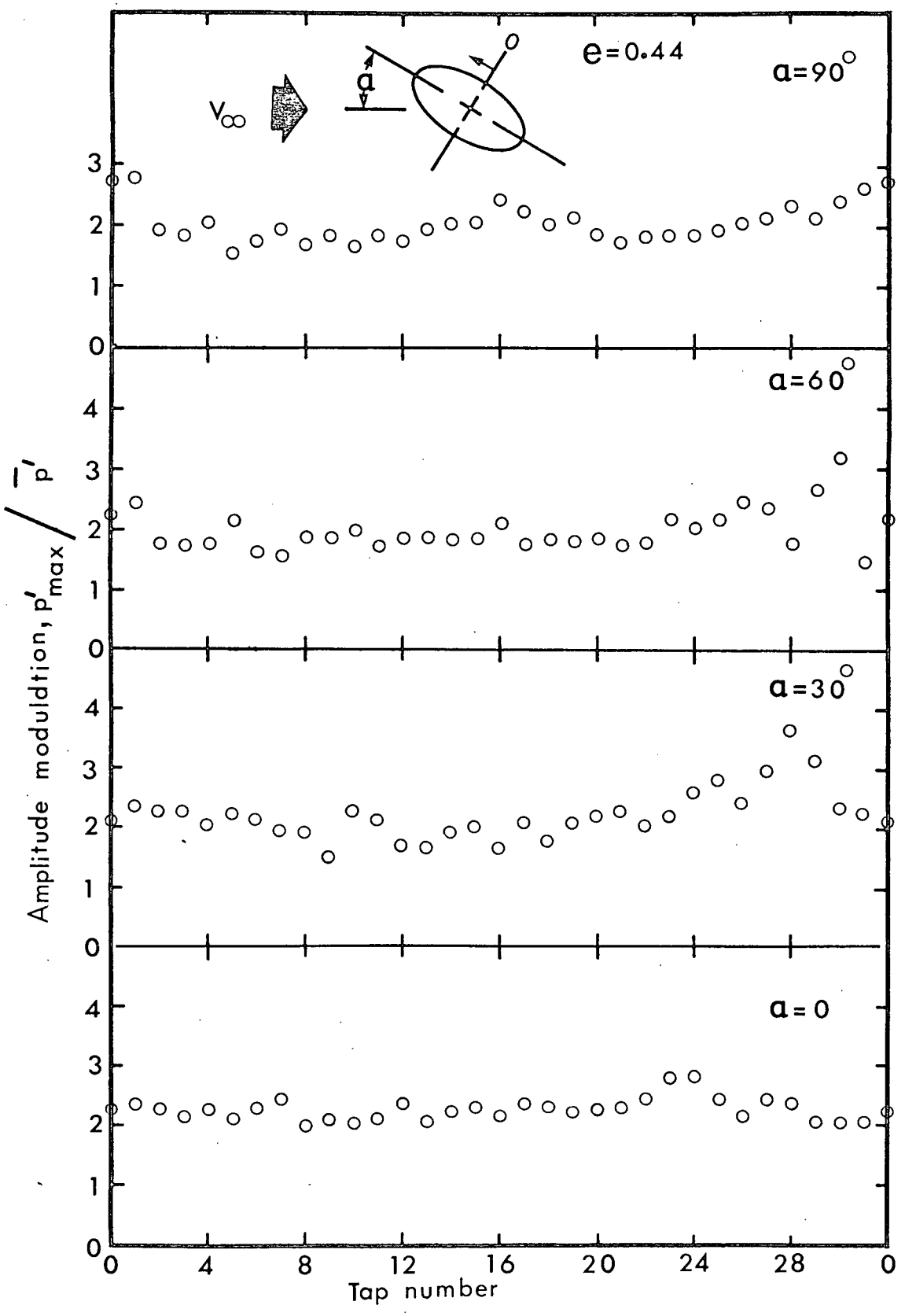

Figure 5-13 Amplitude modulation of pressure signals on the surface of the model: (a) e = 0.44

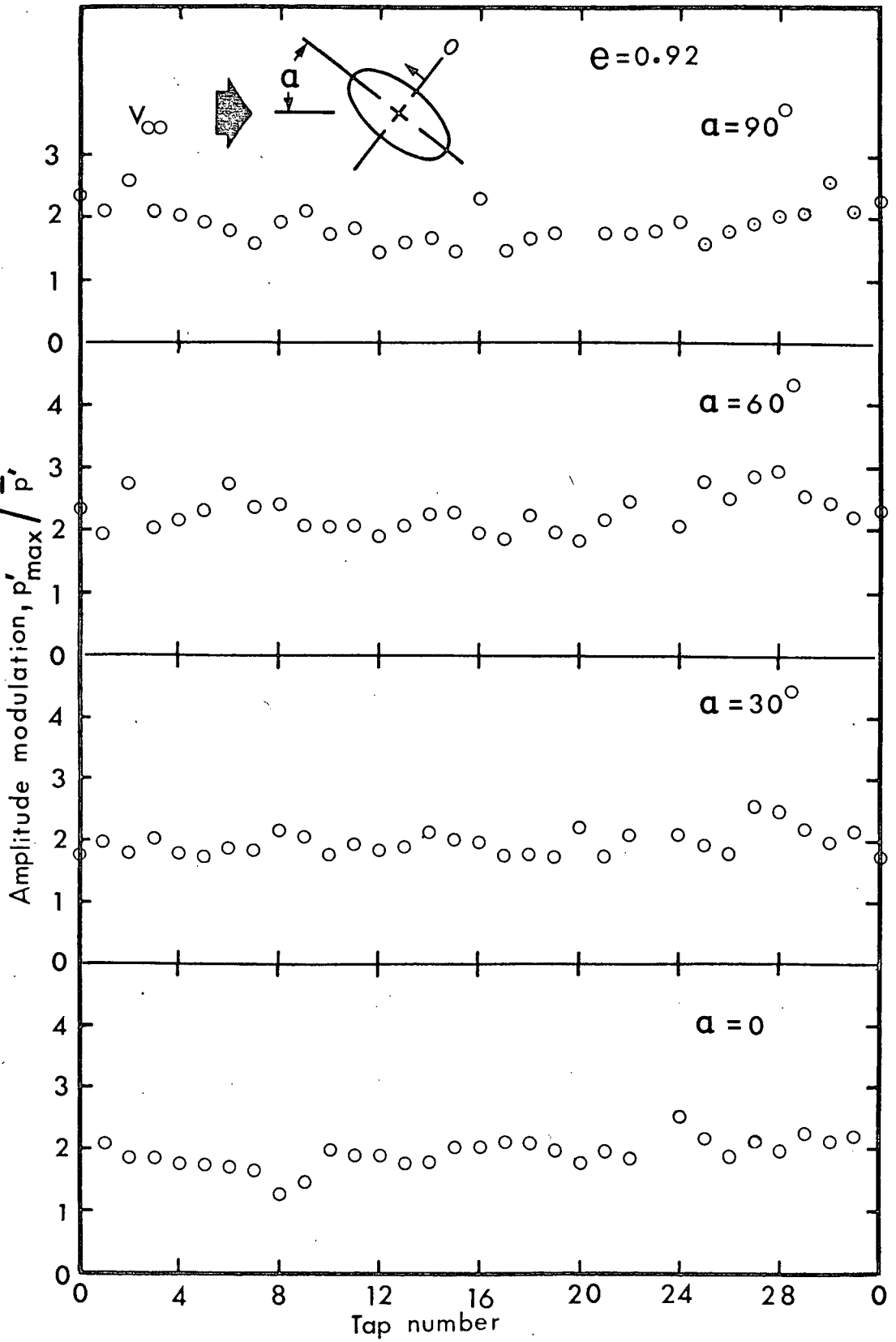

Figure 5-13 Amplitude modulation of pressure signals on the surface of the model: (b) e = 0.92

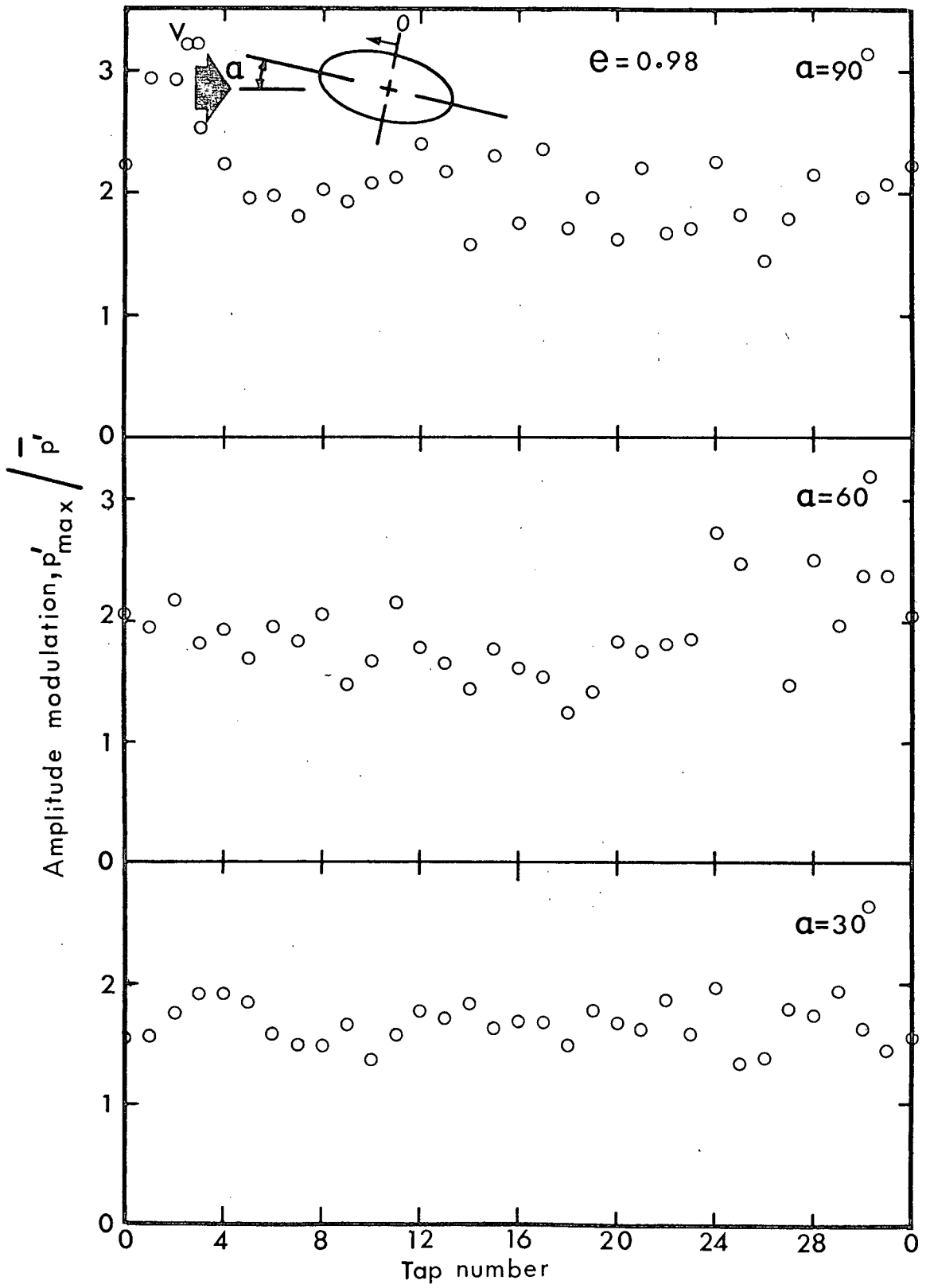

Figure 5-13 Amplitude modulation of pressure signals on the surface of the model: (c) e = 0.98

vortex core. Hence, a systematic study of phase between unsteady pressures as a function of eccentricity was undertaken. The measurements were confined to the extreme attitudes, α=0, 90°. Two pressure taps at 90° position to the flow direction were chosen, each serving as a reference for taps on its side. This led to two sets of data, which, theoretically, should be identical but showed some scatter perhaps due to minor discrepancy in the flow symmetry. The results are presented in Figure 5-14. For α=0, the phase change in general was found to increase with increase in eccentricity and reached a value as high as ≃65° for e=0.92. The effect of eccentricity appears to be more pronounced in and near the separated flow region as compared to the leading edge. It is of interest to note that for cylinders at α=0, the signals from upstream and downstream pressure taps are lagging and leading, respectively, with respect to the reference located at 90° position (taps 0 and 16). On the other hand, for α=90° almost all the pressure signals lag the reference (taps 8 and 24). Relatively large scatter in results near pressure cancellation regions may be partially attributed to rather weak signals, considerably distorted by the noise.

5.7 Fluctuating Lift

The unsteady lift experienced by the elliptic cylinders was determined through the integration of pres-

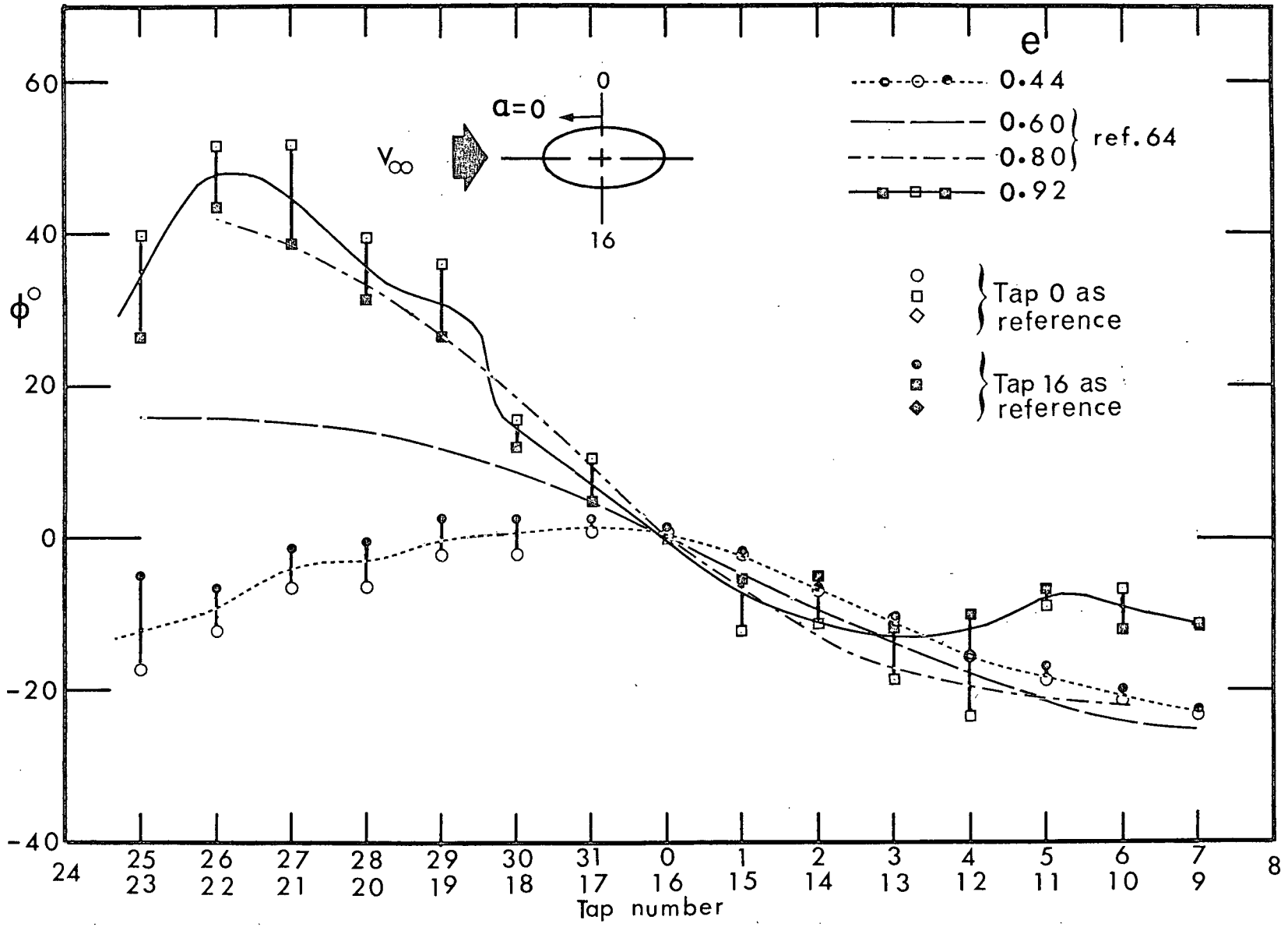

Figure 5-14 Midspan circumferential phase shift between pressure signals on the surface of the model: (a) $\alpha = 0$

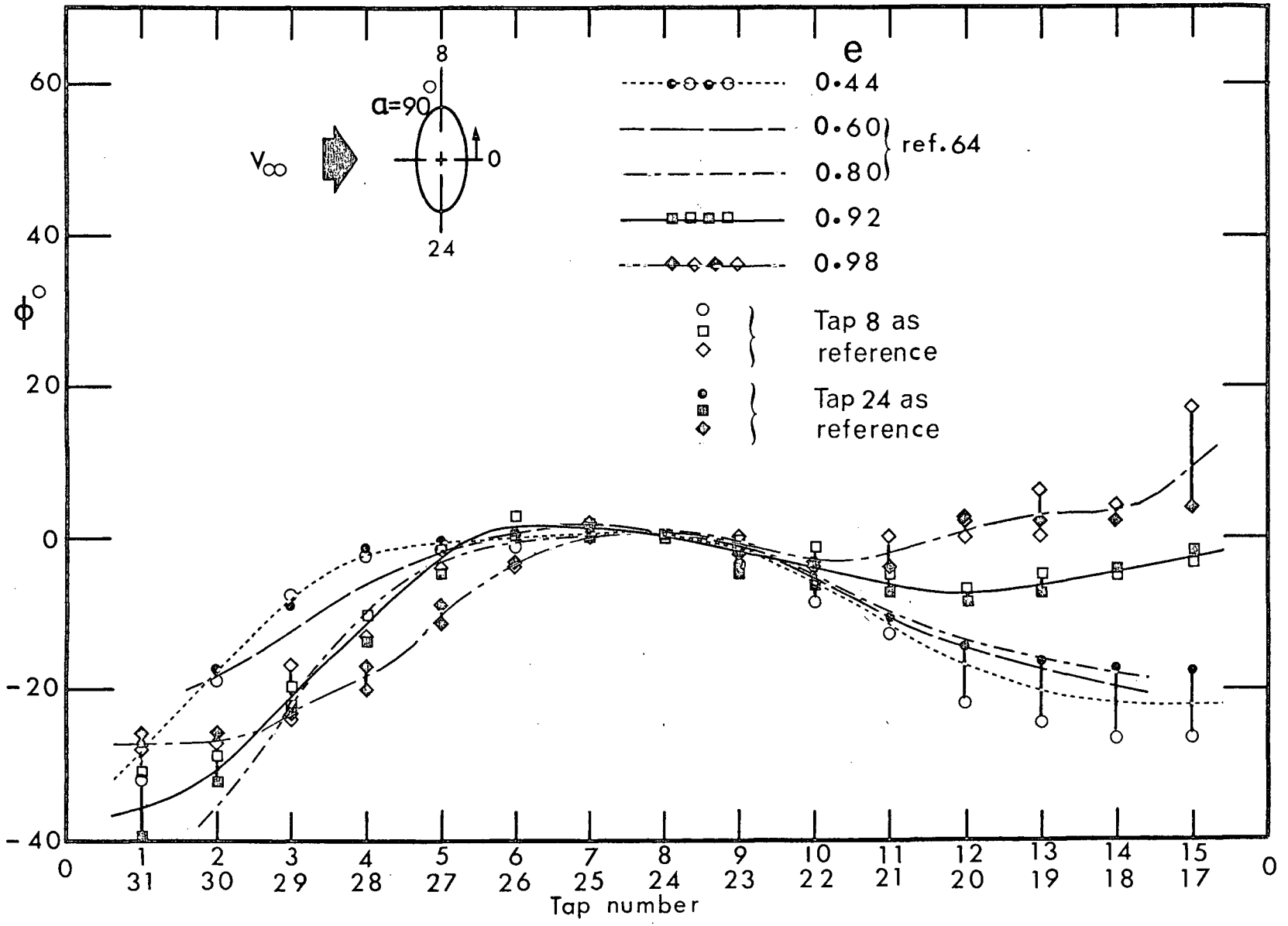

Figure 5-14 Midspan circumferential phase shift between pressure signals on the surface of the model: (b) $\alpha = 90°$

sure distribution plots presented earlier. The variation of the fluctuating lift coefficient, $C_{L'}$, based on the major axis of the ellipse, with angle of attack is shown in Figure 5-15. Integrated values accounting for the circumferential phase are also included.

Except for e=0.44, the elliptic cylinders, in general, show the fluctuating lift to increase with the angle of attack until the critical attitude of ≃70°-80° is attained. Beyond this the fluctuating lift tends to diminish. For e=0.44, $C_{L'}|_{max}$ was found to be 0.58, as compared to the circular cylinder value[42] of 0.45. The substantial magnitude of fluctuating lift for e=0.60, 0.80 ($C_{L'}|_{max}$ ≃ 1.0 and 0.75, respectively[57]) would make them susceptible to large amplitude oscillation during vortex resonance. It is of interest to note that the circumferential phase has negligible effect (<8% at α=0 and 90°) on the fluctuating lift. This may be attributed to the fact that, in general, large pressure fluctuations are associated with small phase differences and viceversa. Hence, the contribution to the fluctuating lift is hardly significant.

5.8 Spanwise Effects

As pointed out by Vickery[51], Prendergast[36] and Feng[42], the spanwise correlation of the flow past the circular cylinder exists only for a finite length. For stationary models this was, typically, two to three cylinder

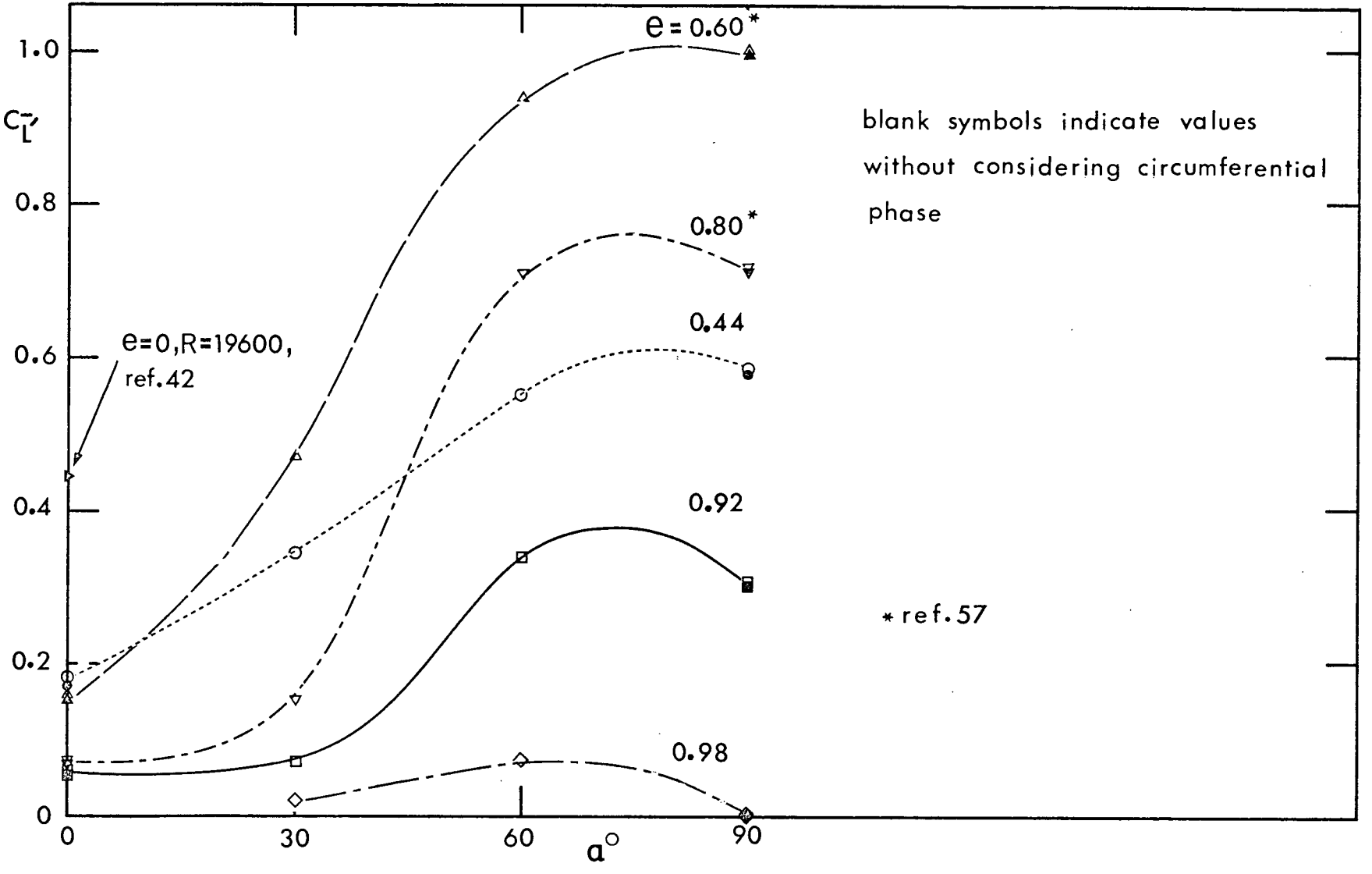

Figure 5-15 Variation of fluctuating lift coefficient with angle of attack

diameters with increased two-dimensionality during model oscillation. In general, the correlation length improves for sharp-edged bodies, and is of the order of five to six diameters for stationary square member in a smooth stream[51]. Normally turbulence affects the spanwise correlation adversely.

With this background, it was decided to undertake a preliminary study of the effect of eccentricity and angle of attack of an elliptic cylinder on the spanwise character of the flow. The experimental program used three models (e=0.44, 0.92, 0.98) at angles of attack of 30°, 60° and 90°. Each model was provided with a set of nine, equally spaced pressure taps along its leading edge (Figure 3-2). The model spanned the test section almost completely, with no gap at the bottom and the top gap less than 0.015 in. The distribution of the mean pressure as shown in Figure 5-16 suggests negligible spanwise effect. The results for α=0 are omitted as no spanwise dependency was noticed. On the other hand, unsteady pressure and phase showed marked variation with spanwise location. These results are presented in Figure 5-17 and 5-18. Feng's[42] results for circular cylinder are also included for comparison. In general, the variation of fluctuating pressure in spanwise direction increases with increase in angle of attack, however, the forms of the plots remain essentially similar. A degree of distorted symmetry about the midspan section

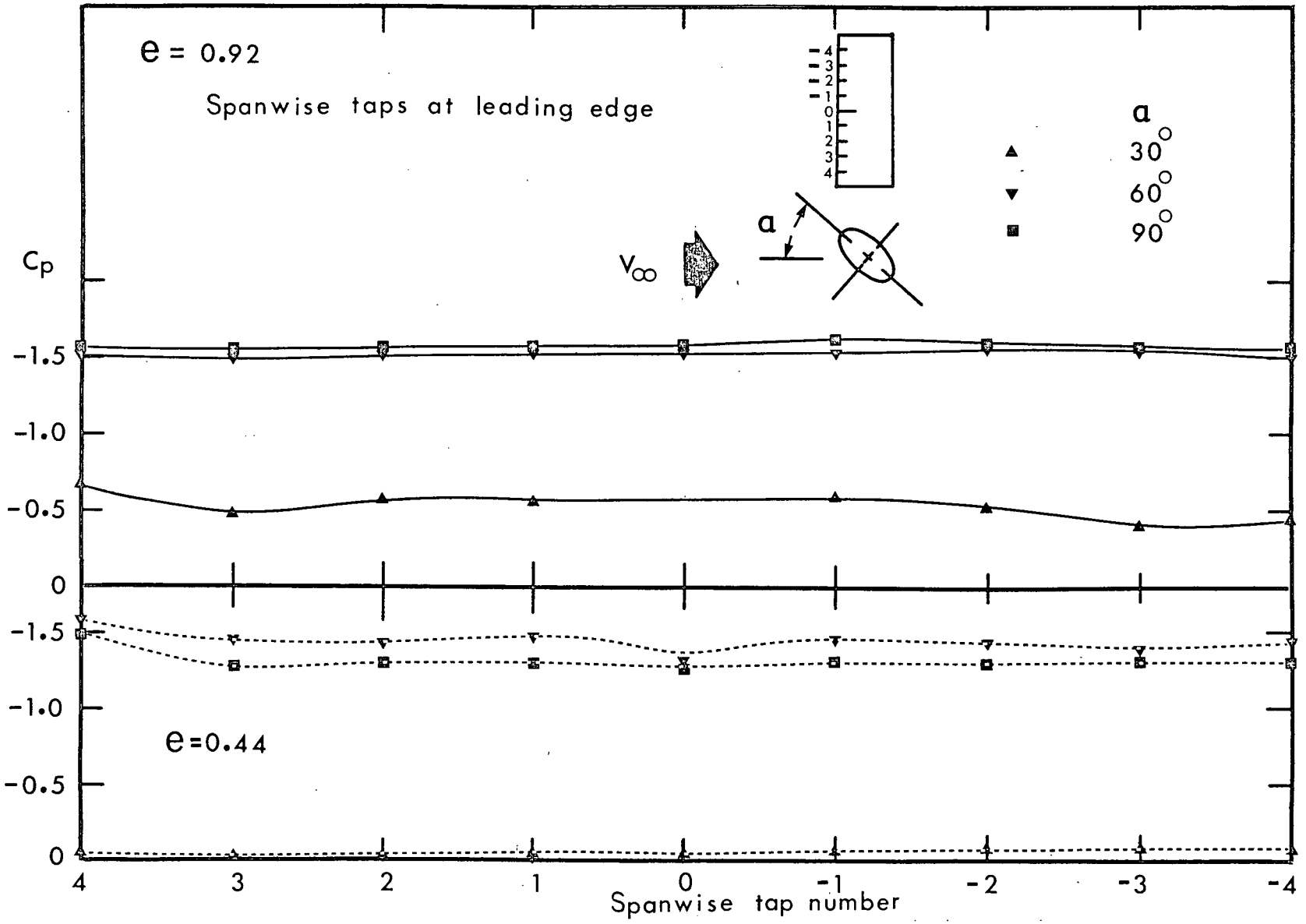

Figure 5-16 Representative spanwise variation of mean pressure coefficient

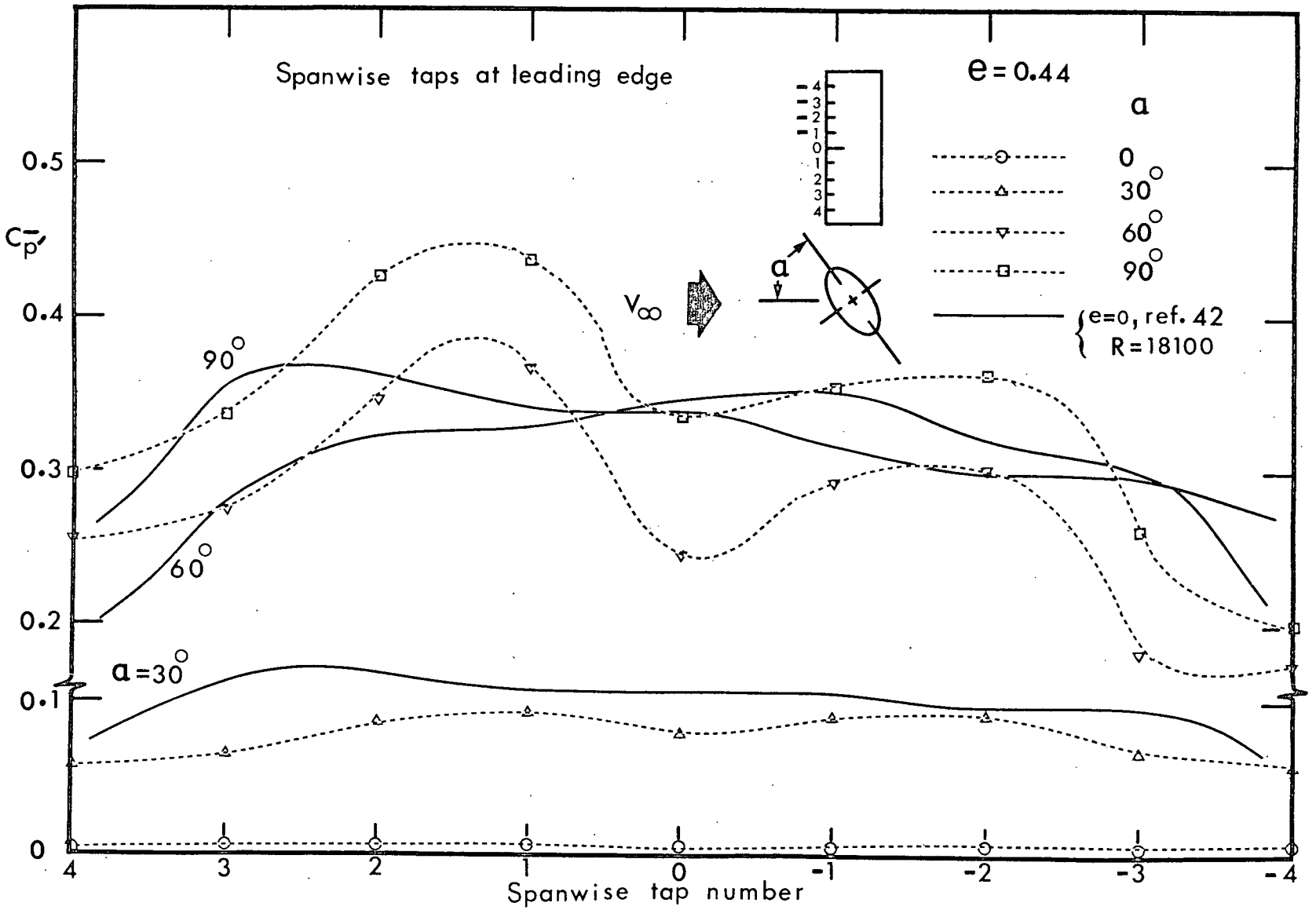

Figure 5-17 Spanwise distribution of fluctuating pressure coefficient: (a) e = 0.44

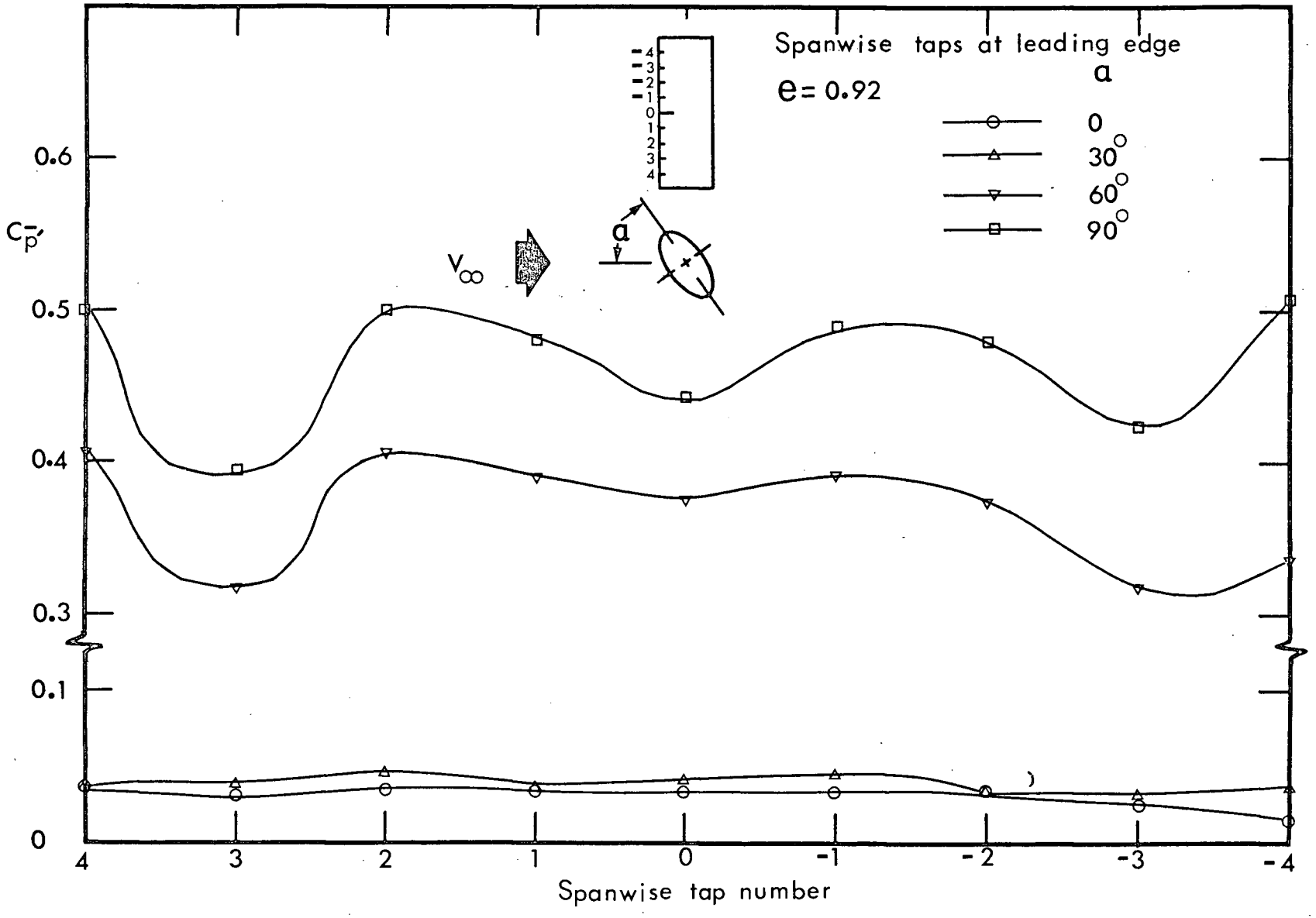

Figure 5-17 Spanwise distribution of fluctuating pressure coefficient: (b) e = 0.92

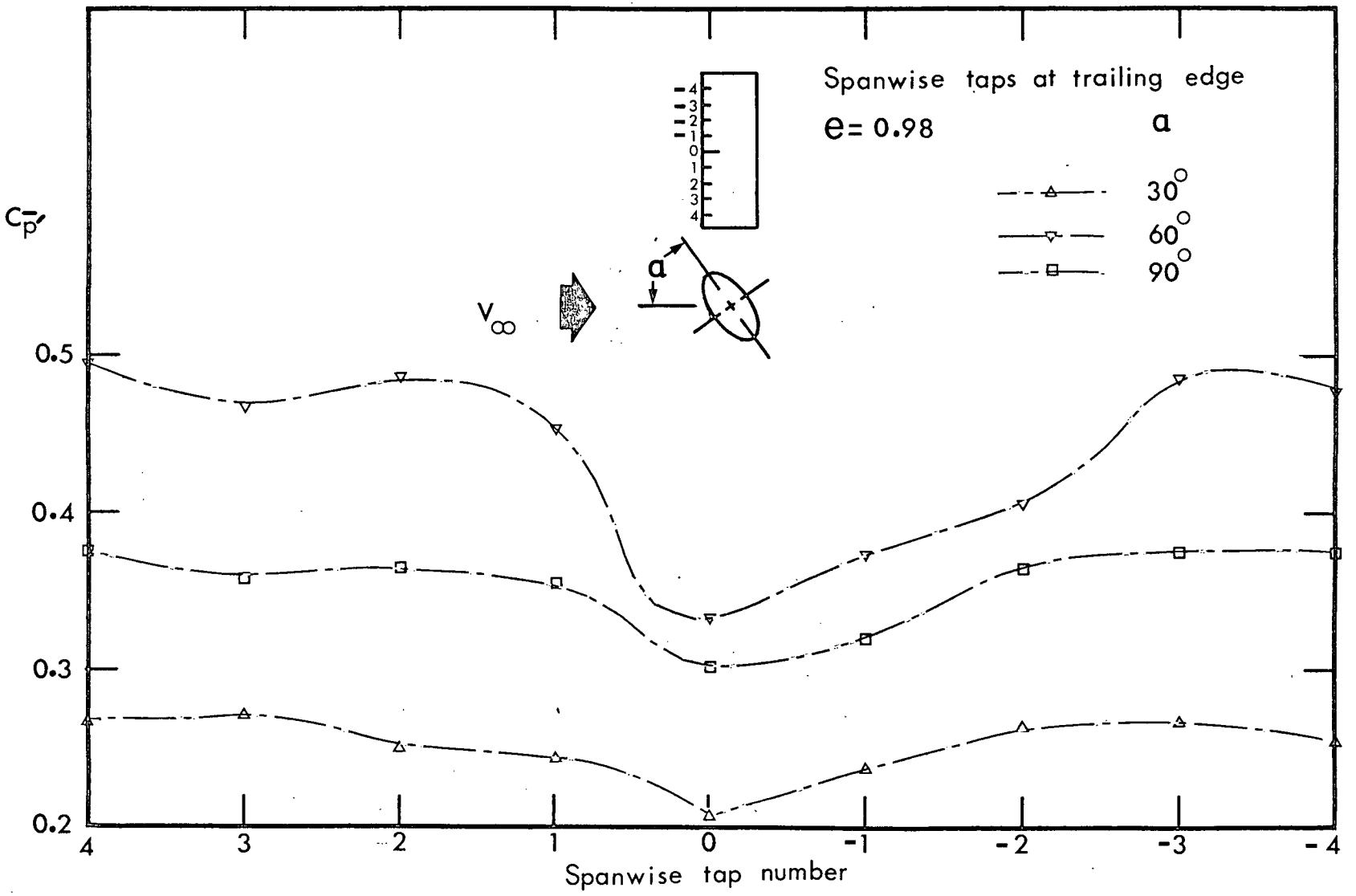

Figure 5-17 Spanwise distribution of fluctuating pressure coefficient: (c) e = 0.98

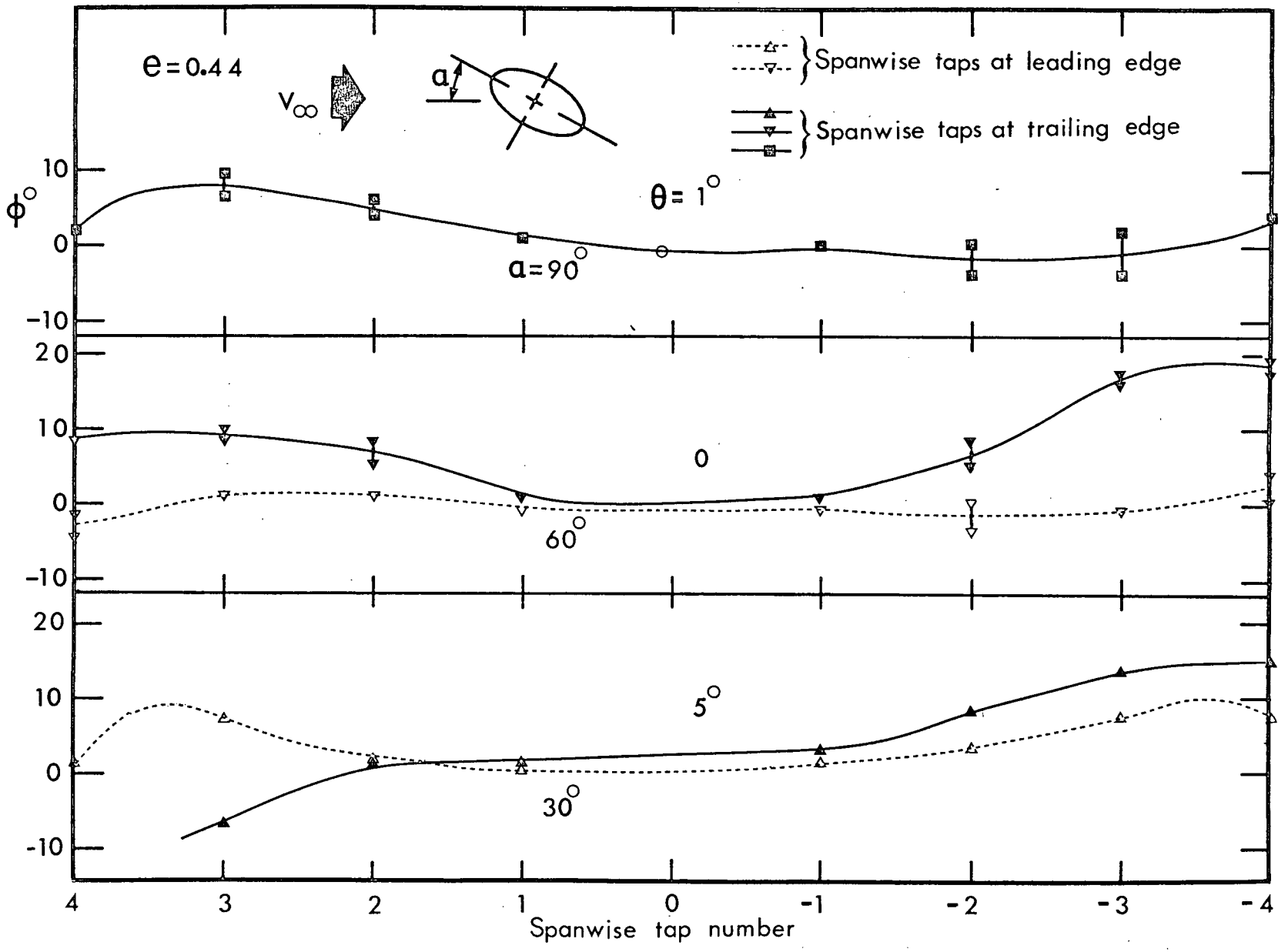

Figure 5-18 Phase difference between pressure signals in spanwise direction: (a) e = 0.44

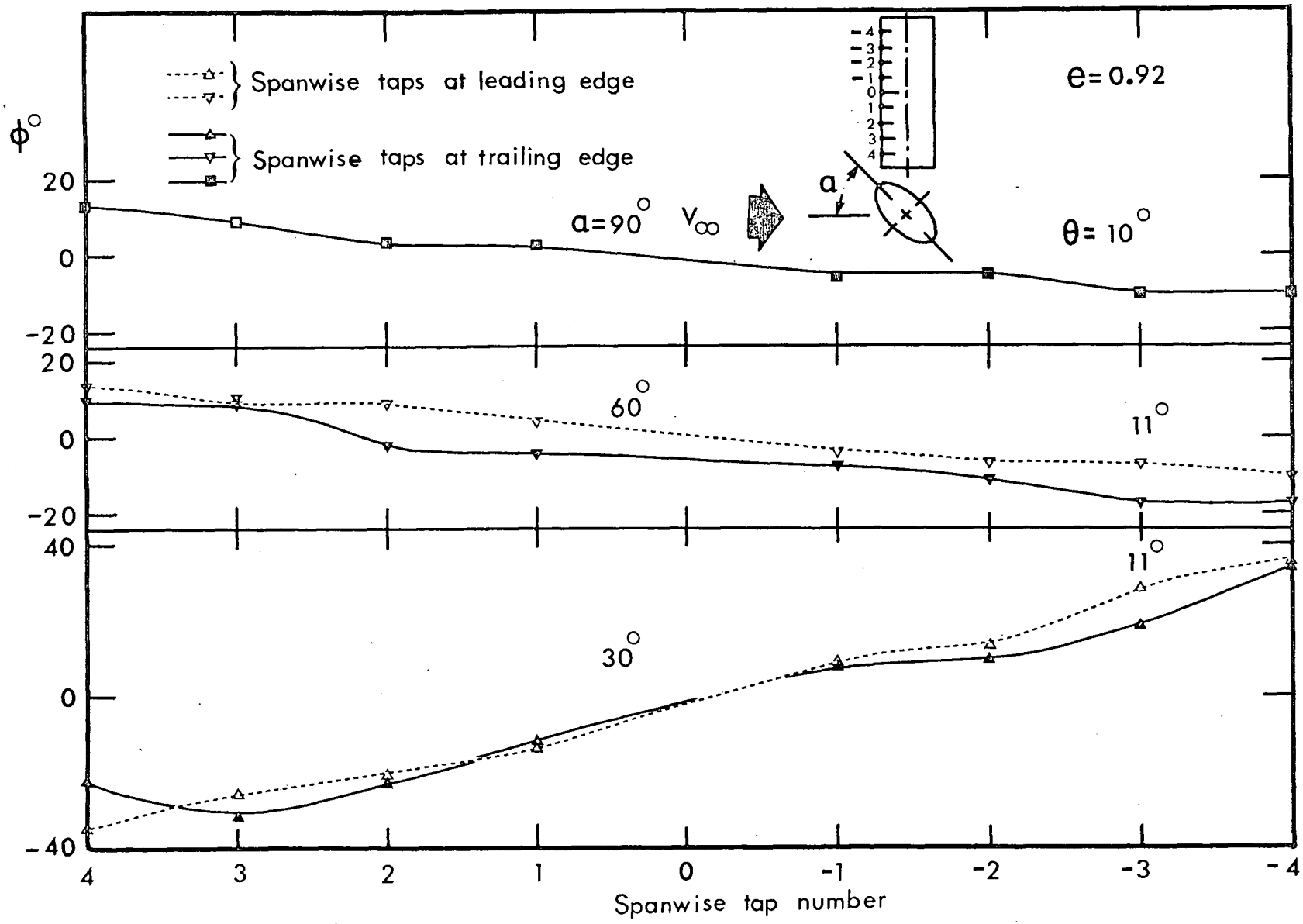

Figure 5-18 Phase difference between pressure signals in spanwise direction: (b) e = 0.92

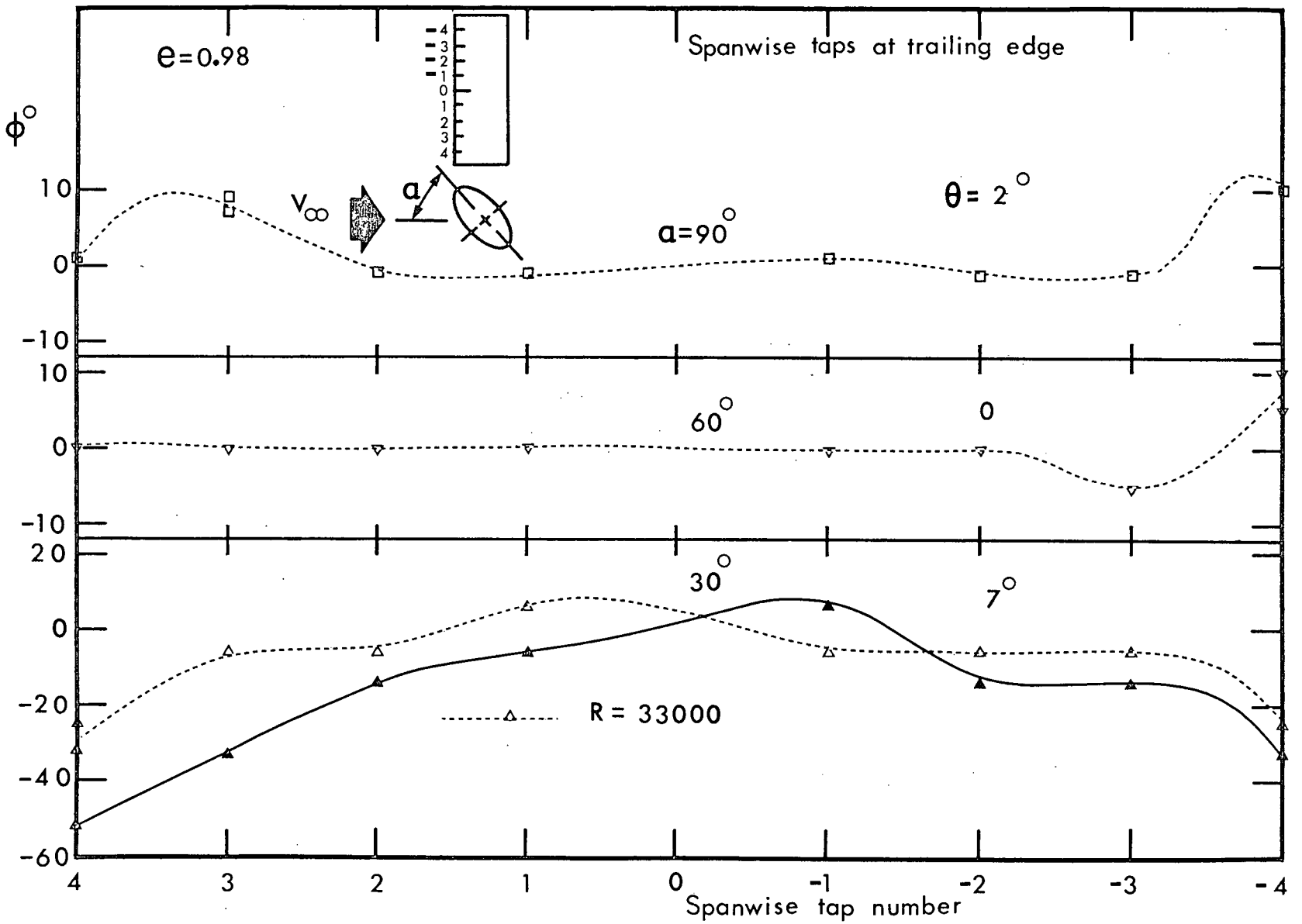

Figure 5-18 Phase difference between pressure signals in spanwise direction: (c) e = 0.98

can also be discerned in most of the cases investigated. The maximum fluctuating pressure invariably occurred away from the midspan. Similar behavior was also observed by Gerrard[15] and Feng[42] for circular cylinder. The spanwise variations were found to be as large as 80% (e=0.44, α=60°) of the reference midspan value.

The variation of phase between unsteady pressure signals along the span is shown in Figure 5-18. Normally the results were obtained for the leading edge as well as the trailing edge by rotating the model through 180°. For a particular case of e=0.98, the experiment was repeated for R=33,000.

In general, the results did not show any well defined trends as to the effect of cylinder eccentricity and angle of attack on the spanwise variation of the phase. However, in most cases the two-dimensional character was maintained only over a short distance around the midspan section with the small aspect ratio effect becoming quite apparent towards the ends. The plots suggest odd or even function type of symmetry about the midspan, however, due to limited number of spanwise stations and inherently unsteady character of the flow, no definite conclusions can be drawn.

As time history of the phase is associated with the spatial location of the vortex sheet, the average inclination of the core line with respect to the cylinder axis

can be calculated. The inclination θ, based on the straight line variation of the phase near midspan station, is shown on the diagram. There is an indication that at high values of α, the vortex line inclination diminishes suggesting improved alignment with the cylinder axis. It is significant to point out that Vickery[51] found improvement in correlation length for square cylinder (5.6 D) compared to the circular cylinder results (3.5 D) of Prendergast[36] and el Baroudi[37].

Gerrard's[18] results on three-dimensional character of the flow past a circular cylinder at $R=2\times10^4$ should be mentioned here. The hot wire measurements made three diameters downstream and over a small axial distance (test length = 9 in., model length = 20 in.) showed vortex lines to be almost straight and parallel to the cylinder axis. This behavior was confirmed through flow visualisation using titanium tetrachloride. The random fluctuations in the vortex line inclination, which was always present, was found to be as large as $\pm15°$, however, it occurred at a frequency an order of magnitude below the fundamental frequency. On the other hand, Feng's[42] results with circular cylinder at the same Reynolds number and present data with elliptic cylinders at R=68,000 showed the presence of vortex line inclination even when based on average phase results at the fundamental frequency.

A comment concerning the effect of cylinder motion as reported by Koopmann[40,41], Toebes[39] and Feng[42] would be

appropriate. For low amplitude (<<10% of the cylinder diameter) forced and wind induced oscillations at low Reynolds number (100-300), Koopmann[40,41] reported vortex line inclination of 17°. However, large amplitude oscillations tended to promote alignment of vortex lines with cylinder axis suggesting improved two-dimensionality of the near wake flow. Some of the results on three-dimensionality of the wake are summarised in Table 5-3.

5.9 Wake Geometry

There appears to be rather scant information concerning the organised wake associated with elliptic cylinder. Modi and Wiland[57] presented preliminary results on its near infinity character, i.e., uniform values of vortex spacings attained five to eight 'diameters' (major axis) downstream, for cylinders of eccentricity 0.60 and 0.80. However, no attempt was made to explore the variation of wake geometry as a function of downstream coordinate. This section discusses the results of a detailed investigation on the wake of cylinders with e=0.44, 0.80, 0.92 and 0.98. To study the dependence of various wake parameters on the attitude of the models, the experiments were conducted at α=0, 30°, 60° and 90°. Since the Reynolds number effect in the range 3×10^4-10^5 is reported[57] to be negligible, all the tests were confined to R=68,000.

The results on phase variation in the downstream direction showed it to attain a constant value suggesting

Table 5-3 Average inclination of vortex line with respect to cylinder axis

Eccentricity	Condition	R	Technique	Inclination	Investigator
e=0	stationary	50	phase measurement using hot-wire	aligned with the axis for at least 30 diameters downstream	Kovásznay[11], 1949
	stationary	<60 75	alumina flake suspension in water	0 10°	Taneda[84], 1952
	stationary	≤100 ≤80	hollow cylinder filled with dye, in water	0, in still water 0, in disturbed water	Phillips[85], 1956
	stationary	117 190	red dye leaked through small holes aligned parallel to cylinder axis	0 <10°, wavy	Hama[86], 1957
	stationary	10^5-3×10^7	use of fine silk threads in wind-tunnel	wave pattern with cell size between 1.4D and 1.7D	Humphreys[31], 1960
	stationary	100-140	hydrogen bubble flow visualization	0-30°	Abernathy[85], 1964
	stationary	85 2×10^4	hot-wire anemometry	14° at 17.2 diameters downstream 0 at 3 diameters downstream	Gerrard[18], 1966
	stationary vibrating: wind induced forced	200 200	smoke visualisation	17.5° at the cylinder and 33° at 14 diameters downstream } 0	Koopmann[41], 1967
	stationary wind induced	17600 20400 17000 20700 26300	measurement of phase between pressure signals at the cylinder surface	9° 7.1° 7.8° 0 9°	Feng[42], 1968
e=0.44 α=0 α=30° α=60° α=90°	stationary	68000		weak signal, absence of well defined phase 5° 0-5° 1°	Present experiment
e=0.92 α=0 α=30° α=60° α=90°	stationary	68000	measurement of phase between pressure signals at the cylinder surface	weak signal, absence of well defined phase 11° 10° 10°	Present experiment
e=0.98 α=30° α=60° α=90°	stationary	68000		7° 0 2°	Present experiment

an uniform vortex velocity and longitudinal spacing. The limited reach of the traversing gear and poor strength of the fluctuating pressure signal restricted the longitudinal measurements to eight diameters. Fortunately, this does not represent a serious limitation as Frimberger's[87] experiments with circular cylinders, in air and water, showed the wake geometry to attain uniform dimensions around the same distance downstream. The variation of longitudinal spacing between vortices obtained using equation (4.2) is presented in Figure 5-19. The plots show a rapid increase in spacing for the distance of two to three diameters behind the cylinder, gradually approaching a constant value by seven diameters. In general, a lower angle of attack is accompanied by early attainment of uniform spacing. The vortex spacing showed increase with increase in angle of attack, the larger change, as expected, being associated with high eccentricity ellipses.

The vortex velocity was deduced from the relation,

$$V_V = fL \qquad (5.3)$$

Although, V_V shows a trend similar to the longitudinal spacing, it is relatively less dependent on the cylinder attitude and eccentricity. In general, the effect of increase in angle of attack and eccentricity is to delay the establishment of near infinity values downstream.

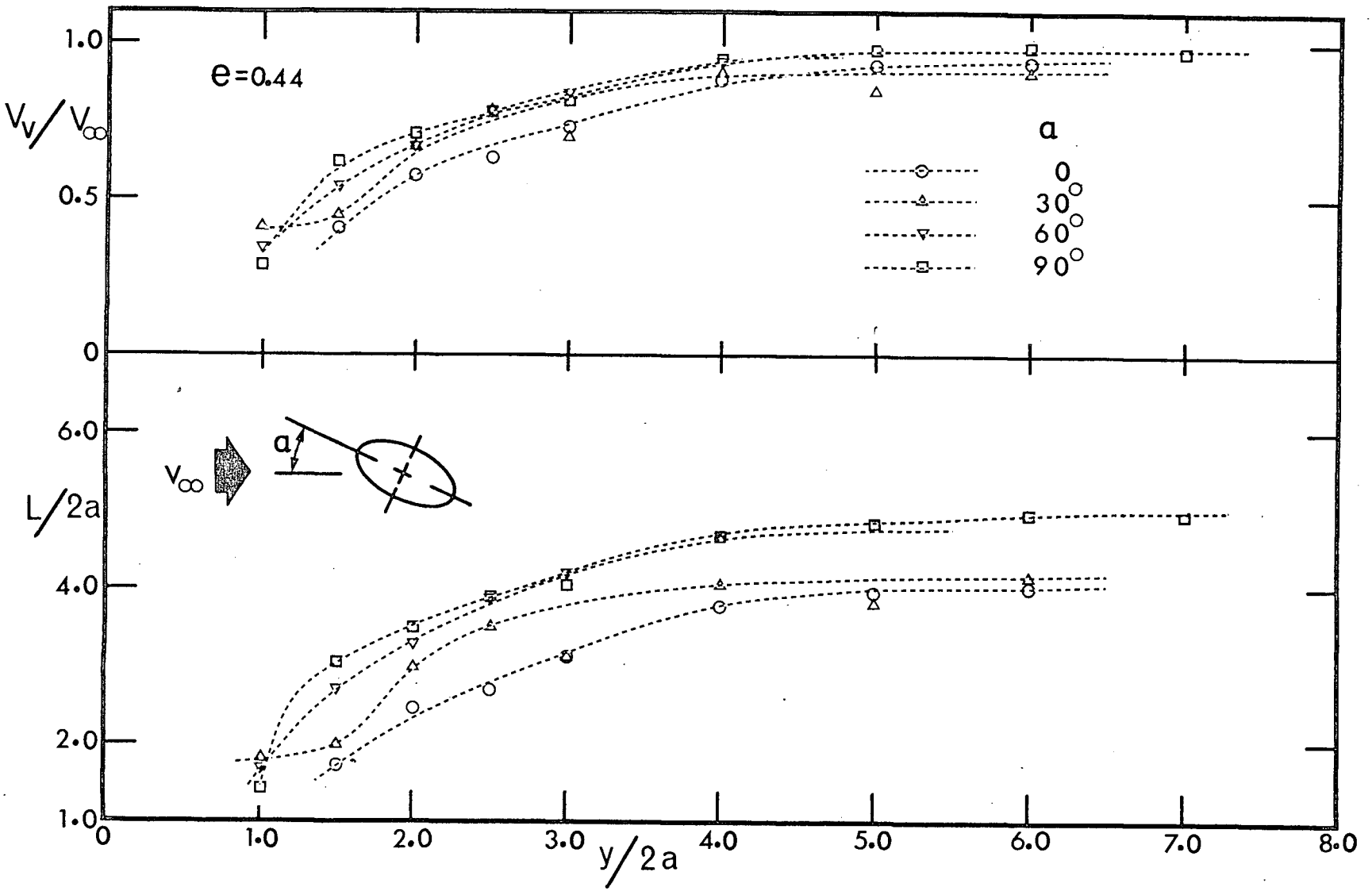

Figure 5-19 Streamwise variation of longitudinal vortex spacing and vortex velocity: (a) e = 0.44

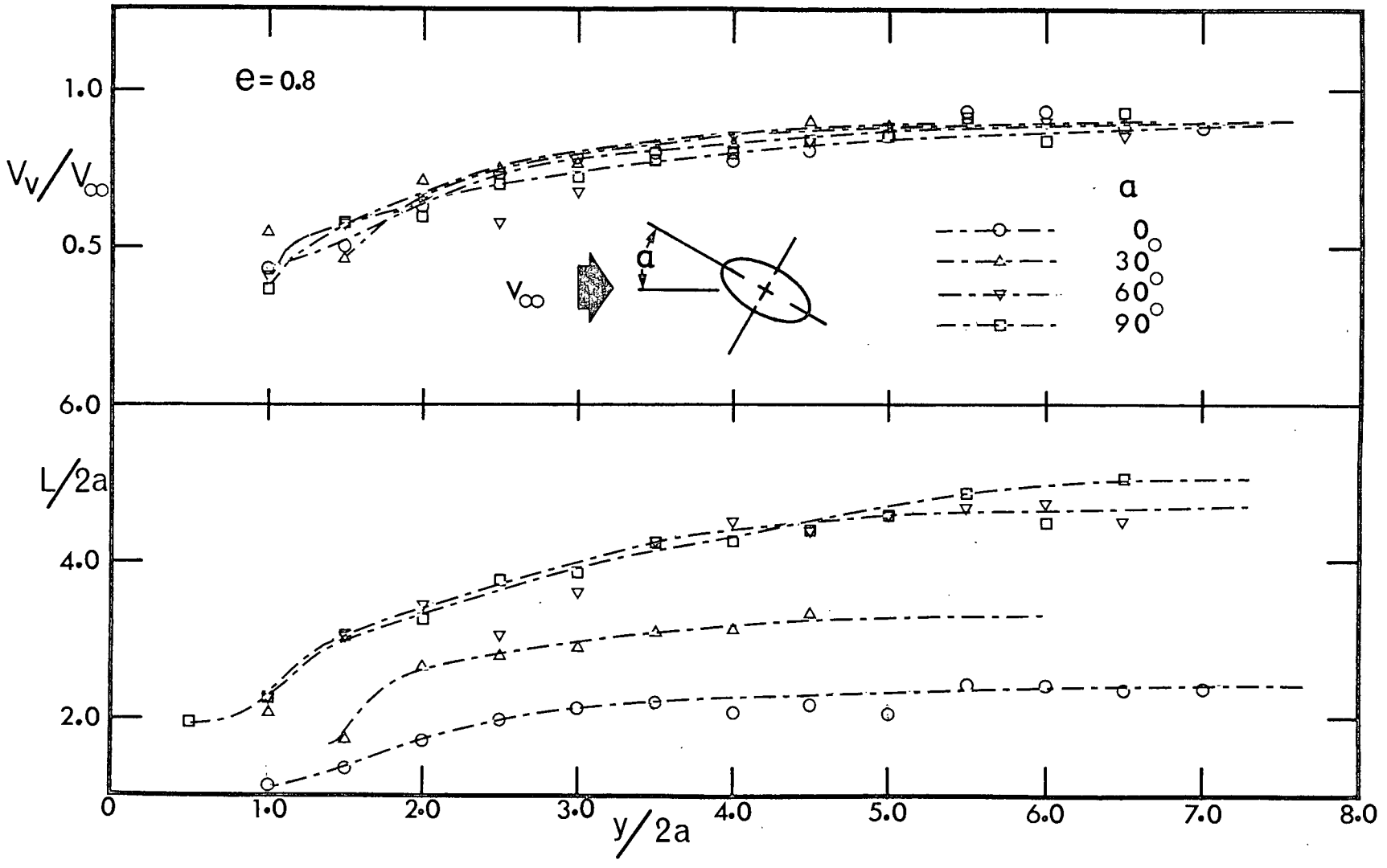

Figure 5-19 Streamwise variation of longitudinal vortex spacing and vortex velocity: (b) e = 0.80

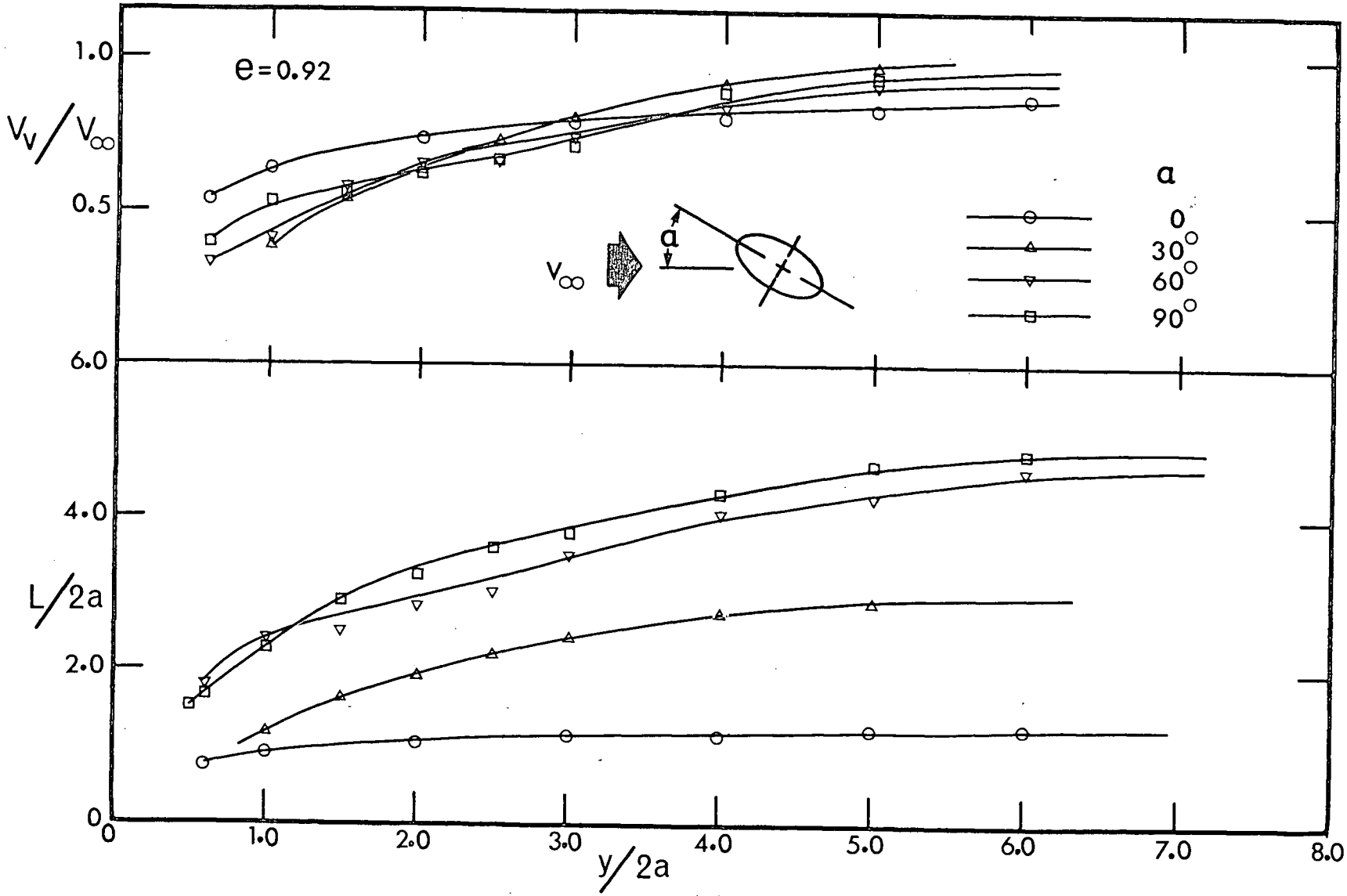

Figure 5-19 Streamwise variation of longitudinal vortex spacing and vortex velocity: (c) e = 0.92

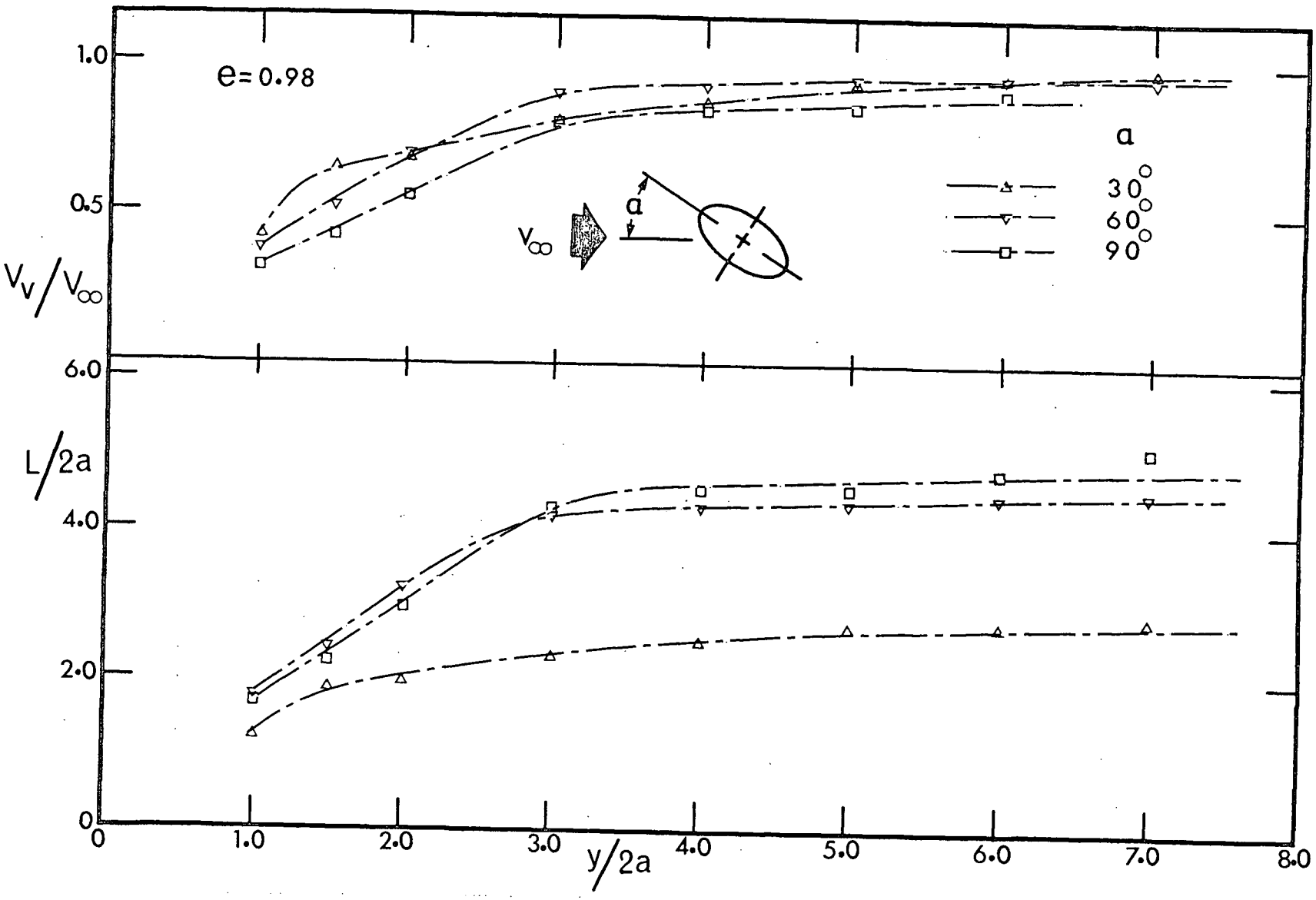

Figure 5-19 Streamwise variation of longitudinal vortex spacing and vortex velocity: (d) e = 0.98

Figure 5-20 summarises the dependence of longitudinal spacing at two extreme attitudes of the models. As can be expected, the effect of eccentricity at $\alpha=90°$ is relatively small. On the other hand, the plots at $\alpha=0$ show significant dependence on eccentricity. At a given station, the longitudinal spacing increases as the cylinder becomes more slender, which also promotes early attainment of its uniform value. For the ellipses of e=0.92 and 0.44, the near infinity values were reached approximately three and five diameters downstream, respectively. It may be mentioned here that basing downstream distance and longitudinal spacing on minor axis showed reduction in latter's variation with e at $\alpha=0$. In particular the near infinity value of the parameter was found to be $\simeq 4$ except for e=0.92 in which case it was 3.2. For other angles of attack the values ranged between 4.0 and 5.5.

Table 5-4 presents the results on uniform values attained by longitudinal spacing and vortex velocity as a function of cylinder attitude and eccentricity. It is apparent that longitudinal spacing diminishes with increase in eccentricity at small angles of attack. However, at $\alpha=60°$ and 90°, no definite trend can be observed although, in general, the variation is relatively small. The variation of vortex velocity does not seem to follow any systematic behavior and for the cases investigated its non-dimensional value was confined to the range 0.77-0.97.

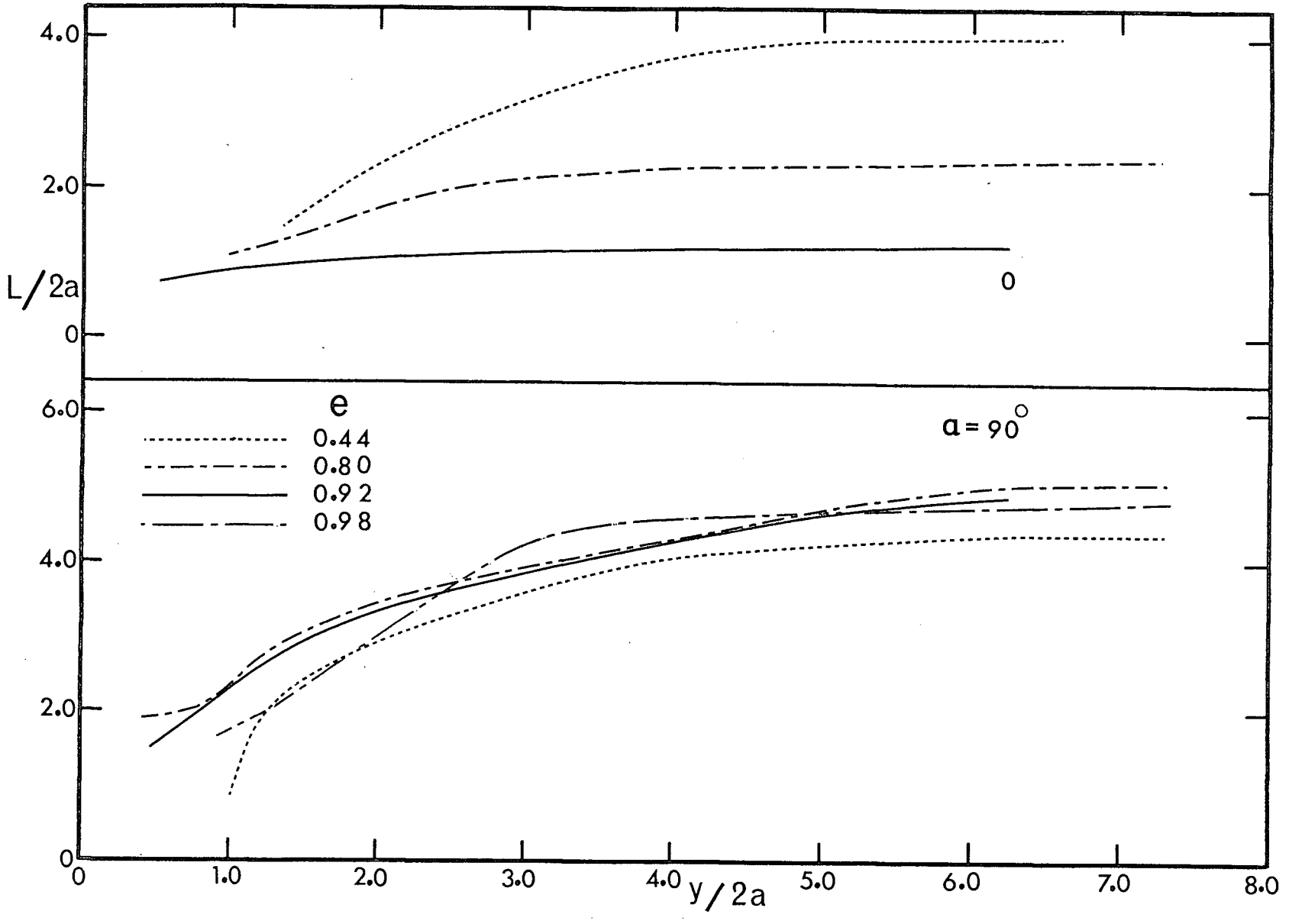

Figure 5-20 Dependence of longitudinal spacing on eccentricity at extreme values of angle of attack

Table 5-4 Variation of longitudinal vortex spacing and vortex velocity with eccentricity and angle of attack

e	$\alpha=0$		$\alpha=30°$		$\alpha=60°$		$\alpha=90°$	
	$(L/2a)_\infty$	$(V_v/V_\infty)_\infty$	$(L/2a)_\infty$	$(V_v/V_\infty)_\infty$	$(L/2a)_\infty$	$(V_v/V_\infty)_\infty$	$(L/2a)_\infty$	$(V_v/V_\infty)_\infty$
0*	4.27	0.80						
0.44	4.1	0.95	4.2	0.92	4.8	0.96	5.0	0.97
0.60†	3.2	0.86	3.9	0.93	4.4	0.94	4.6	0.93
0.80	2.4	0.89	3.3	0.90	4.7	0.90	5.1	0.90
0.92	1.3	0.86	3.0	0.97	4.7	0.92	4.9	0.96
0.98	-	-	2.8	0.96	4.5	0.95	4.8	0.90
∞^Δ	-	-	2.8	0.84	4.5	0.76	5.2	0.77

*Fage and Johansen[88], †Modi and Wiland[57], ΔFage and Johansen[70]

The lateral variations of the fluctuating pressure amplitude in the wake at various downstream stations is presented in Figure 5-21. As expected, the unsteady pressure distributions are similar on both sides of the wake for symmetrically oriented models. The wake centreline, thus, coincides with the y-axis. However, for other orientations, the wake is unsymmetrical with the higher peak value on the side for which the separation of the shear layer is more rearward. Similar behavior was also observed by Slater[27] in his study with structural angle section. As the vorticity rate associated with the upper and lower surfaces of a body is the same[88], the presence of higher pressure peak on one side may be explained by relatively shorter distance and hence reduced dissipation suffered by the corresponding vortex. Figure 5-22 shows the position of the wake obtained by considering, approximately, the location of peak fluctuation as the position of the vortex core. However, as pointed out by Hooker[89], the maximum velocity fluctuations (and hence pressure variations) do not occur along the path of vortex centres as some experimenters have asserted but rather develop in the neighbourhood of the core farthest from the street centreline. Thus, the distance between the peaks as presented here would overestimate the wake width by an amount equal to the diameter of the vortex core. Based on Schaefer and Eskinazi's[14] mathematical model for vortex street in

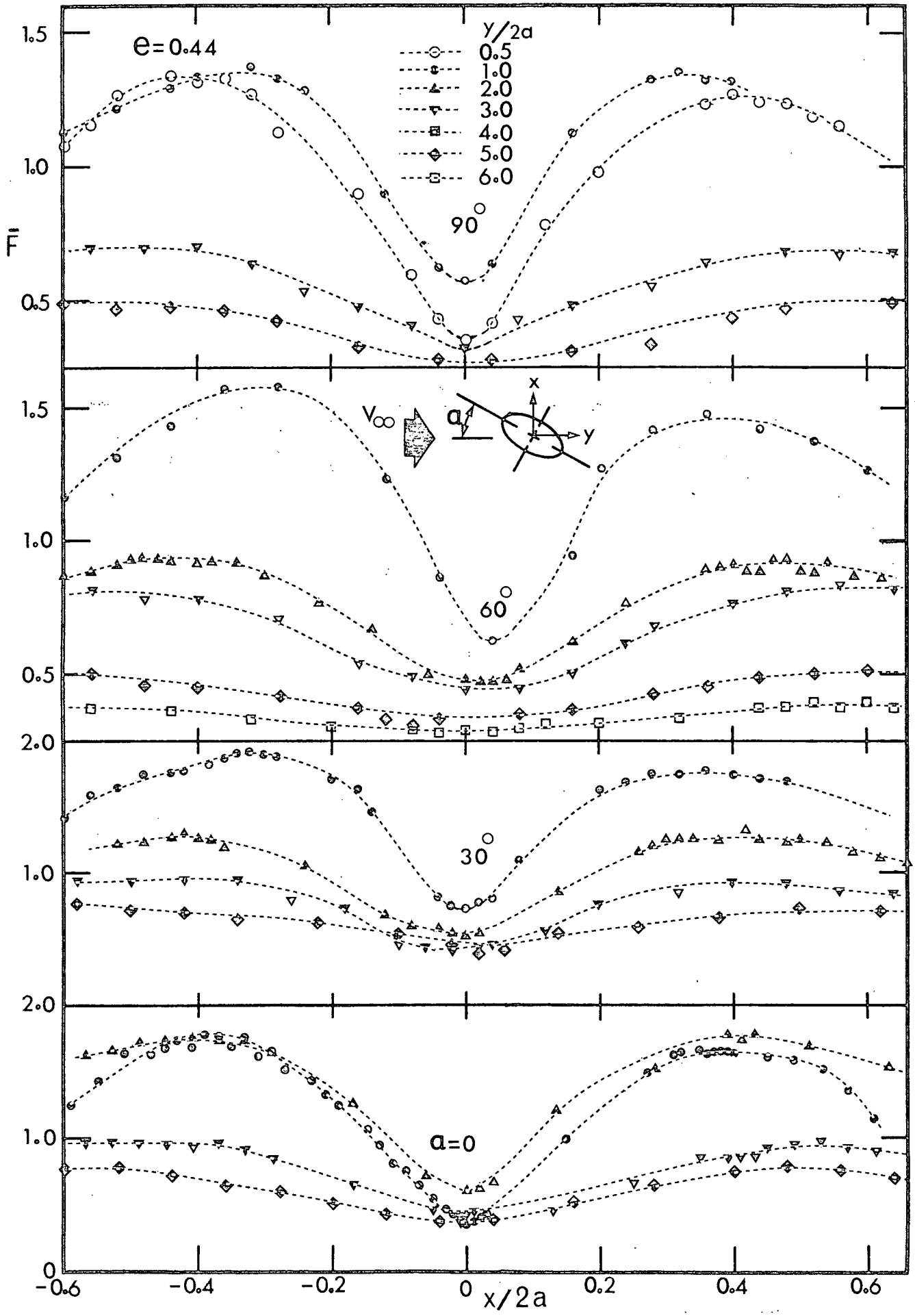

Figure 5-21 Lateral variation of the fluctuating pressure in the wake of elliptic cylinders: (a) e = 0.44

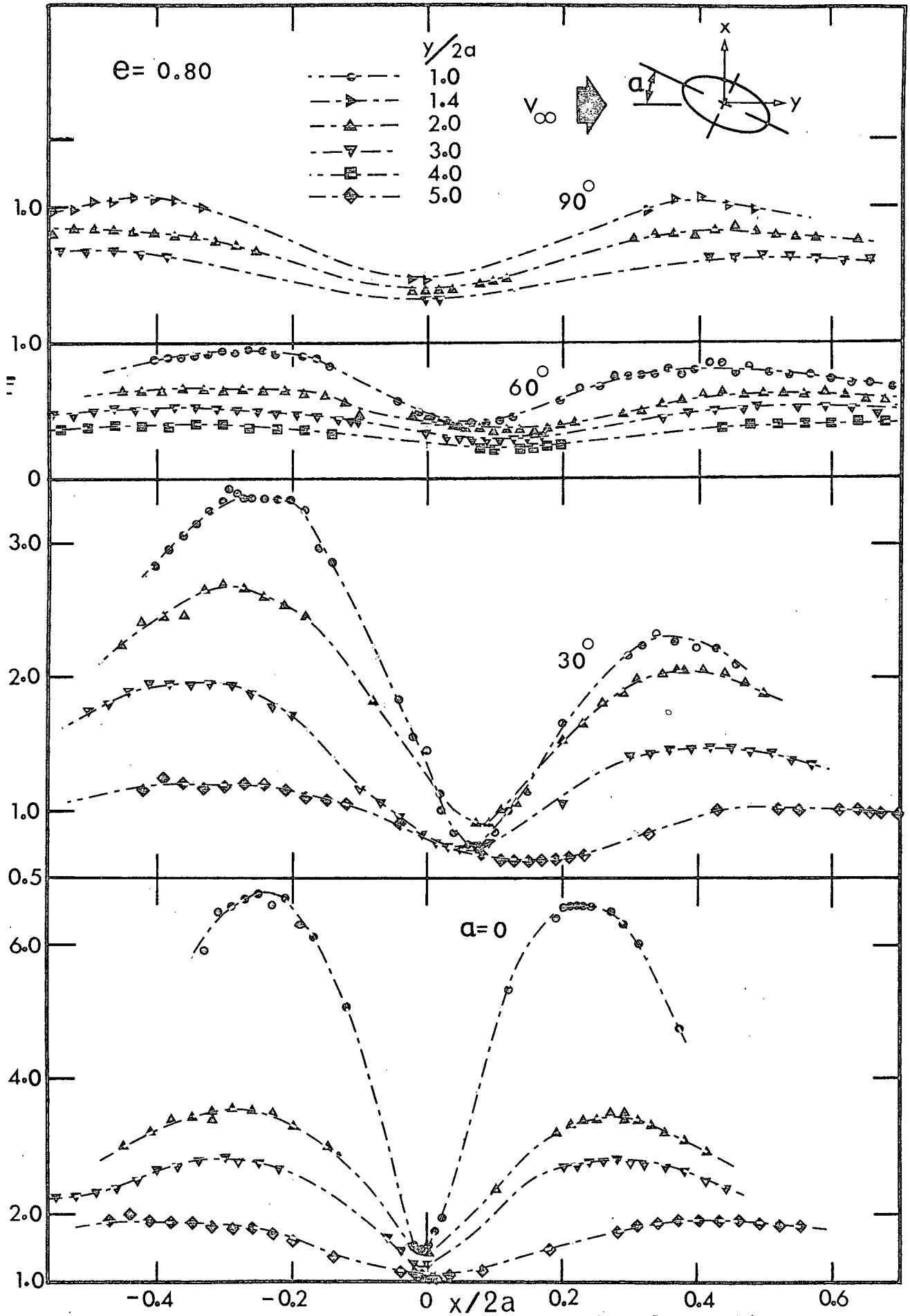

Figure 5-21 Lateral variation of the fluctuating pressure in the wake of elliptic cylinders: (b) e = 0.80

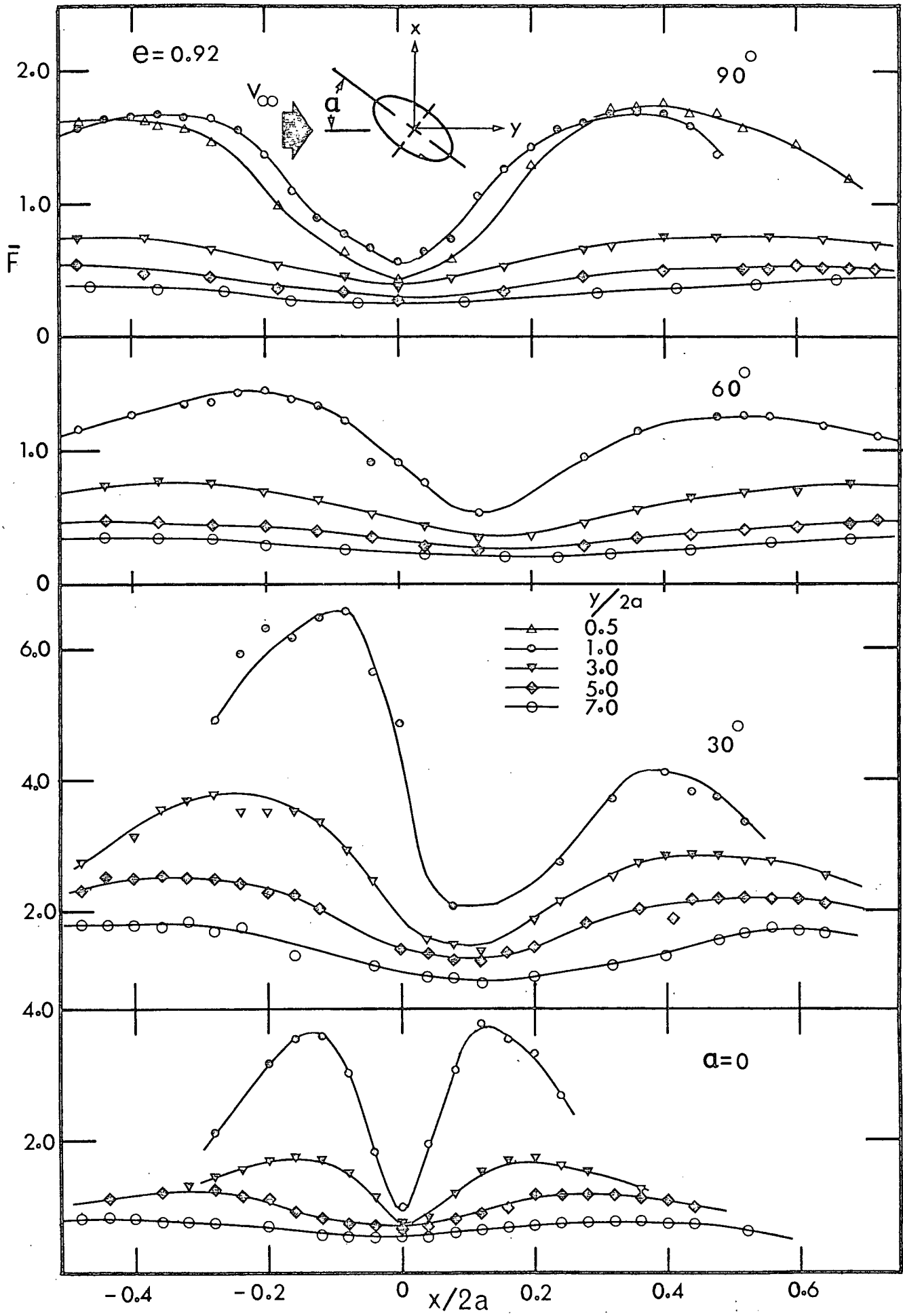

Figure 5-21 Lateral variation of the fluctuating pressure in the wake of elliptic cylinders: (c) e = 0.92

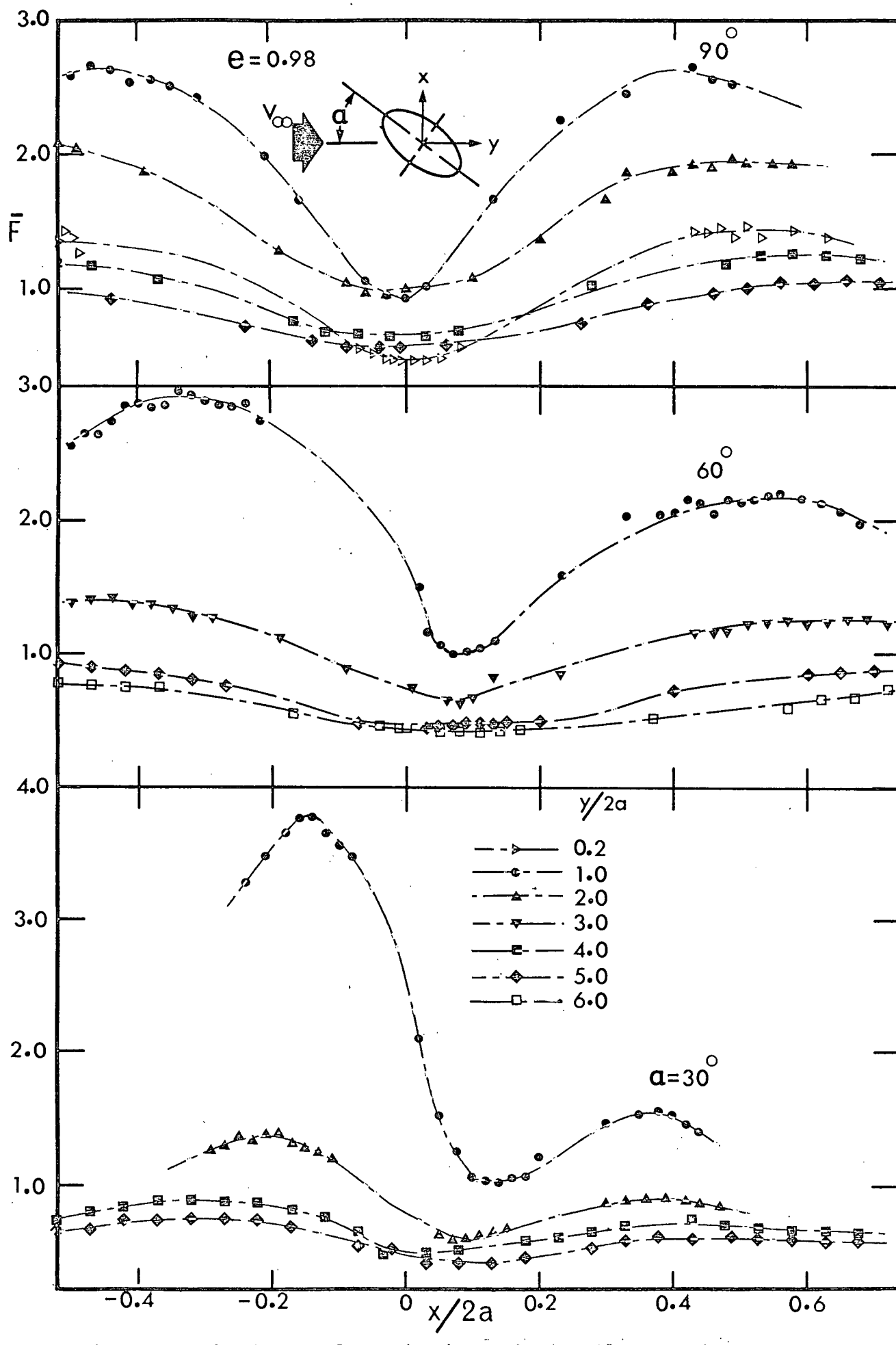

Figure 5-21 Lateral variation of the fluctuating pressure in

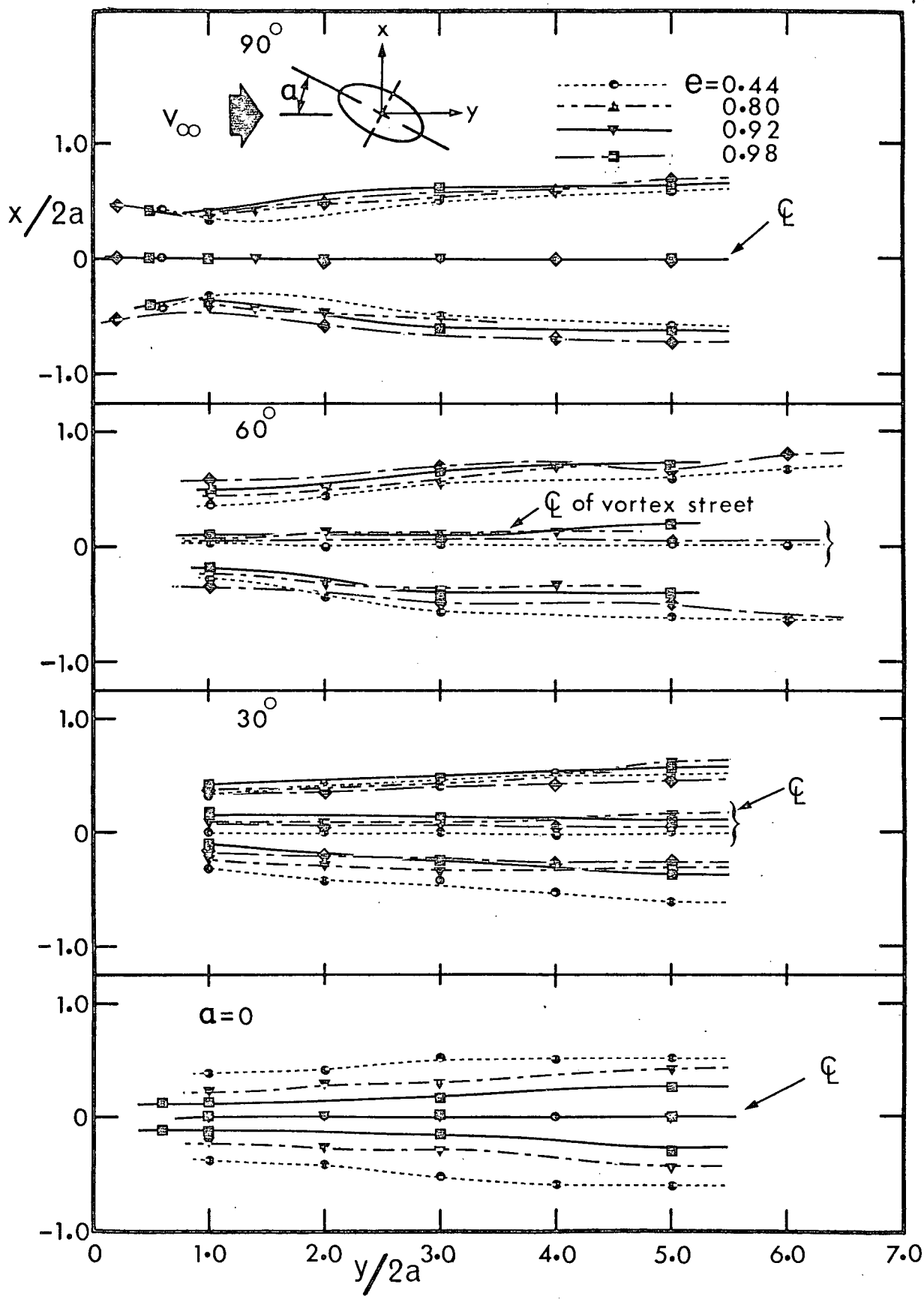

Figure 5-22 Lateral position of vortex cores behind elliptic cylinders

viscous fluid showed correction in the wake width to be negligible (<1%) at the model and less than 5% eight diameters downstream. It may be pointed out, however, that the correction would fail far downstream as it does not account for turbulence or wake instability which would influence the position and growth of the vortex cores.

The variation of the lateral spacing with downstream distance is presented in Figure 5-23 for various ellipses as a function of angle of attack. It is apparent that both the model geometry and attitude have substantial effect on the spacing between the vortex rows. In general, the spacing increased with downstream coordinate except for the short formation region, and in some cases failed to attain the uniform value within the limit of the traverse. As pointed out by several investigators[13,70,90], vortices do not flow downstream indefinitely in parallel rows but always move away from the centreline with increasing y even when an intermediate sequence of vortices have some uniformity of configuration. This point is well emphasized by the wake width results for flat plate[70], circular[91] and elliptic cylinders presented in Table 5-5.

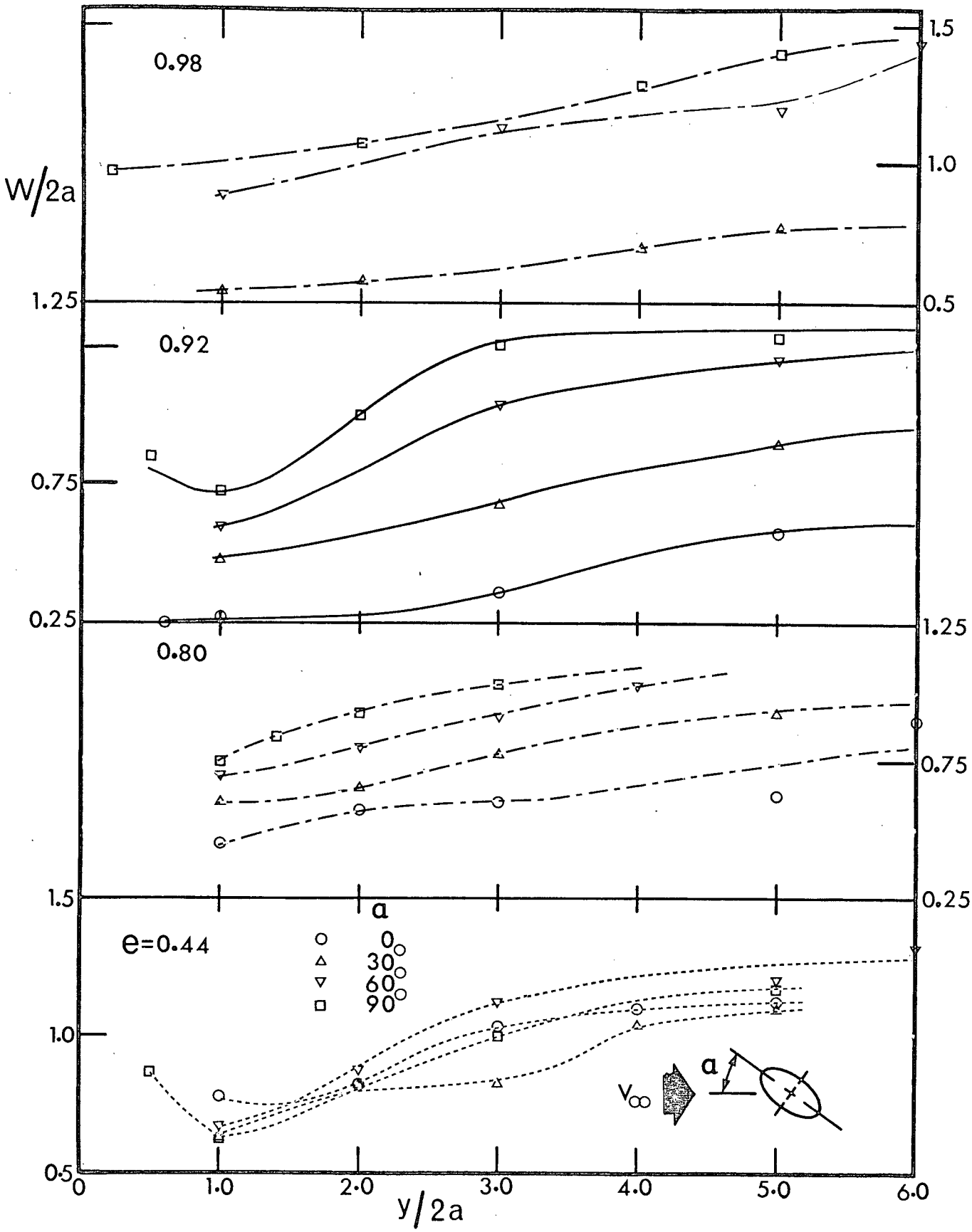

Figure 5-23 Variation of lateral vortex spacing with downstream coordinate and angle of attack

Table 5-5 Variation of lateral spacing with downstream coordinate for several bluff bodies

circular cylinder,† e=0,R=4,900		elliptic cylinder e=0.92,α=90°,R=68,000		flat plate* e=∞,α=90°,R=31,000	
y/2a	w/2a	y/2a	w/2a	y/2a	w/2a
3.22	1.06	1.0	0.72	5.0	1.30
4.60	1.19	3.0	1.20	10.0	2.00
7.00	1.34	5.0	1.20	20.0	2.75
8.80	1.40	7.0	1.40		

†Tyler[91], *Fage and Johansen[70]

Longitudinal and lateral spacing results may be combined to obtain classical wake geometry parameter, W/L (Figure 5-24). With increase in downstream coordinate, in general, there is a drop in the value up to, approximately, 2-4 diameters downstream followed by a region of constant value and finally a tendency towards rise in W/L. In particular for e=0.98, the ratio ranged between 0.4 to 0.6 at y/2a=1.0, diminished to ≃0.3 in the vicinity of y/2a=4.0 and showed upward trend thereafter. This corresponds reasonably well with Kármán's observation of W/L ≃0.36 behind the body approaching the value 0.281 farther downstream. A rise in the wake geometry ratio when far downstream is also reported by several investigators[70,90]

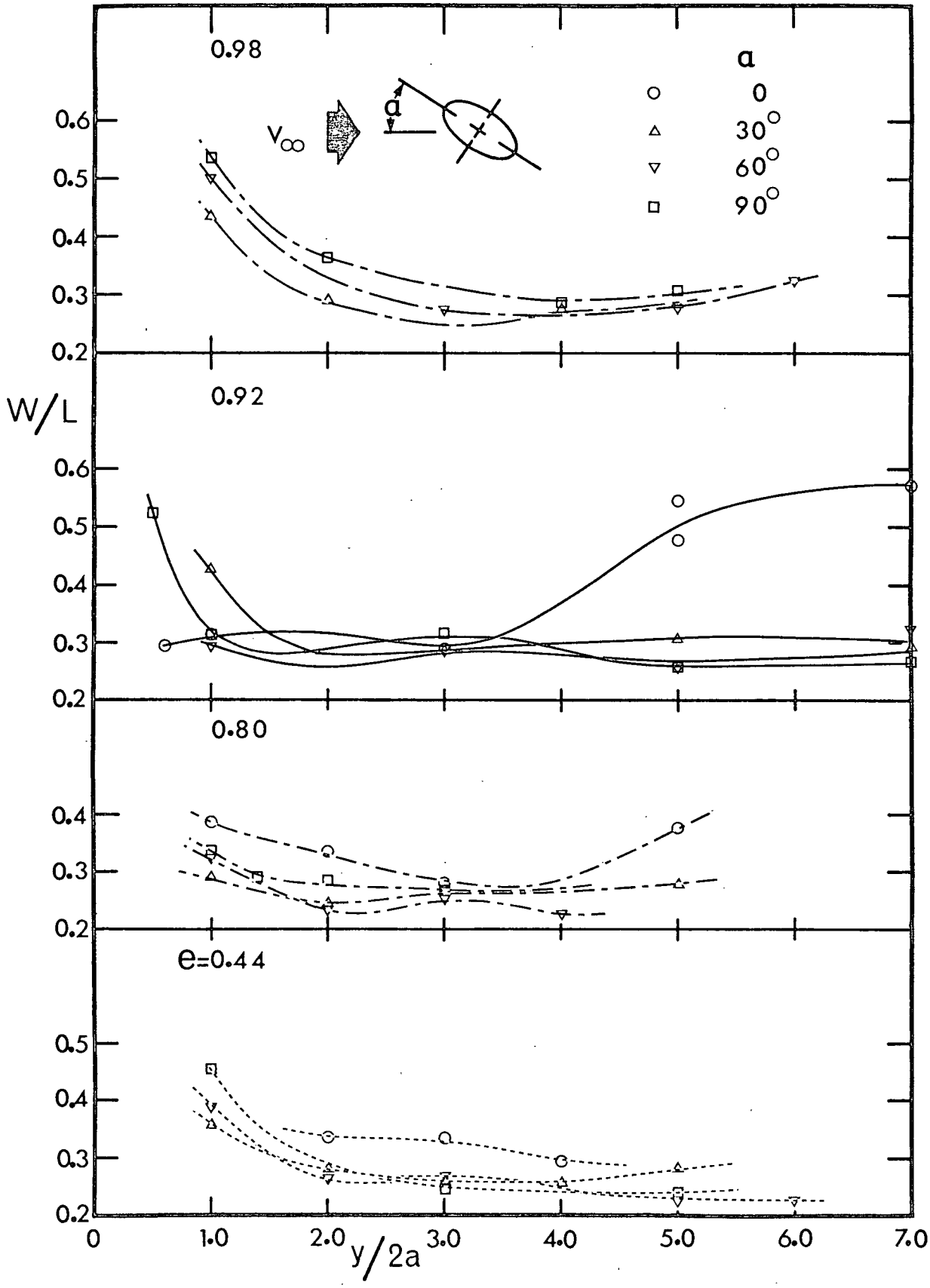

Figure 5-24 Wake geometry ratio for elliptic cylinders as a function of downstream distance

in the flat plate and circular cylinder studies. In fact Fage and Johansen[70], in their experiment with flat plate normal to the flow, found W/L to increase by more than 100% over the downstream distance of 5-20 plate widths. It is of interest to note that the location of minimum wake geometry ratio seems to move downstream with increase in eccentricity of an ellipse. The wake width did not show any well defined dependence on cylinder attitude.

The near infinity values for the wake width and geometry ratio as affected by cylinder eccentricity and attitude are summarised in Table 5-6. The quoted figures occur around six to seven diameters downstream. For $\alpha=0$, the wake width diminishes with increase in eccentricity, however, the wake geometry ratio increases suggesting greater reduction in longitudinal spacing. Essentially the same behavior was observed at $\alpha=30°$. No clear pattern can be discerned at $\alpha=60°$, however, at higher attitude, there appears to be a complete reversal in the trend of $(W/2a)_\infty$ observed earlier. Furthermore, the wake geometry ratio remains reasonably close to Kármán's stability value of 0.281.

It would be appropriate to emphasize a degree of similarity in the variation of $(h/L)_\infty$, $(W/L)_\infty$, S_h and $(1/C_{D_h})$ with model orientation. This is shown in Figure 5-25. In general, they appear to attain the peak value at $\alpha=0$, diminsh with increase in angle of attack to reach

Table 5-6 Dependence of lateral vortex spacing and wake geometry ratio on eccentricity and angle of attack

e	$\alpha=0$		$\alpha=30°$		$\alpha=60°$		$\alpha=90°$	
	$(w/2a)_\infty$	$(W/L)_\infty$	$(w/2a)_\infty$	$(W/L)_\infty$	$(w/2a)_\infty$	$(W/L)_\infty$	$(w/2a)_\infty$	$(W/L)_\infty$
0*	1.3-1.8	0.24-0.28						
0.44	1.12	0.27	1.10	0.26	1.28	0.27	1.14	0.23
0.60†	1.0	0.31	1.04	0.27	1.14	0.26	1.16	0.25
0.80	0.90	0.38	0.96	0.29	1.12	0.24	1.20	0.24
0.92	0.62	0.48	0.96	0.32	1.25	0.27	1.32	0.27
0.98	-	-	0.78	0.28	1.25	0.28	1.45	0.30
∞^Δ							1.65	0.32

*Schaefer and Eskinazi[14], †Modi and Wiland[57], ΔFage and Johansen[70]

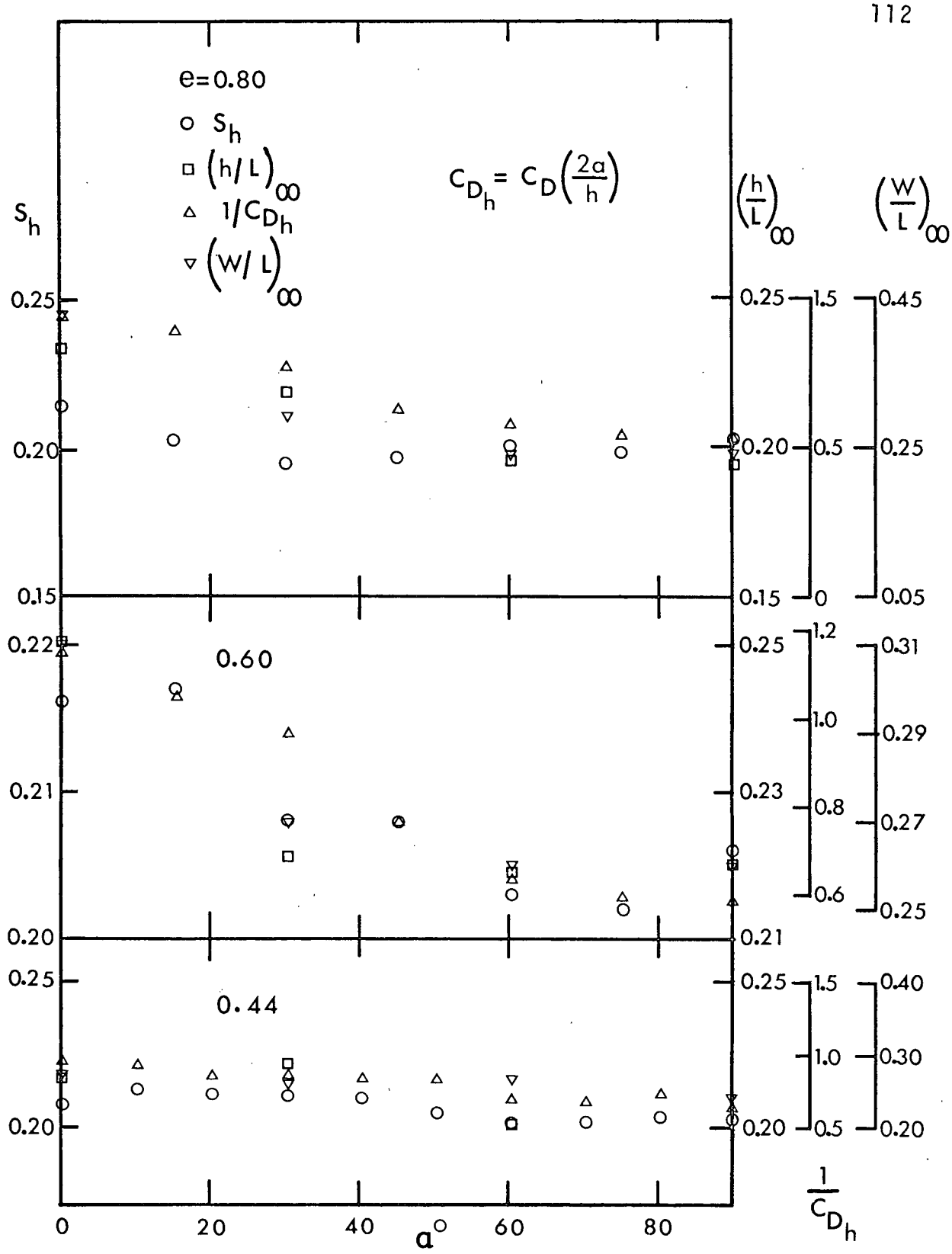

Figure 5-25 Variation of Strouhal number, drag coefficient and near infinity values of wake parameters with cylinder attitude: (a) e = 0.44, 0.60, 0.80

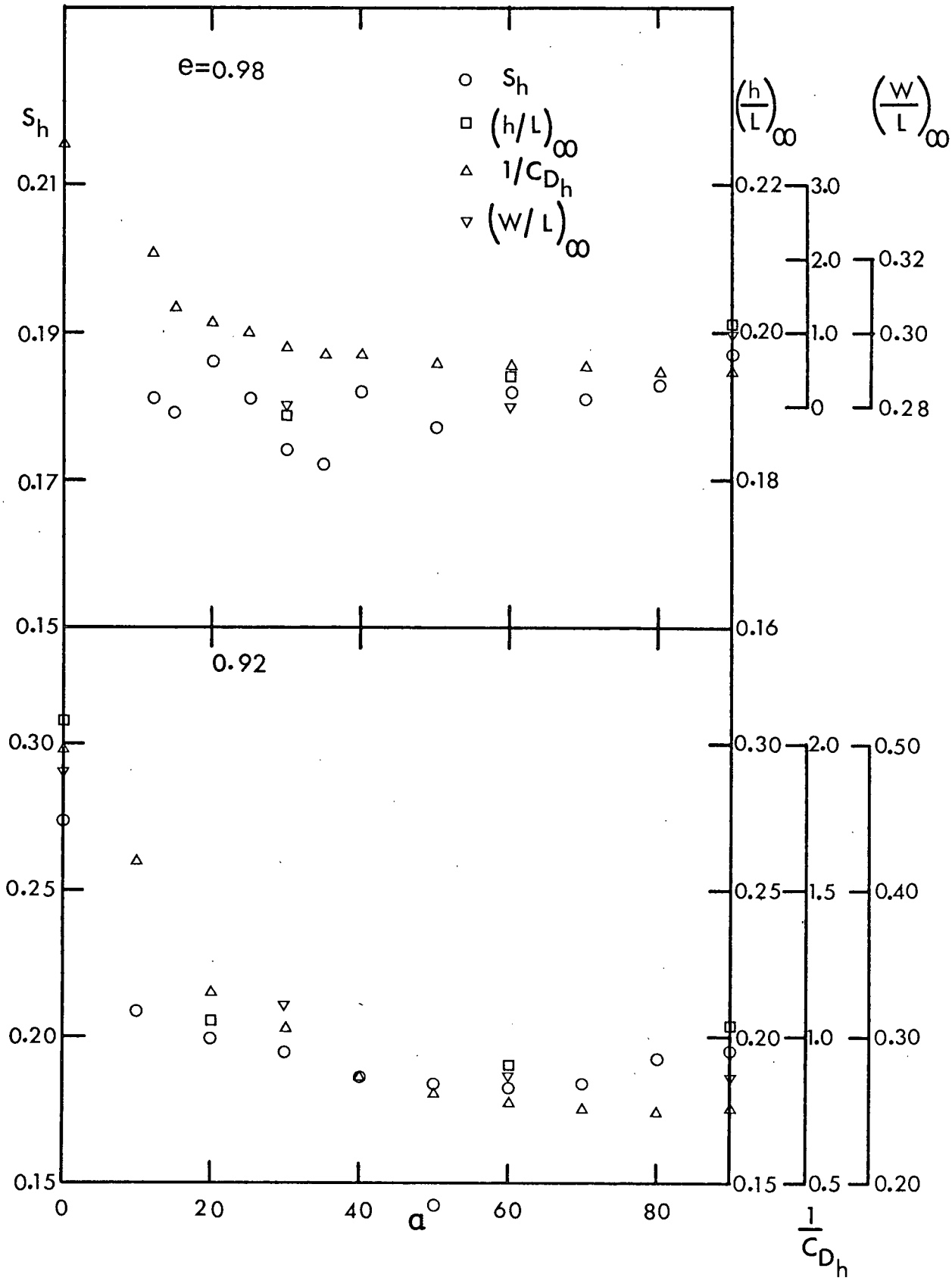

Figure 5-25 Variation of Strouhal number, drag coefficient and near infinity values of wake parameters with cylinder attitude: (b) e = 0.92, 0.98

a minimum around 50° followed by a small rise over the remaining range. Apparently, this suggests significant relationship between the wake geometry and body aerodynamics. The use of universal numbers in such a study by several authors may be attributed to the similar observation of wake-body interaction.

The results of lateral traverse also provide information about variation of peak fluctuating pressure with downstream coordinate (Figure 5-26). It appears that peak pressure amplitude attains a maximum value around one diameter downstream. The pressure decay that follows compares favourably with the analytical results obtained using vortex street model of Schaefer and Eskinazi[14]. Ferguson[66] (circular cylinder) and Slater[27] (structural angle section) also observed similar decay of unsteady pressure in the wake. However, a systematic study of its rise and decay in the downstream direction and as a function of cylinder eccentricity and attitude does not seem to be reported in literature. In general, the increase in angle of attack tends to move pressure peak upstream. This may suggest closer formation of the first vortex at higher angles of attack. The behavior was confirmed through flow visualisation.

Figure 5-27 shows typical frames from the high speed 16 mm. movie of the near wake region. It provides some information concerning the position of the first

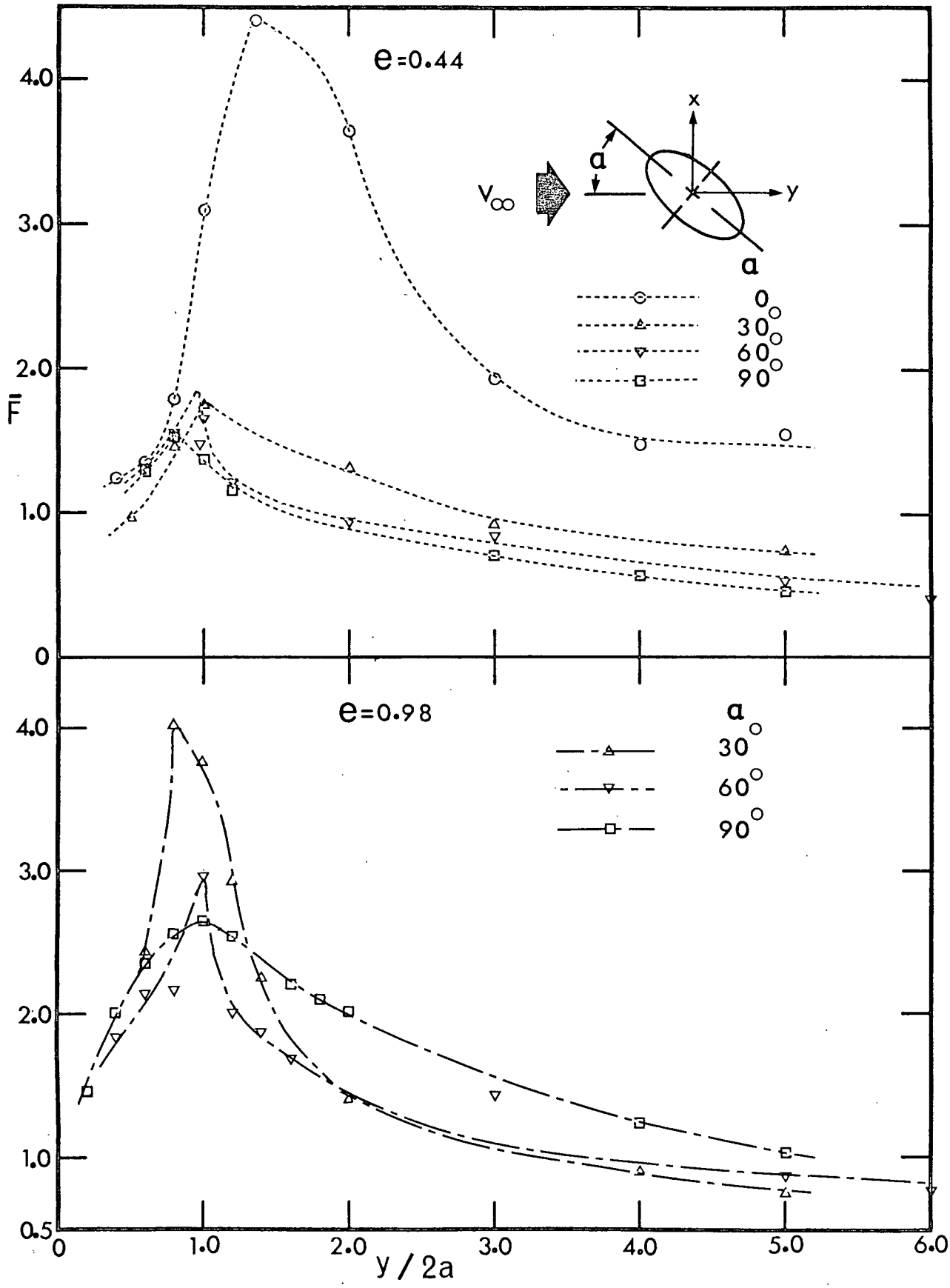

Figure 5-26 Variation of peak fluctuating pressure in the wake: (a) e = 0.44, 0.98

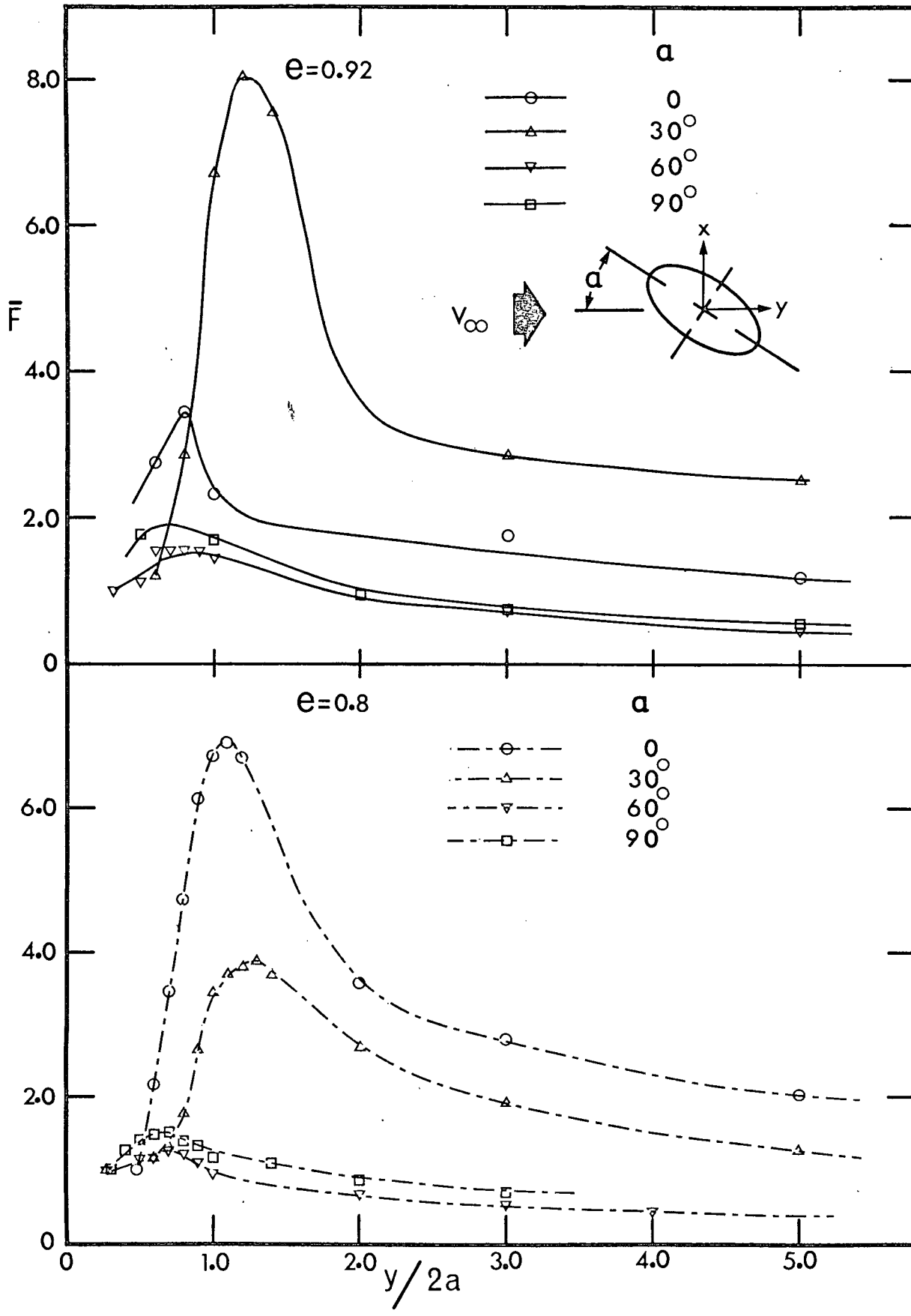

Figure 5-26 Variation of peak fluctuating pressure in the wake: (b) e = 0.92, 0.80

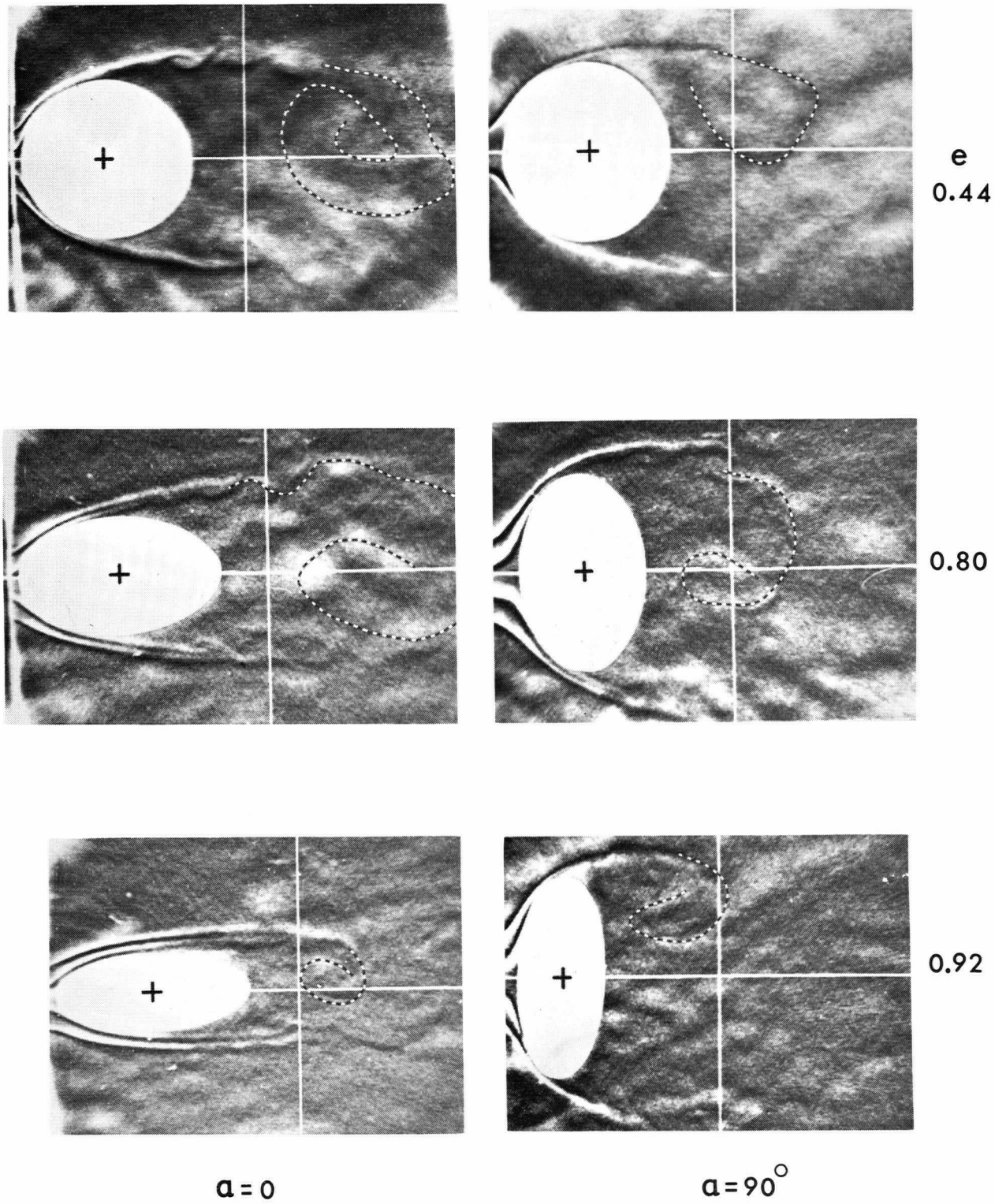

Figure 5-27 Visual study of near wake showing:
(a) position of the first vortex as affected by angle of attack

e=0.60

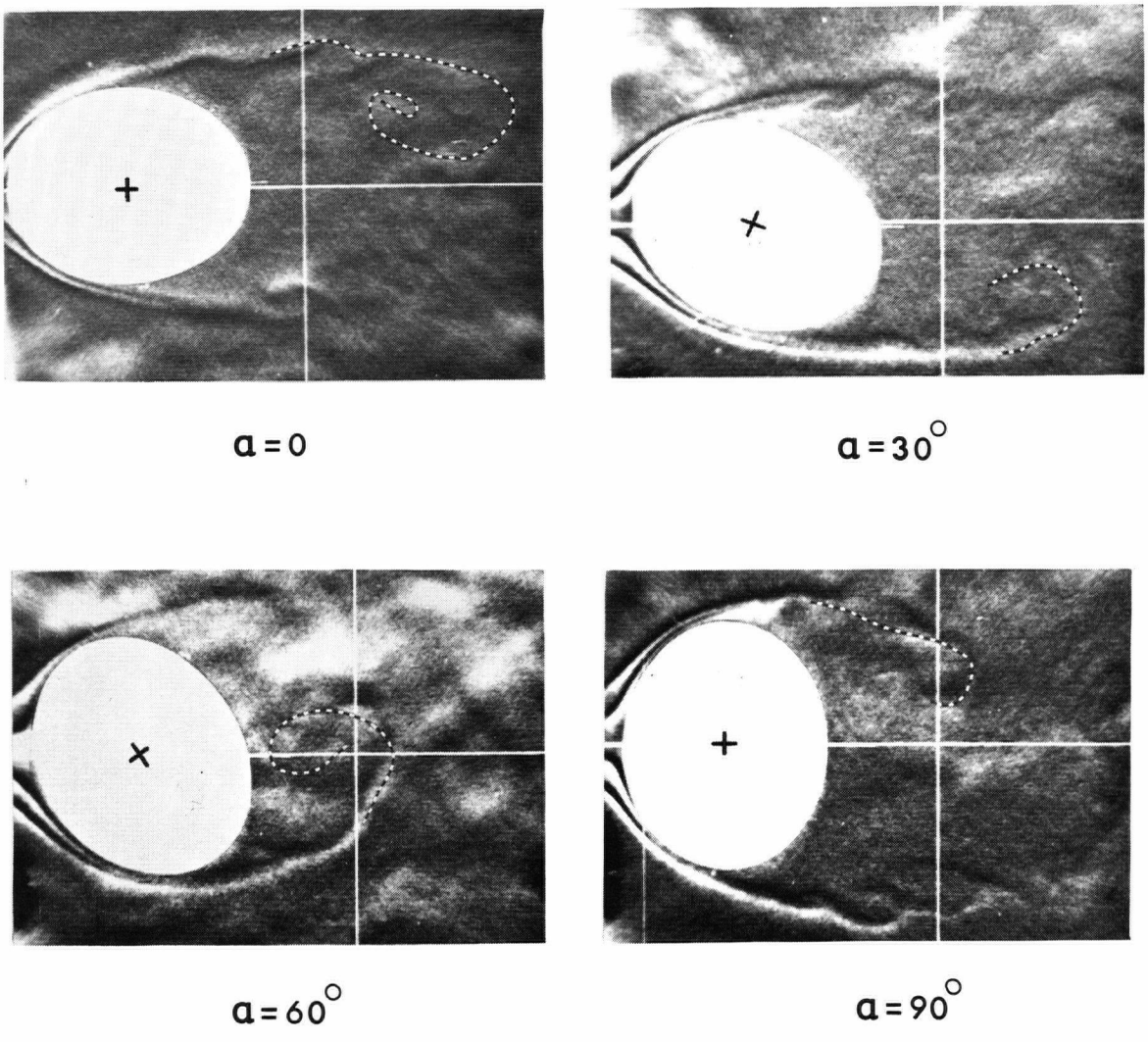

Figure 5-27 Visual study of near wake showing:
(a) position of the first vortex as affected by angle of attack

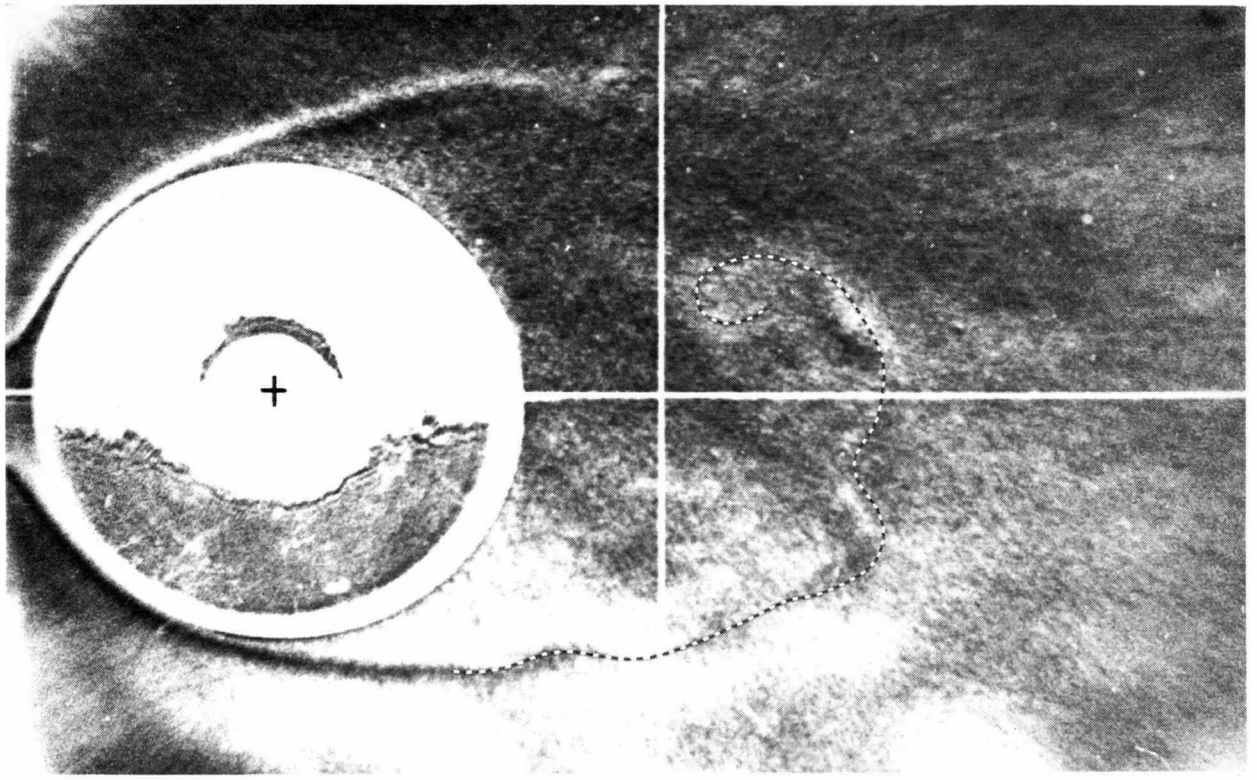

e = 0

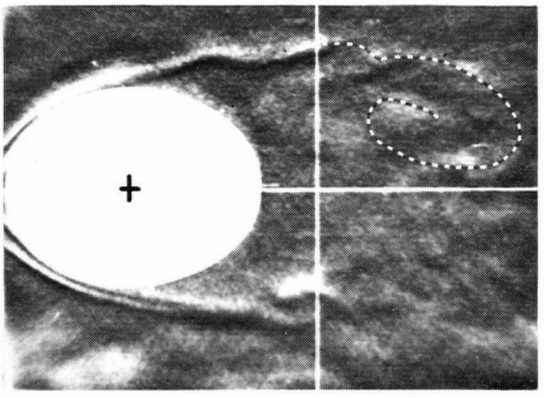

e = 0.60; α = 0

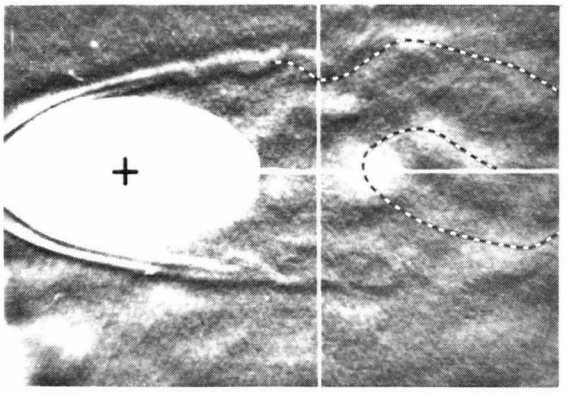

e = 0.80; α = 0

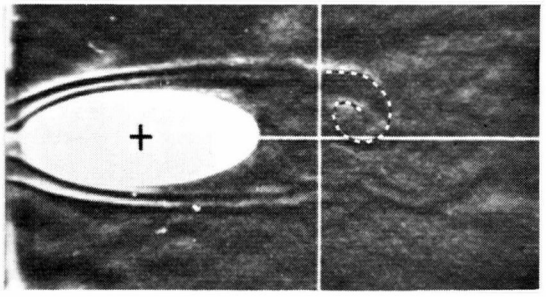

e = 0.92; α = 0

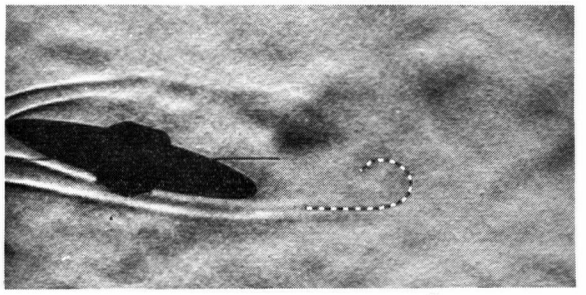

e = 0.98; α = 15°

Figure 5-27 Visual study of near wake showing:
(b) effect of eccentricity

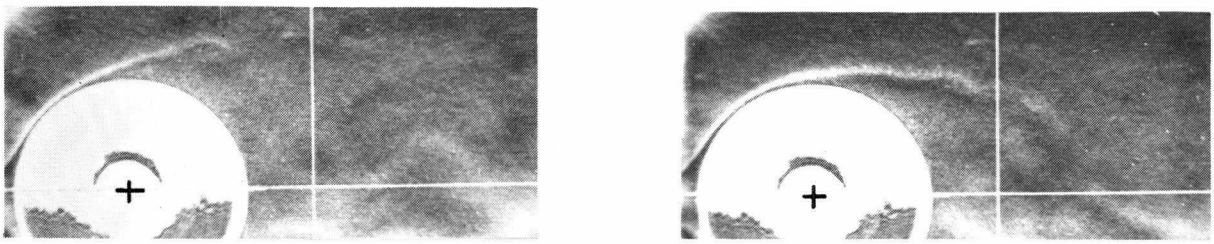

e=0

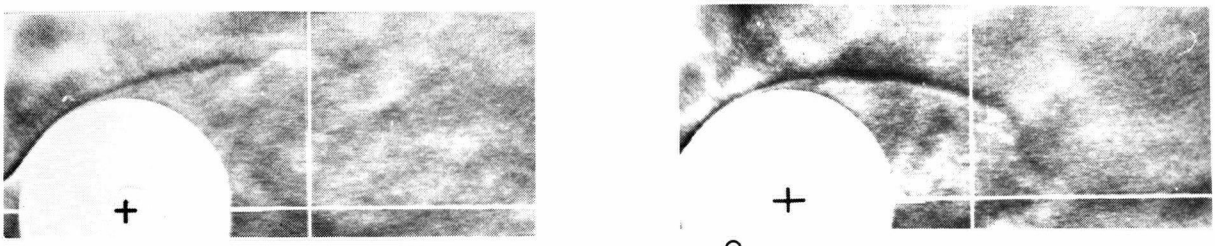

e=0.44 ; α=90°

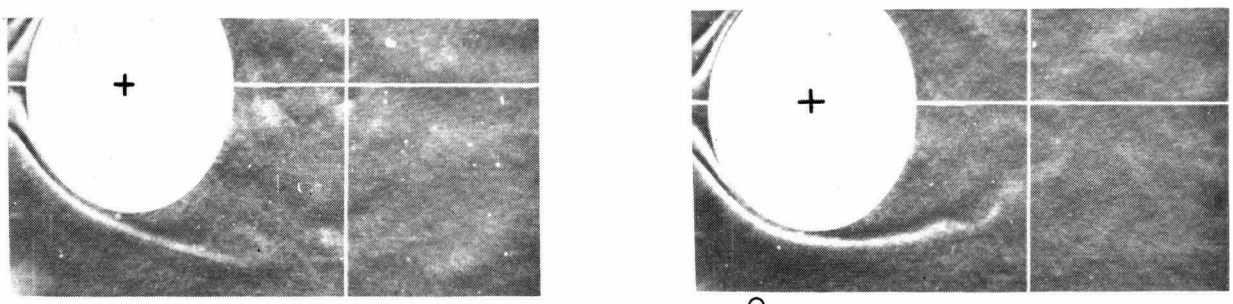

e=0.60; α=90°

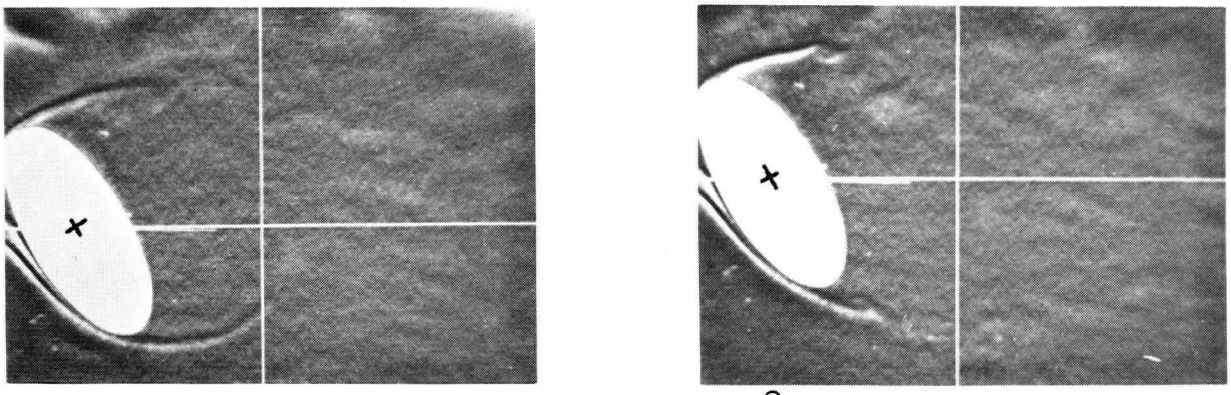

e=0.92 ; α=60°

Figure 5-27 Visual study of near wake showing:
(c) unsteady character of shear layer

vortex and hence the vortex formation length[21,92] as affected by cylinder eccentricity and angle of attack. Several aspects of interest become apparent:

(i) The photographs suggest that the first vortex is located around 0.75-1.5 diameters downstream from the cylinder axis. This is in agreement with the location of pressure peaks in Figure 5-26.

(ii) A comparison of vortex positions at α=0 and 90° for a set of ellipses shows forward movement of the first vortex at higher angles of attack. This, in general, confirms the trend indicated by pressure peaks in the wake. On the other hand, no conclusive remarks can be made about the effect of eccentricity at the same angle of attack.

(iii) The unsteady character of the position of separation is quite evident. For circular cylinder it was observed to be, approximately, over the range of 70° to 88°. This movement is accompanied with the periodic change in the inclination of separating shear layer.

These observations on the near wake should be considered preliminary and hence only indicative of qualitative features of the phenomenon.

6. CONCLUDING REMARKS

Based on the experimental results the following general remarks can be made concerning the unsteady aerodynamics of the stationary elliptic cylinders:

(i) The mean lift, drag and pitching moment show considerable dependence on angle of attack and eccentricity of an ellipse. However, they are substantially independent of the Reynolds number in the range 2×10^4-10^5. The balance results compare favourably with the pressure integrated steady aerodynamic coefficients thus indicating two-dimensional character of the mean flow. The plots suggest that the ellipse with eccentricity of 0.98 is susceptible to galloping type of instability in the vicinity of $\alpha=10°$.

(ii) Eccentricity and the attitude of the model affect mean pressure distribution on its surface substantially. The location of minimum pressure on the top surface moves forward while that on the lower surface moves rearwards with increase in angle of attack. However, this trend reverses at around 40°. The study of separating shear layer through flow visualisation using Schlieren technique

confirmed this trend. The agreement between the analytical data on the separation points, obtained using Görtler's series solution, and the experimental values appears to be quite acceptable.

(iii) The Strouhal frequency increases linearly with wind speed in the Reynolds number range of $2x10^4$-10^5. Strouhal number exhibits considerable dependence on the cylinder eccentricity and angle of attack, ranging from 0.037 (e=0.98, α=90°) to 0.274 (e=0.92, α=0). The variation of Strouhal number can be reduced by basing it on the projected dimension, wake width or transverse distance between separation points. Roshko's criterion provides satisfactory collapse around the value of 0.164 except for the slender ellipses at small angles of attack. However, S_S has the advantage of offering the smoother trend even at low angles of attack for ellipses of high eccentricity.

(iv) The midspan fluctuating pressure distribution is essentially independent of the Reynolds number except for the ellipses at α=0 in the range $2.5x10^4$-10^5. In general, for a given ellipse, the maximum fluctuating pressure coefficient increases with increase in angle of attack. The pressure signals are always amplitude modulated although

the extent of modulation is less in the laminar region. Considerable phase difference can exist even between the pressure signals on the same side of the model. For the slender ellipse of e=0.92, at α=0, the phase change as large as 65° was recorded.

(v) In general, the fluctuating lift coefficient increases with increase in angle of attack reaching maximum value around 70°-80°, beyond which it tends to drop. Highest fluctuating lift recorded was $\simeq$1.0 for e=0.60. The phase between the pressure signals has negligible effect on unsteady lift data.

(vi) The unsteady aerodynamics of elliptic cylinders exhibits three dimensional character, fluctuating pressure and phase being substantially dependent on spanwise location. Average inclination of vortex lines was found to be around 0-11° with improved alignment with the cylinder axis at higher angles of attack.

(vii) Both longitudinal and lateral spacings between the vortices are substantially independent of the Reynolds number in the range 3×10^4-10^5.

Longitudinal spacing between vortices increases rapidly behind the model and attains a constant value around seven diameters (limit of the traversing gear) downstream.

It increases with increase in angle of attack, the larger change being associated with high eccentricity ellipses. The vortex velocity has relatively small dependence on attitude and eccentricity of an ellipse.

The lateral spacing continues to increase with downstream coordinate, for some cases even beyond the limit of traverse. At small angles of attack, the effect of increase in eccentricity is to diminish the wake width. However, at $\alpha=90°$, the trend undergoes a complete reversal.

A certain amount of similarity can be discerned between the variation of $(h/L)_\infty$, $(b/a)_\infty$, S_h and $1/C_{D_h}$ with angle of attack. This emphasizes the interaction between wake geometry and body aerodynamics. In general, the wake geometry ratio remains close to Kármán stability value of 0.281.

(viii) The rise and decay of fluctuating pressure in the wake suggests formation of the first vortex to occur in the vicinity of one diameter downstream. The flow visualisation confirms this observation.

(ix) The high speed photography indicates, qualitatively, unsteady character of position and inclination of the separating shear layers.

7. RECOMMENDATIONS FOR FUTURE WORK

The concept of a systematic change of eccentricity to cover a wide range of geometrical shapes, though attractive, does not seem to have received sufficient attention in the study of bluff body aerodynamics. Through the investigation presented here come to light several areas where available information is limited thus suggesting possible course for future research. Some of the more important problems are listed below:

(i) It would be useful to establish the limit of applicability of the Görtler's series approach for determining separation points, which, as pointed out in the text, could be used only in the analysis of cylinders at zero angle of attack, particularly for high eccentricity ellipses. The probable limiting factor is likely to be steep pressure gradients on the surface of the model at higher angles of attack. The use of more terms in ξ series may extend the limit of applicability of this approach. The study would require, obviously, measurement of mean pressure distribution at finer interval of attitude.

(ii) The dependence of fluctuating pressure on the Reynolds number at $\alpha=0$ should be explored further.

Although the preliminary results suggest correlation between this behaviour and base pressure, a detailed investigation is necessary to prove it conclusively. Apparently, the phenomenon is likely to be associated with changes in separation and near wake condition. The measurement of instantaneous fluctuating pressure or shear stress with a view to establish excursion of the separation points, and the length of formation region as discussed by Gerrard[21] may throw some light on this unexplained behaviour. Flow visualisation studies may also prove to be of some use.

(iii) A systematic study of the three dimensional character of flow around elliptic cylinders as a function of end conditions, eccentricity and attitude should provide information of fundamental interest. The investigation of pressure correlation length in spanwise direction and inclination of vortex filament would supplement the existing information on circular cylinder presented by Prendergast[36], el Baroudi[37], Toebes[39], Koopmann[40,41] et al.

(iv) A systematic study of wake associated with circular and elliptical cylinders with particular emphasis on far downstream behaviour would be relevent.

(v) The aerodynamics and dynamics of elliptic cylinders in vortex induced and galloping mode of oscillations appear to be the logical extension of this study.

BIBLIOGRAPHY

1. Strouhal, V., "Über eine besondere Art der Tonerregung," Wied. Ann. Physik u. Chem., Neue Folge, Vol. V, 1878, pp. 216-251.

2. Kármán, Th. Von.,"Flüggigkeit u. Luftwiderstand," Phys. Ż., Vol. 13, 1911, p. 49; "Über den Mechanismus des Flüssigkeits -und Luftwiderstandes," Physik. Ż., Vol. 13, 1912, pp. 49-59; "Über den Mechanismus des Widerstands, den ein bewegter Körper in einer Flüssigkeit erfährt," Göttinger Nachrichten, Math. Physik. Kl., 1911, pp. 509-519; and, 1912, pp. 547-556.

3. Heisenberg, W. Von.,"Die Absoluten Dimensionen der Kármánschen Wirbelbewegung," Physik. Ż., Vol. 23, 1922, pp. 363-366.

4. Bénard. H., "Hydrodynamique expérimentale-formation de centres de giration à l'arrière d'un obstacle en mouvement," Comptes Rendus (Académie des Sciences), Vol. 147, 1908, pp. 839-842; "Hydrodynamique experimentale-sur les lois de la fréquence des tourbillons atternés détachés derrière un obstacle," Comptes Rendus, Vol. 182, 1926, pp. 1375-1377; "Hydrodynamique expérimentale-sur l' inexatitude, pour les liquides réels, des lois théoriques de Kármán relatives á la stabilité des tourbillons alternés," Comptes Rendus, Vol. 182, 1926, pp. 1523-1525.

5. Roshko, A., "On the Drag and Shedding Frequency of Two-Dimensional Bluff Bodies," NACA, Tech. Note 3169, 1953.

6. Roshko, A., "On the Development of Turbulent Wakes From Vortex Streets," NACA, Tech. Note 2913, 1954.

7. Roshko, A.,"A New Hodograph for Free-Streamline Theory," NACA, Tech. Note 3168, July 1954.

8. Roshko, A., "On the Wake and Drag of Bluff Bodies," J. Aeronautical Sciences, Vol. 22, No. 2, February 1955, pp. 124-133.

9. Roshko, A., "Experiments on the Flow Past a Circular Cylinder at Very High Reynolds Number," J. Fluid Mech., Vol. 10, 1961, pp. 345-356.

10. Roshko, A., "Transition in Incompressible Near-Wakes," The Physics of Fluids Supplement, Vol. 10, No. 9, 1967, pp. S181-S183.

11. Kovásznay, L.S.G., "Hot-Wire Investigation of the Wake Behind Cylinders at Low Reynolds Numbers," Proc. Roy. Soc. of London, Series A, Vol. 198, 1949, pp. 174-190.

12. Rosenhead, L., "The Kármán Street of Vortices in a Channel of Finite Breadth," Phil. Trans., Series A, Vol. 228, June 1929, pp. 275-329.

13. Rosenhead, L. and Schwabe, M., "An Experimental Investigation of the Flow Behind Circular Cylinders in Channels of Different Breadths," Proc. Roy. Soc. of London, Series A, Vol. 129, 1930, pp. 115-135.

14. Schaefer, J.W. and Eskinazi, S., "An Analysis of the Vortex Street Generated in a Viscous Fluid," J. Fluid Mech., Vol. 6, 1959, pp. 241-260.

15. Gerrard, J.H.,"An Experimental Investigation of the Oscillating Lift and Drag of a Circular Cylinder Shedding Turbulent Vortices," J. Fluid Mech., Vol. 11, 1961, pp. 244-256.

16. Gerrard, J.H., "The Calculation of the Fluctuating Lift on a Circular Cylinder and its Application to the Determination of Aeolian Tone Intensity," AGARD Rep. No. 463, April, 1963.

17. Gerrard, J.H., "A Disturbance-Sensitive Reynolds Number Range of the Flow Past a Circular Cylinder," J. Fluid Mech., Vol. 22, Part I, 1965, pp. 187-196.

18. Gerrard, J.H., "The Three-Dimensional Structure of the Wake of a Circular Cylinder," J. Fluid Mech., Vol. 25, Part I, 1966, pp. 143-164.

19. Gerrard, J.H., "Numerical Computation of the Magnitude and Frequency of the Lift on a Circular Cylinder," Trans. Royal Society of London., Series A, Vol. 261, January 1967, pp. 137-162.

20. Gerrard, J.H., "Experimental Investigation of Separated Boundary Layer Undergoing Transition to Turbulence," The Physics of Fluids Supplement, Vol. 10, No. 9, 1967, pp. S98-S100.

21. Gerrard, J.H., "The Mechanics of the Formation Region of Vortices Behind Bluff Bodies," J. Fluid Mech., Vol. 25, Part 2, 1968, pp. 401-413.

22. Rosenhead, L., "Vortex Systems in Wakes," Adv. In Applied Mechanics, Vol. 3, 1953, pp. 185-195.

23. Wille, R., "Über Strömungserscheinungen im Übergangsgebiet von geordneter zu ungeordneter Bewegung," Jahrb. Schiffbautechn. Ges., Vol. 46, 1952, pp. 176-187.

24. Wille, R., "Kármán Vortex Streets," Adv. in Applied Mechanics, Vol. 6, 1960, pp. 273-287.

25. Marris, A.W., "A Review on Vortex Streets, Periodic Wakes, and Induced Vibration Phenomena," J. Basic Eng., ASME, Vol. 86, 1964, pp. 185-196.

26. Morkovin, M.V., "Flow Around Circular Cylinder-A Kaleidoscope of Challenging Fluid Phenomena," Sym. on Fully Separated Flows, ASME, 1964, pp. 102-118.

27. Slater, J.E., "Aeroelastic Instability of A Structural Angle Section," University of British Columbia, Ph.D.Thesis, March 1969.

28. McGregor, D.M., "An Experimental Investigation of the Oscillating Pressures on a Circular Cylinder in a Fluid Stream," University of Toronto Inst. of Aerophysics, Tech. Note 14, 1957.

29. Keefe, R.T., "An Investigation of the Fluctuating Forces Acting on a Stationary Circular Cylinder in a Subsonic Stream, and of the Associated Sound Field," University of Toronto Inst. of Aerophysics, Report 76, 1961.

30. Molineux, W.G., "Measurement of the Aerodynamic Forces on Oscillating Airfoils," AGARD Report 35, 1956.

31. Humphreys, J.S., "On a Circular Cylinder in a Steady Wind at Transition Reynolds Numbers," J. Fluid Mech., Vol. 9, 1960, pp. 603-612.

32. Fung, Y.C., "Fluctuating Lift and Drag Acting on a Cylinder in a Flow at Supercritical Reynolds Number," J. Aerospace Sciences, Vol. 27, No. 11, November 1960, pp. 801-814.

33. Grove, A.S., Shair, F.H., Peterson, E.E. and Acrivos, A., "An Experimental Investigation of the Steady Separated Flow Past a Circular Cylinder," J. Fluid Mech., Vol. 19, Part 1, 1964, pp. 60-80.

34. Bishop, R.E.D., and Hassan, A.Y., "The Lift and Drag Forces on a Circular Cylinder in a Flowing Fluid," Proc. Roy. Soc. of London, Series A, Vol. 277, 1964, pp. 32-50.

35. Ferguson, N. and Parkinson, G.V., "Surface and Wake Flow Phenomena of the Vortex-Excited Oscillation of a Circular Cylinder," ASME Vibration Conference, Paper 67-Vibr.-31, 1967.

36. Prendergast, V., "Measurement of Two-Point Correlations of the Surface Pressure on a Circular Cylinder," University of Toronto Inst. of Aerophysics, Tech. Note 23, 1958.

37. EL Baroudi, M.Y., "Measurement of Two-Point Correlations of Velocity Near a Circular Cylinder Shedding a Kármán Vortex Street," University of Toronto Inst. of Aerophysics, Tech. Note 31, 1960.

38. Mattingly, G.E., "An Experimental Study of the Three Dimensionality of the Flow Around a Circular Cylinder," University of Maryland, Tech. Note BN-295, 1962.

39. Toebes, G.H., "Fluidelastic Features of Flow Around Cylinders," Int. Research Seminar: Wind Effects on Bldgs. and Structures, NRC, Ottawa, Vol. 2, September 1967, pp. 323-341.

40. Koopmann,G.H., "On the Wind Induced Vibrations of Circular Cylinders," Catholic University, M.A.Sc. Thesis, March 1967.

41. Koopmann,G.H., "The Vortex Wakes of Vibrating Cylinders at Low Reynolds Numbers," J. Fluid Mech., Vol. 28, 1967, pp. 501-512.

42. Feng, C.C., "The Measurement of Vortex Induced Effects in Flow Past Stationary and Oscillating Cylinder and D-Section Cylinders," University of British Columbia, M.A.Sc. Thesis, October 1968.

43. Surry, D., "The Effect of High Intensity Turbulence on the Aerodynamics of a Rigid Circular Cylinder at Subcritical Reynolds Number," University of Toronto Inst. for Aerospace Studies, Report 142, October 1969.

44. Parkinson, G.V. and Brooks, N.P.H., "On the Aeroelastic Instability of Bluff Cylinders," J. Appl. Mech., ASME, Vol. 83, No. 2, June 1961, pp. 252-258.

45. Toebes, G.H. and Eagleson, P.S., "Hydroelastic Vibrations of Flat Plates Related to Trailing Edge Geometry," J. Basic Engng., ASME, Vol. 83, No. 4, December 1961, pp. 671-678.

46. Eagleson, P.S., Noutsopoulos, G.K. and Daily, J.W., "The Nature of Self-Excitation in the Flow-Induced Vibration of Flat Plates," J. Basic Engng., ASME, Vol. 86, No. 3, September 1964, pp. 599-606.

47. Parkinson, G.V. and Smith J.D., "The Square Prism as an Aeroelastic Non-Linear Oscillator," Quart. J. Mech. and Appl. Math., Vol. 17, Part 2, May 1964, pp. 225-239.

48. Wardlaw, R.L. and Davenport, A.G., "Some Experiments on the Fluctuating Forces on Flat Plates in Turbulent Flow," National Research Council of Canada, Aeronautical Report LR-416, December 1964.

49. Modi, V.J. and Heine, W., "On the Pressure Fluctuations and Wake Geometry Associated with Several Bluff Bodies," JSME Proc. 15th Japan Nat. Cong. Appl. Mech., 1965, pp. 7-18.

50. Schramm, W., "Wirbelfrequenzmessungen an umströmten Bauteilen," IfL-Mitt., Vol. 5, No. 8, 1966, pp. 308-318.

51. Vickery, B.J., "Fluctuating Lift and Drag on a Long Cylinder of Square Cross-Section in a Smooth and in a Turbulent Stream," J. Fluid Mech., Vol. 25, Part 3, 1966, pp. 481-494.

52. Parkinson, G.V. and Santosham, T.V., "Cylinders of Rectangular Section as Aeroelastic Nonlinear Oscillators," ASME Vib. Conf., Paper No. 67-VIBR-50, March 1967.

53. Wardlaw, R.L., "Aerodynamically Excited Vibrations of a 3-inch x 3-inch Aluminum Angle in Steady Flow," National Research Council of Canada, Aeronautical Report No. LR-482, June 1967.

54. Modi, V.J. and Slater, J.E., "On the Aeroelastic Instability of A Structural Angle," JSME Semi-International Sym., September 1967, pp. 207-214.

55. Kosko, E., "The Frequency Spectrum of a Structural Member in Coupled Flexural-Torsional Vibration," J. Sound and Vibration, Vol. 7, No. 2, 1968, pp. 143-155.

56. Peake, D.J., "Three-Dimensional Flow Separations on Upswept Rear Fuselages," Canadian Aeronautics and Space Jour., Vol. 15, No. 10, December 1969, pp. 399-408.

57. Modi, V.J. and Wiland, E., "Unsteady Aerodynamics of Stationary Elliptic Cylinders in Subcritical Flow," CASI/AIAA Subsonic Aero-and-Hydro-Dynamics Meeting, Paper No. 69-745, July 1969; In Press AIAA Jour.

58. Hiemenz, K., "Die Grenzschicht an einem in den gleichförmigen Flüssigkeitsstrom eingetauchten geraden Kreiszylinder," Dissertation Göttingen, 1911.

59. Chiu, W.S., "The Boundary Layer Formation and Vortex Shedding on Yawed Cylinders," Washington State University, College of Engng., Bulletin 299, 1966.

60. Achenbach, A., "Distribution of Local Pressure and Skin Friction Around a Circular Cylinder in Cross-Flow up to $Re=5x10^6$," J. Fluid Mech., Vol. 34, Part 4, 1968, pp. 625-639.

61. Schlichting, H., "Boundary-Layer Theory," McGraw Hill Book Co., New York, 1968, Chapters IX and X.

62. Parkinson, G.V., "Aeroelastic Galloping in One Degree of Freedom," Proc. First Int. Conf. on Wind Effects on Bldgs. and Structs., NPL., London, Vol. II, 1965, pp. 581-609.

63. Parkinson, G.V. and Modi, V.J., "Recent Research on Wind Effects on Bluff Two-Dimensional Bodies," Int. Research Seminar: Wind Effects on Bldgs. and Structs., NRC, Ottawa, Vol. 1, September 1967, pp. 485-513.

64. Wiland, E., "Unsteady Aerodynamics of Stationary Elliptic Cylinders in Subcritical Flow," University of British Columbia, M.A.Sc. Thesis, April 1968.

65. Görtler, H., "A New Series for the Calculation of Steady Laminar Boundary Layer Flows," J. of Maths. and Mechanics, Vol. 6, No. 1, 1957, pp. 1-66.

66. Ferguson, N., "The Measurement of Wake and Surface Effects in the Subcritical Flow Past a Circular Cylinder at Rest and in Vortex Excited Oscillations," University of British Columbia, M.A.Sc. Thesis, 1965.

67. Bryer, D.W., Walshe, D.E. and Garner, H.C., "Pressure Probes Selected for Three-Dimensional Flow Measurement," Aeronautical Research Council, R. and M. No. 3037, 1958.

68. Pankhurst, R.C. and Holder, D.W., "Wind Tunnel Techniques," Pitman and Sons Limited, London, 1952, Chapter 8.

69. Whitbread, R.E., "Model Simulation of Wind Effects on Structures," Proc. First Int. Conf. on Wind Effects on Bldgs. and Structs., NPL, London, Vol. 1, 1965, pp. 283-306.

70. Fage, A. and Johansen, F.C.,"On the Flow of Air Behind an Inclined Flat Plate of Infinite Span," Proc. Roy. Soc. of London, Series A, Vol. 116, 1927, pp. 170-197.

71. Hoerner, S.F., Fluid-Dynamic Drag, 1965, Chapter 3, p. 11.

72. Flachsbart, O., "Winddruck auf Gasbehälter," Rep. of the Aerodyn. Versuchsanstalt in Göttingen, IV Series, 1932, pp. 134-138.

73. Rosenhead, L., Laminar Boundary Layers, Clarendon Press, Oxford, 1963, pp. 258-348.

74. Blasius, H., "Grenzschichten in Flüssigkeiten mit kleiner Reibung," Z. Math. u. Phys., Vol. 56, 1927, pp. 1-37.

75. Pohlhausen, K., "Zur näherungsweisen Integration der Differentialgleichung der laminaren Reibungsschicht," ZAMM 1, 1921, pp. 252-268.

76. Schlichting, H., and Ulrich, A., "Zur Berechung des Umschlages laminar-turbulent," Jahrbuch d. dt. Luftfahrtforschung, Vol. I, 1942, pp. 8-35.

77. Howarth, L., "On the Solution of the Laminar Boundary Layer Equations," Proc. Roy. Soc. of London, Series A, Vol. 164, 1938, pp. 547-579.

78. Tani, I., "On the Solution of the Laminar Boundary Layer Equations," J. Phys. Soc. of Japan, Vol. 4, 1949, pp. 149-154.

79. Rotem, Z., Hauptmann, E.G., and Claassen, L., "Semi-focusing Color Schlieren System for Use in Fluid Mechanics and Heat Transfer," Applied Optics, Vol. 8, No. 11, November 1969, pp. 2326-2328.

80. Rotem, Z., and Claassen, L., "Natural Convection above Unconfined Horizontal Surface," J. Fluid Mech., Vol. 38, Part I, 1969, pp. 173-192.

81. Meksyn, D., New Methods in Laminar Boundary-Layer Theory, Pergamon Press, London, 1961, Chapter 11.

82. Schubauer, G.B., "Airflow in a Separating Laminar Boundary Layer," NACA, Rep. No. 527, 1935.

83. Heine, W., "On the Experimental Investigation of Vortex Excited Pressure Fluctuations," University of British Columbia, M.A.Sc. Thesis, 1964.

84. Taneda, S., "Experimental Investigation of the Wakes Behind Cylinders and Plates at Low Reynolds Number," J. Physical Society of Japan, Vol. 11, No. 3, March 1956.

85. Abernathy, F.H., Communication at IUTAM Conference on Concentrated Vortex Motions, Ann Arbor, 1964.

86. Hama, F.R., "Three Dimensional Vortex Pattern Behind a Circular Cylinder," J. Aerospace Sciences, Vol. 24, No. 2, February 1957, pp. 156-158.

87. Frimberger, R., "Experimentelle Untersuchungen an Kármánschen Wirbelstraßen," Z. Flugwiss., Vol. 5, 1957, pp. 355-359.

88. Fage, A. and Johansen, F.C., "The Structure of Vortex Sheets," Phil. Mag., Series 7, Vol. 5, No. 28, 1928, pp. 317-440.

89. Hooker, S.G., "On the Action of Viscosity in Increasing the Spacing Ratio of a Vortex Street," Proc. Roy. Soc. of London, Series A, Vol. 154, 1936, pp. 67-89.

90. Wille, R. and Timme, A., "Über des Verhalten von Wirbelstraßen, Jahrbuch der Schiffbautechn. Gesellschaft," Vol. 51, 1957, pp. 215-221.

91. Tyler, E., "Vortex Formation Behind Obstacles of Various Sections," Phil. Mag., Series 7, Vol. 11, No. 72, 1931, pp. 849-890.

92. Bloor, M.S., "The Transition to Turbulence in the Wake of a Circular Cylinder," J. Fluid Mech., Vol. 19, Part II, 1964, pp. 290-304.